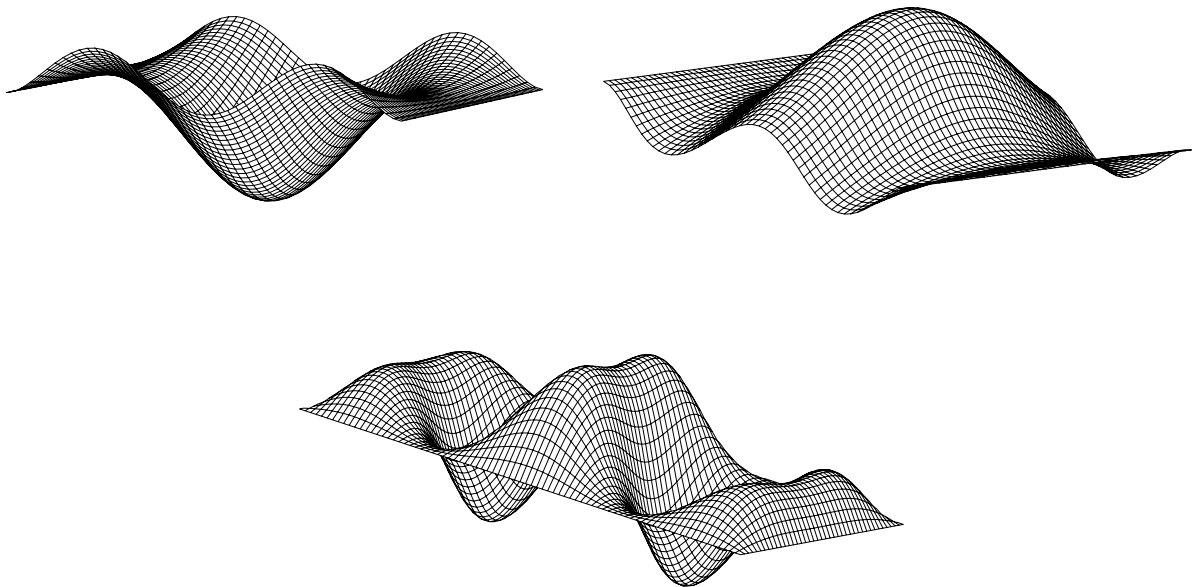




CHALMERS
UNIVERSITY OF TECHNOLOGY



Calculation of vibrations in the early design phase

A comparative study of the dynamic response of plates subjected to ground motion using Response Spectrum Analysis and Time History Analysis

Master's thesis in Master's Programme Structural Engineering and Building Technology

Fredrik Hellquist
Nils Rasmak

MASTER'S THESIS 2018:55

Calculation of vibrations in the early design phase

A comparative study of the dynamic response of plates subjected to ground motion using Response Spectrum Analysis and Time History Analysis

Master's thesis in the Master's Programme Structural Engineering and Building Technology

Fredrik Hellquist
Nils Rasmark



CHALMERS
UNIVERSITY OF TECHNOLOGY

Department of Mechanics and Maritime Sciences

Division of Dynamics

CHALMERS UNIVERSITY OF TECHNOLOGY

Gothenburg, Sweden 2018

Calculation of vibrations in the early design phase
A comparative study of the dynamic response of plates subjected to ground motion
using Response Spectrum Analysis and Time History Analysis
FREDRIK HELLQUIST, NILS RASMARK

© FREDRIK HELLQUIST, NILS RASMARK, 2018.

Supervisor: Mattias Carlsson, ÅF Infrastructure AB, Buildings
Examiner: Peter Folkow, Department of Mechanics and Maritime Sciences, Division
of Dynamics

Master's Thesis 2018:55
Department of Mechanics and Maritime Sciences
Division of Dynamics
Chalmers University of Technology
SE-412 96 Gothenburg
Telephone +46 31 772 1000

Cover: Displacement of plates subjected to ground motion.

Typeset in L^AT_EX
Printed by Chalmers reproservice
Gothenburg, Sweden 2018

Calculation of vibrations in the early design phase

A comparative study of the dynamic response of plates subjected to ground motion using Response Spectrum Analysis and Time History Analysis

Master's thesis in the Master's Programme Structural Engineering and Building Technology

FREDRIK HELLQUIST

NILS RASMARK

Department of Mechanics and Maritime Sciences

Division of Dynamics

Chalmers University of Technology

Abstract

Buildings exposed to vibrations from heavy road or train traffic do not normally risk being damaged, but the vibrations can cause discomfort to the users. Performing a detailed dynamic analysis is expensive and time consuming. Consequently, they are rarely performed with regard to comfort vibrations. Fagerström and Lindorsson (2017) studied a simple method of analysing beams and frame structures with respect to comfort vibrations. As a continuation of their work, this thesis aims to further develop a simple and effective method for studying comfort vibrations of buildings by incorporating plates into the method. In addition, it is investigated if the vibration of a plate can be predicted by interpolation of the known vibrations of similar plates. A calculation program in MATLAB is developed where the simplified analyses can be performed. The results are compared to analyses performed with a commercial FE program.

The study shows a large spread in the results between the simple and the more advanced method. The behaviour of plates are more complicated than beams and requires a higher understanding to be able to interpret the results correctly. If one takes careful measures with regards to the mesh, the dominant frequency range of the applied response spectrum and the natural frequencies of the studied plates, the simplified method provides results with reasonable accuracy. The study also shows that an interpolation between plates with similar geometry and boundary conditions to obtain the response is not easily performed, due to relatively small parameter differences potentially causing profound changes in the behaviour.

Keywords: RSA, THA, plates, MPF, response spectrum, structural dynamics, vibrations, Natural frequency, eigenfrequency, FEM.

Beräkning av vibrationer i det tidiga projekteringsskedet
En jämförande studie av den dynamiska responsen på plattor utsatta för markrörelse
med användning av responspektrumanalys och tidshistorieanalys
Examensarbete inom masterprogrammet Konstruktionsteknik och Byggnadsteknologi
FREDRIK HELLQUIST
NILS RASMAR
Institutionen för Mekanik och maritima vetenskaper
Avdelningen Dynamik
Chalmers tekniska högskola

Sammanfattning

En byggnad utsatt för vibrationer från exempelvis tung väg- eller tågtrafik riskerar normalt inte att skadas av vibrationerna, men vibrationerna kan orsaka obehag för människor i byggnaden. Att utföra en detaljerad dynamisk analys är dyrt och tidskrävande och därför utförs de sällan med avseende på komfortvibrationer. Fagerström and Lindorsson (2017) studerade en enkel metod för analys av balkar och ramkonstruktioner med avseende på komfortvibrationer. Som en fortsättning på deras arbete syftar detta examensarbete till att vidareutveckla en enkel och effektiv metod för analys av komfortvibrationer för byggnader genom att inkorporera plattor i metoden. Dessutom undersöks om vibrationen hos en platta kan förutsägas genom interpolering av kända vibrationer i liknande plattor. Ett beräkningsprogram i MATLAB utvecklas där de förenklade analyserna kan utföras. Resultaten jämförs med analyser utförda med ett kommersiellt FE-program.

Studien visar en stor spridning i resultaten mellan den enkla och den mer avancerade metoden. Plattors beteende är mer komplicerat än balkars och kräver en högre förståelse för att kunna tolka resultaten korrekt. Om stor noggrannhet läggs på plattans elementindelning, det dominerande frekvensområdet för det applicerade responspektrumet och de naturliga frekvenserna hos de plattor som studeras, kan den förenklade metoden ge resultat med rimlig noggrannhet. Studien visar också att en interpolering mellan liknande plattor för att erhålla responsen av en platta är svårt att genomföra på ett säkert sätt på grund av de många parametrar som påverkar olika plattor olika mycket.

Nyckelord: RSA, THA, plattor, MPF, responspektrum, strukturdynamik, vibrationer, naturlig frekvens, egenfrekvens, FEM.

Contents

List of Figures	xiii
List of Tables	xvii
List of Items	xx
1 Introduction	1
1.1 Background	1
1.2 Aim	2
1.3 Scope of the study	2
1.4 Limitations	2
1.5 Method	2
1.6 Outline of the report	3
2 Theory	5
2.1 Orientation	5
2.2 Basic concepts of vibration	5
2.2.1 Orientation	5
2.2.2 Introduction to vibrations	5
2.2.3 Free vibrations, Forced vibrations and natural modes	6
2.2.3.1 Beam vibration	6
2.2.3.2 Plate vibration	7
2.2.3.3 Example of free vibration with mass-spring system	8
2.2.3.4 Damping	9
2.2.3.5 Resonance	10
2.2.4 Relative and absolute response	11
2.2.5 Comfort vibration	12
2.3 Basic equations for dynamic systems	12
2.3.1 Orientation	12
2.3.2 Basic equations for SDOF-systems	12
2.3.3 Basic equations for MDOF-systems	14
2.3.4 Plate elements	15
2.3.5 Mode superposition	15
2.3.6 Direct integration methods	17
2.4 Applications of structural dynamics	18
2.4.1 Orientation	18

2.4.2	Time History Analysis	19
2.4.3	Response Spectrum Analysis	19
2.4.3.1	Orientation	19
2.4.3.2	Calculation of response spectrum	20
2.4.3.3	Spectral displacement, pseudovelocity and pseudoac- celeration	22
2.4.3.4	Modal participation factor	23
2.4.3.5	Calculation of the influence coefficient vector	24
2.4.3.6	Product of MPF and eigenvector	25
2.4.3.7	Modal combination rules	25
3	Method	27
3.1	Calculation tools	27
3.1.1	Orientation	27
3.1.2	MATLAB	27
3.1.2.1	Description of general properties	27
3.1.2.2	Purpose and function of the script	28
3.1.3	ADINA	29
3.1.3.1	Description of general properties	29
3.1.3.2	Horizontal modes	29
3.1.3.3	Generation of response spectrum with ADINA	29
3.1.3.4	MPF with ADINA	30
3.1.3.5	RSA with ADINA	30
3.1.3.6	THA with ADINA	30
3.1.4	Number of elements and convergence	30
3.2	General properties and information with regard to the plate analysis .	31
3.2.1	Orientation	31
3.2.1.1	Names of the plate sides	31
3.2.1.2	Nodal map and introduction to terminology used in the following chapters	31
3.2.1.3	Properties in common for all plates	32
3.2.2	Ground motions used as input for the analysis	32
3.2.2.1	Traffic load 1	32
3.2.2.2	Traffic load 2	33
4	Results	35
4.1	Orientation	35
4.2	Study of modal contribution	35
4.2.1	Orientation	35
4.2.2	Plates analysed in modal contribution study	36
4.2.2.1	Geometry of studied quadratic plates	36
4.2.2.2	Geometry of studied rectangular plates	36
4.2.2.3	Geometry of plates in parameter study	37
4.2.3	Number of elements used in modal contribution study	38
4.2.4	Modal contribution in MATLAB verified with modal contri- bution in ADINA	40
4.2.5	Results from the study of modal contribution	41

4.2.5.1	Study of modal contribution for quadratic plates . .	41
4.2.5.2	Study of modal contribution for rectangular plates .	43
4.2.5.3	Study of possibilities for interpolation of modal contribution for different plates	46
4.2.5.4	Study of modal contribution for plates in Parameter study	46
4.3	Comparison of THA and RSA	47
4.3.1	Orientation	47
4.3.2	Geometry of studied plates in parameter study	47
4.3.3	Initial number of elements used in parameter study	47
4.3.4	Verification of response spectrum calculated with ground motion from Traffic load 1	48
4.3.5	RSA with MATLAB verified through RSA with ADINA . . .	49
4.3.6	Parameter study of THA compared with RSA using coarse mesh	49
4.3.7	Refined mesh in parameter study	50
4.3.8	Parameter study of THA compared with RSA using refined mesh	52
4.3.8.1	Orientation	52
4.3.8.2	Plate type A	52
4.3.8.3	Plate type B	52
4.3.8.4	Plate type C	53
4.3.8.5	Plate type D	53
4.3.8.6	Plate type E	54
4.3.8.7	Summary of difference between THA and RSA from parameter study	54
4.3.9	Comparison of results from parameter study with fine and coarse mesh	56
4.3.10	Convergence study of a plate sensitive to mesh size	57
4.3.11	RSA using modal combination rule ABSSUM	58
4.4	In depth study of plates from parameter study	59
4.4.1	Orientation	59
4.4.2	Response spectrum from Traffic load 2	59
4.4.3	In depth analysis of plate with large deviation between THA and RSA, plate D5	60
4.4.3.1	Analysis of the entire time history	60
4.4.3.2	Study of general response in plate D5	62
4.4.3.3	Investigation on how the time-step length influence THA response	62
4.4.3.4	Investigation on how the number of modes influence the response of RSA	63
4.4.3.5	How mode interaction influences the difference of RSA and THA	64
4.4.3.6	Analysis with Traffic load 2	67
4.4.3.7	Maximum response of plate D4, E4 and E5.	67
4.4.4	In depth analysis of plate with small deviation between THA and RSA, plate B3	68

4.4.4.1	Analysis of the entire time story	68
4.4.4.2	Investigation on how the modes influence the response	70
4.4.4.3	Analysis with Traffic load 2	72
5	Conclusion	73
5.1	Orientation	73
5.2	Interpretation and analysis of results	73
5.2.1	Plates with large differences between results of THA and RSA, plates D4, D5 and E5.	73
5.2.2	General accuracy of results	74
5.2.3	Convergence	75
5.2.4	Interpolation of modal contribution	75
5.2.5	Natural modes activated with uniform vibration	76
5.3	Advice and options when using the method	76
5.3.1	Importance of conservative results and use of the modal com- bination rules	76
5.3.2	Optimisation of MATLAB script	77
5.3.3	Application of symmetry conditions to reduce model size . . .	77
5.3.4	Relationship between boundary conditions and accuracy of results	78
5.4	Further studies	78
5.4.1	Modal combination rules and widening of response spectra . .	78
5.4.2	Absolute response	78
5.4.3	Comfort weighting	79
5.5	Final conclusions	79
	Bibliography	81
	A Graphs from the parameter study of modal contribution	I
	B Results from the comparison of THA and RSA using a coarse mesh	XI
	C Results from the comparison of THA and RSA using ABSSUM	XV
	D MATLAB code	XIX
D.1	RSA code	XIX
D.2	MPF code	XXVI

List of Figures

2.1	Mode shapes for SS beam	6
2.2	Mode shapes for SS Plate	7
2.3	Mass-spring system with its free-body diagram for dynamic equilibrium	8
2.4	Graph of $u(t) = u_0 \cos(\omega_n t)$ starting from u_0 with period time $T_n = \frac{2\pi}{\omega_n}$	9
2.5	Linear viscous dashpot damping element.	9
2.6	The three different cases of damping: underdamped ($\zeta < 1$), critically damped ($\zeta = 1$) and overdamped ($\zeta > 1$).	10
2.7	Resonance behaviour, when the frequency of an external load $\Omega = \omega_n$	11
2.8	Ground motion, relative motion and absolute motion.	11
2.9	Mass-spring-damper with moving base and the free body diagram. . .	13
2.10	Mass-spring-damper system with external force and moving base. . .	14
2.11	Free body diagram of the MDOF mass-spring-damper system.	14
2.12	Example of ground motion and the associated THA.	19
2.13	Procedure for calculation of response spectra.	21
2.14	Graph of response spectrum with the relative acceleration response for the frequency range 1-200 [Hz].	22
3.1	Four node rectangular quadrilateral element with three DOF per node, vertical displacement and $x - y$ rotations.	28
3.2	Cantilever beam with point mass, model used for generation of response spectrum in ADINA.	29
3.3	Name of the sides of the studied plates.	31
3.4	Rectangular plate with the node names and positions.	32
3.5	Ground acceleration 1. Vibration is the result of a train passage. . . .	33
3.6	Ground acceleration 2.	34
4.1	Schematic of the different plate types, exemplifying with the dimensions and BCs of plate type D.	37
4.2	Graph of how the first mode frequency of plate A3/Q4 calculated with the MATLAB program converges depending on number of elements. . .	39
4.3	Convergence of frequencies calculated with ADINA.	39
4.4	Study of the impact on modal contribution with different element sizes	40
4.5	Comparison of modal contribution calculated with MATLAB and ADINA for plate Q4 with thickness of 0.2 m and 400 elements.	40

4.6	Modal contribution plotted in relation to frequency which has been normalised with the first mode frequency of the plate. For clarity, modal contributions smaller than 10^{-9} are not shown in the graph. Calculations were performed with MATLAB	45
4.7	Modal contribution on vertical mid DOF plotted in relation to normalised frequency.	46
4.8	Response spectrum calculated with ADINA and MATLAB in form of relative responses based on ground acceleration.	48
4.9	Convergence study of the first mode frequency and responses with RSA and THA for plate A1/A5.	51
4.10	Convergence study of the first mode frequency and responses with RSA for plate E1.	57
4.11	The ground acceleration for Traffic load 2 and the response spectra calculated from the ground acceleration.	60
4.12	The applied ground motion signal and complete time history of the mid node in plate D5 for all three responses.	61
4.13	Influence on the response of the mid DOF according RSA with MATLAB and ADINA.	63
4.14	Increase of the response on the mid node with increasing number of modes calculated with MATLAB and a 20×20 mesh. The contributing modes are modes 1, 4, 10 and 17.	64
4.15	The four modes that contributes to the majority of the response for plate D5 according to RSA.	65
4.16	Displacements of plate D5 at time steps with largest displacements according THA.	65
4.17	Illustration of how responses from modes are combined to a total response in RSA and THA.	66
4.18	Modes 8 and 13 for plate D5, which contributes to the response at the free edge.	67
4.19	Plates D4, D5, E4 and E5 at the time of maximum displacement in THA.	68
4.20	Complete THA of the mid node in plate B3.	69
4.21	Influence on the response of the mid DOF according to RSA with MATLAB and ADINA.	70
4.22	Increase of the response on the mid node with increasing number of modes.	70
4.23	The two modes that contributes to the majority of the response for plate B3 according to RSA.	71
4.24	Displacements at the time of largest response in plate B3 in THA. . .	71
A.1	Modal contribution on the vertical mid DOF of plate A1.	I
A.2	Modal contribution on the vertical mid DOF of plate A2.	I
A.3	Modal contribution on the vertical mid DOF of plate A3.	II
A.4	Modal contribution on the vertical mid DOF of plate A4.	II
A.5	Modal contribution on the vertical mid DOF of plate A5.	II
A.6	Modal contribution on the vertical mid DOF of plate B1.	III

A.7	Modal contribution on the vertical mid DOF of plate B2.	III
A.8	Modal contribution on the vertical mid DOF of plate B3.	III
A.9	Modal contribution on the vertical mid DOF of plate B4.	IV
A.10	Modal contribution on the vertical mid DOF of plate B5.	IV
A.11	Modal contribution on the vertical mid DOF of plate C1.	IV
A.12	Modal contribution on the vertical mid DOF of plate C2.	V
A.13	Modal contribution on the vertical mid DOF of plate C3.	V
A.14	Modal contribution on the vertical mid DOF of plate C4.	V
A.15	Modal contribution on the vertical mid DOF of plate C5.	VI
A.16	Modal contribution on the vertical mid DOF of plate D1.	VI
A.17	Modal contribution on the vertical mid DOF of plate D2.	VI
A.18	Modal contribution on the vertical mid DOF of plate D3.	VII
A.19	Modal contribution on the vertical mid DOF of plate D4.	VII
A.20	Modal contribution on the vertical mid DOF of plate D5.	VII
A.21	Modal contribution on the vertical mid DOF of plate E1.	VIII
A.22	Modal contribution on the vertical mid DOF of plate E2.	VIII
A.23	Modal contribution on the vertical mid DOF of plate E3.	VIII
A.24	Modal contribution on the vertical mid DOF of plate E4.	IX
A.25	Modal contribution on the vertical mid DOF of plate E5.	IX

List of Tables

3.1	Properties used for all the studied plates.	32
4.1	Geometry of the studied quadratic plates.	36
4.2	Geometry of the studied rectangular plates.	36
4.3	Name and geometry of plates in parameter study. SS is short for simply supported.	38
4.4	Comparison of frequency and modal contribution from MATLAB and ADINA for plate Q4 with thickness of 0.2 <i>m</i> and 400 elements.	41
4.5	Comparison of the first mode frequency calculated analytically, and with ADINA and MATLAB.	42
4.6	Comparison of modal contribution of the first mode calculated with ADINA and MATLAB.	42
4.7	Comparison of the first mode frequency calculated analytically, and with ADINA and MATLAB.	42
4.8	Comparison of the modal contribution calculated with ADINA and MATLAB.	43
4.9	Modal contribution of the first five contributing modes on the centre node for 6 rectangular plates calculated with MATLAB.	43
4.10	Comparison of RSA calculated with MATLAB and ADINA. The responses at the centre of the plates is compared.	49
4.11	Comparison of responses with RSA and THA with coarse mesh	50
4.12	Comparison of response with THA and RSA in the plates of type A.	52
4.13	Comparison of response with THA and RSA in the plates of type B.	53
4.14	Comparison of response with THA and RSA in the plates of type C.	53
4.15	Comparison of response with THA and RSA in the plates of type D.	54
4.16	Comparison of response with THA and RSA in the plates of type E.	54
4.17	Comparison of responses, as percentage difference between RSA and THA with the fine mesh. Positive difference means the THA is larger than RSA.	55
4.18	Percentage difference of responses between analyses with 20×20 mesh and 10 cm ² mesh.	56
4.19	Difference between the responses with THA and RSA using modal combination rule ABSSUM.	58
4.20	Comparison of the relative response of plate D5 calculated with THA and RSA.	62

4.21	Comparison of RSA and THA in the centre of the plates, i.e node d, including 1 and 4 modes.	63
4.22	Comparison of THA and RSA of plate D5 calculated with Traffic load 2.	67
4.23	Comparison of RSA and THA including 1 and 6 modes.	71
4.24	Comparison of THA and RSA of plate B3 calculated with Traffic load 2.	72
B.1	Comparison of relative acceleration with THA and RSA using a mesh of 20×20 elements.	XI
B.2	Comparison of relative velocity with THA and RSA using a mesh of 20×20 elements.	XII
B.3	Comparison of relative displacement with THA and RSA using a mesh of 20×20 elements.	XIII
C.1	Comparison of relative acceleration with THA and RSA using ABSSUM.	XV
C.2	Comparison of relative velocity with THA and RSA using ABSSUM.	XVI
C.3	Comparison of relative displacement with THA and RSA using ABSSUM.	XVII

Preface

This Master's thesis investigates how comfort vibrations can be assessed in a simplified manner. The thesis is the second in a series on the subject and a continuation on previous Master's thesis by Fagerström and Lindorsson (2017). The study is a collaboration between the Master's program Structural Engineering and Building Technology at Chalmers University of Technology and ÅF Infrastructure AB. The work has been carried out at ÅF Infrastructure at business area Buildings, and both writers contributed in all parts of the thesis.

First and foremost we would like to thank our supervisor Mattias Carlsson at ÅF Infrastructure for his continuous support and commitment throughout the work. His experience and expertise has been very helpful when we encountered obstacles. We would also like to thank our supervisor and examiner, Peter Folkow at Chalmers University of Technology. He has supported us with his knowledge throughout the work and also been helpful with connecting us with other expertise's when needed. We would also like to thank Morgan Johansson at Norconsult, for giving some advice and comments during the work.

Further, we would like to thank Patrik Höstmad at Chalmers University of Technology for lending his time and for his inputs on comfort weighting early on in the project.

Finally, we would like to thank the staff at ÅF Infrastructure for letting us be a part of their team during the writing of the thesis.

Gothenburg, June 2018
Fredrik Hellquist and Nils Rasmark

List of Items

Acronyms

<i>BC</i>	Boundary conditions
<i>DOF</i>	Degree of freedom
<i>MDOF</i>	Multiple degree of freedom
<i>MPF</i>	Modal participation factor
<i>RSA</i>	Response spectrum analysis
<i>SDOF</i>	Single degree of freedom
<i>SS</i>	Simply supported
<i>THA</i>	Time history analysis
<i>VBA</i>	Visual basic for applications

Greek letters

α	Newmark coefficient	
β	Newmark coefficient	
Γ	Modal participation factor	
Ω	Frequency of external dynamic load	<i>rad/s</i>
ω_d	Damped circular natural frequency	<i>rad/s</i>
ω_n	Undamped circular natural frequency	<i>rad/s</i>
Φ	Eigenmatrix	
ϕ	Eigenvector	
ζ	Viscous damping factor	

Matrix and Vector notation

\mathbf{X}	Matrix
\mathbf{x}	Vector
x	Scalar

Roman letters

\mathbf{C}_m	Generalized damping matrix or Model damping matrix	
\mathbf{C}	Damping matrix	
\mathbf{K}_d	Condensed stiffness matrix	
\mathbf{K}_m	Modal stiffness matrix	
\mathbf{K}	Stiffness matrix	
\mathbf{M}_m	Modal mass matrix	
\mathbf{M}	Mass matrix	
\mathbf{R}	Influence coefficient matrix	
\mathbf{r}	Influence coefficient vector	
\ddot{u}, a	Acceleration	<i>m/s²</i>
\dot{u}, v	Velocity	<i>m/s</i>
c_{cr}	Critical damping	

List of Items

c_i	Coefficient of viscous damping	Ns/m
f	Frequency	Hz
f_d	Damping force	N
f_s	Spring force	N
k_i	Elastic spring constant	N/m
m	Mass	kg
p	Correlation coefficient	
S_a	Relative acceleration spectrum	m/s^2
S_d	Relative displacement spectrum	m
S_v	Relative velocity spectrum	m/s
$S_{a.abs}$	Absolute acceleration spectrum	m/s^2
$S_{d.abs}$	Absolute displacement spectrum	m
$S_{v.abs}$	Absolute velocity spectrum	m/s
T_n	Period time	s
u, d	Displacement	m
u_0	Displacement at time $t = 0$	m
v_0	Velocity at time $t = 0$	m/s

1

Introduction

1.1 Background

Vibrations in structures are of large importance for several reasons, ranging from ultimate limit capacity when the structure is subjected to earthquake or impact loads, to serviceability cases when for example traffic vibrations or human activity induce discomfort for the users of the building. The dynamic properties of the building have a large influence on the behaviour when subjected to dynamic loads. Performing detailed dynamic analysis is costly and time consuming, and as a result, dynamic analyses with regards to comfort vibrations are often not performed. Since the comfort of the users of a structure is an important aspect of construction there is a need to investigate the dynamic properties of the structure while avoiding the issue of increased cost that a detailed dynamic analysis requires. Therefore, there is a general need for a simplified efficient method to predict problems with comfort vibrations, or in unclear cases give an indication if a more detailed analysis would be needed.

One method for simplified dynamic analysis is the Response Spectrum Analysis (RSA), which is in frequent use for earthquake analysis worldwide. Combining a response spectrum with a structure's Modal Participation Factors (MPF) and eigenvectors is a fast and simple method to obtain results of comparable accuracy to the much more resource- and time consuming Time History Analysis (THA) for earthquake applications.

Fagerström and Lindorsson (2017) studied the RSA method for beams and frame structures with regard to comfort vibrations. They obtained good results for vibration response at the connection between the walls and floors. To analyse the vibrations a person would experience in a building, it is necessary to find the vibrational response on the floor that they are standing or sitting on. In order to perform such an analysis, the incorporation of plates is a necessity.

1.2 Aim

Following the work of Fagerström and Lindorsson (2017), this thesis aims to continue development of a simple and efficient method for the study of comfort vibrations for buildings by incorporating plates into the method.

1.3 Scope of the study

The study primarily revolves around the accuracy of results between RSA and THA for various plates. The effect that plate geometry, support conditions and element mesh have on the MPF and eigenfrequencies are also studied. In addition, it is investigated if MPF and eigenfrequencies can be interpolated from data of other plates with similar dimensions and support conditions.

1.4 Limitations

Several key elements of analysing comfort vibrations are omitted from the study, these include absolute response, methods of combining local and global analysis and methods to incorporate comfort weighting. The concepts are explained in theory and discussed, as they are important parts of the comfort vibration analysis. Simple linear elastic material models are used, and nonlinear phenomena such as concrete cracking are not included in the analyses. Effects of damping are considered in a simplified way in the models through modal damping. No in-depth study of the damping phenomenon is made and the subject is only briefly touched upon. Vibrational loads that are studied are assumed to have fully reached the structure. Hence, geotechnical conditions and transfer of vibrations through the foundation are not considered. Of the various integration methods, this study applies the Newmark- β method.

1.5 Method

A literature study of structural dynamics through textbooks, technical reports and scientific articles comprise the first part of the study. The literature study focuses on numerical integration methods, THA and RSA.

To be able to run fast analyses a script that is able to perform a RSA is developed in MATLAB. THA, verification of RSA results, and RSA of computationally heavier models are done in ADINA FEM.

Using the RSA and THA, plates with varying support conditions and dimensions are studied. The accuracy of the MATLAB RSA script is verified with ADINA RSA and comparison of RSA against THA is made. An investigation is made into how the MPF and eigenfrequencies are affected by plate geometry and support conditions. In addition, a study on how mesh refinement affects THA and RSA is made.

1.6 Outline of the report

The report consists of a theory chapter (Chapter 2), a method chapter (Chapter 3), a result chapter (Chapter 4) and finally a conclusion chapter (Chapter 5).

In Chapter 2 background theory needed to perform and understand the methods and results in upcoming chapters of the thesis is given. It includes an introduction of vibration and basic theory of structural dynamics. Also explanations of the THA, RSA and numerical integration methods are given here.

Chapter 3 describes how the calculation tools MATLAB and ADINA have been used to calculate the MPF and perform the RSA and THA. General properties and information of the plate analysis performed in Chapter 4 are introduced as well as the traffic loads that have been used.

Chapter 4 presents the results of the modal contribution study and the comparative study of RSA and THA for various plates. An in-depth analysis of two plates were made and the results are also presented in this chapter. In addition of presenting the results an introductory discussion is held for some of the results.

Chapter 5 covers more in depth discussions and conclusions of the results. Propositions for further studies are given as well as recommendations for improvements of the analysis carried out in the thesis.

In the appendices, graphs from the modal contribution study and some additional tables from the THA and RSA comparison are shown.

2

Theory

2.1 Orientation

The theory chapter explains the theory on which the thesis work is based on. It covers the basics of vibrations, fundamentals of structure dynamics, Response spectrum analysis (RSA), Time history analysis (THA), numerical integration methods and comfort weighting.

2.2 Basic concepts of vibration

2.2.1 Orientation

This section covers some of the basic concepts of vibrations such as natural vibration modes, free and forced vibration, relative and absolute response, illustrations of beam and plate vibration and an example of free vibration in order to explain the basic concepts.

2.2.2 Introduction to vibrations

At the most basic level, a vibration is when a particle or a system of particles oscillates periodically around its equilibrium point, which is a consequence of the particle or system being disturbed from its equilibrium state in some way (Merriam-Webster, 2018). Ways to disturb a particle or system from equilibrium include displacement, velocity, acceleration or an external force. All these terms are in reality very much related to each other, but in the mathematical study of dynamic systems they are viewed separately. The vibration of any system depends on the four parameters mass, stiffness, damping and external force.

2.2.3 Free vibrations, Forced vibrations and natural modes

A system which is excited by a short disturbance from its equilibrium state will continue to vibrate for a time, even when no external exciting source remain on the system. This is known as free vibration, and an intuitive example of it can be seen by striking a guitar string. The system will vibrate with a combination of its *natural modes*. A continuous system has an infinite amount of natural modes, while a n -degree of freedom system will have n natural modes. The free vibration is a simultaneous combination of all of a systems' natural modes, but the lower modes contain more energy and are typically the most significant while the low energy higher modes are of less significance. A natural mode is accompanied by a natural frequency, in structural dynamics a natural mode is described by an eigenvector and the natural frequency by its associated eigenvalue, this is covered in Section 2.3.5. Forced vibrations implies, unlike free vibrations, that the disturbing factor remains on the system. Often this disturbance is in the shape of an external dynamic force.

2.2.3.1 Beam vibration

Simply supported beams vibrate much like the aforementioned example of a guitar string, see Figure 2.1. The first mode, also known as the *fundamental mode* is a half sine wave. Each following mode will have an extra hump and an extra *node*. The nodes are the points of the beam that have zero movement in a natural mode. For the n -DOF beam in the example there are n modes with n associated natural frequencies.

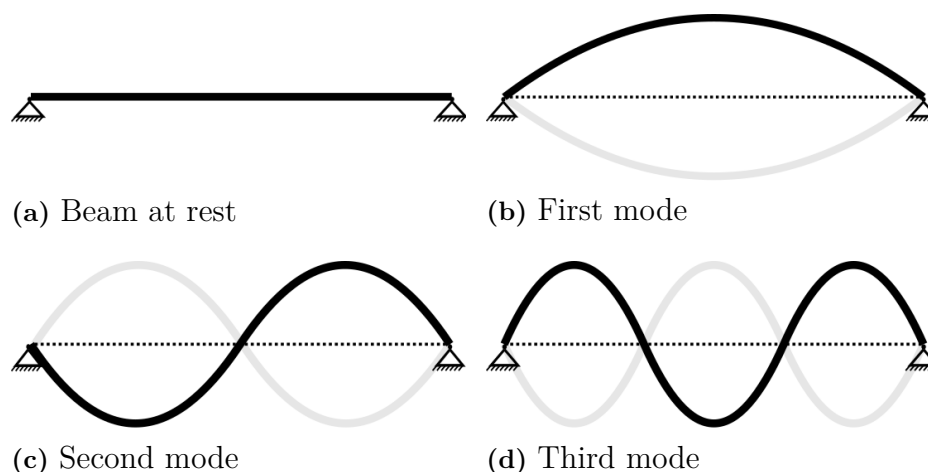


Figure 2.1: The first natural vibration modes for a simply supported beam: (a) Beam at rest, no vibration; (b) Beam vibrating in its first natural mode; (c) Beam vibrating in its second natural mode; and, (d) Beam vibrating in its third natural mode.

2.2.3.2 Plate vibration

Unlike the beam element, plates are two-dimensional and thus exhibit a more complex vibrational behaviour. For instance, many modes will have a twin mode in the perpendicular direction, which will have a different natural frequency than its twin mode if the plate is not symmetrical with regards to support conditions and dimensions. The plate vibration behaviour is studied thoroughly in later sections of the thesis, but examples of the first few vibrational modes of a simply supported quadratic plate can be seen in Figure 2.2.

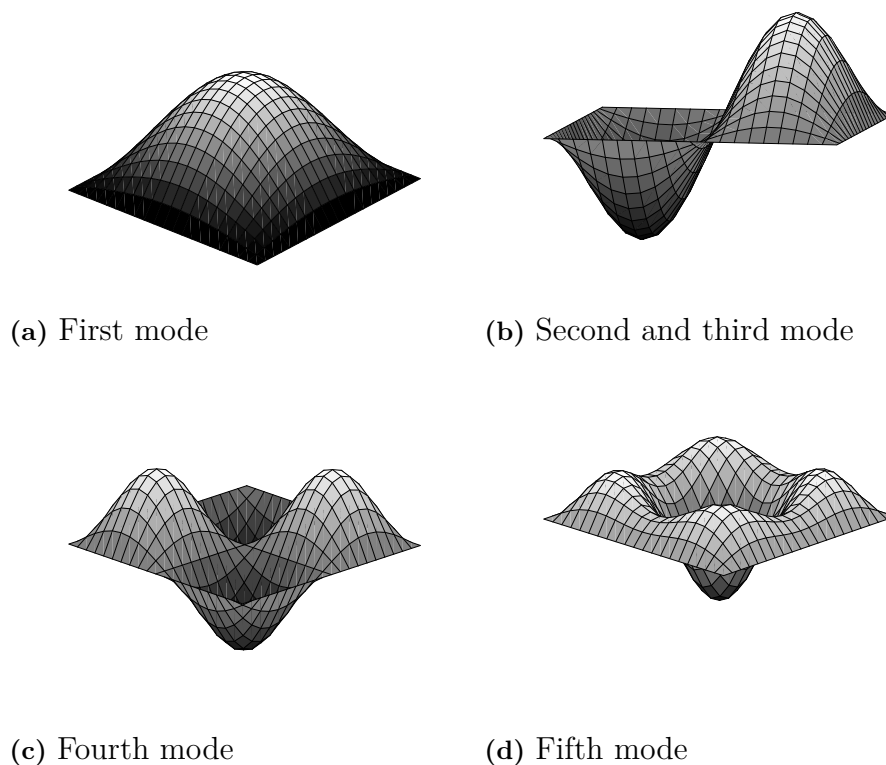


Figure 2.2: The first natural vibration modes for a simply supported quadratic plate. (b) Shows a twin mode.

The natural frequency of a plate can easily be analytically calculated. Equation 2.1 shows a formula that can be used to calculate the fundamental frequency for a simply supported quadratic or rectangular plate (Feldmann, Heinemeyer, and Völling, 2007).

$$f = \frac{\alpha}{a^2} \sqrt{\frac{Et^3}{12m(1-\nu)}} \quad \alpha = 1.57\left(1 + \left(\frac{a}{b}\right)^2\right) \quad (2.1)$$

Where E is the Young's Modulus, m is the mass of the plate, ν is the Poisson's ratio, t is the thickness of the plate, a and b are the length and width of the plate.

2.2.3.3 Example of free vibration with mass-spring system

To illustrate a basic example of free vibration, a mass-spring system is used, as shown in Figure 2.3a. In the mass-spring system a linear elastic spring is assumed. This means that the spring force f_s is proportional to the displacement u with the spring constant k , i.e the constitutive relation:

$$f_s = ku. \quad (2.2)$$

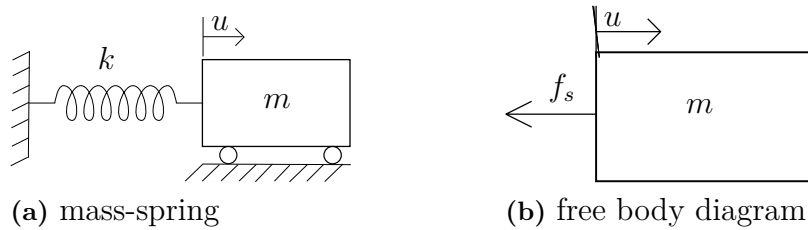


Figure 2.3: Mass-spring system with its free-body diagram for dynamic equilibrium

In the free body diagram in Figure 2.3b using Newton's second law: $\sum F_x = m\ddot{u}_x$, and the constitutive relation $f_s = ku$ the equation of motion for the system is obtained as

$$m\ddot{u} + ku = 0. \quad (2.3)$$

Equation 2.3 is a *second-order linear ordinary differential equation* with the complementary (homogeneous)¹ solution as in Equation 2.4. As there is no external force present in this system the particular solution $u_p = 0$, which makes the general solution $u(t) = u_c + u_p = u_c$. When there is an external force the system undergoes *forced vibration*, which is covered in Section 2.3.2

$$u(t) = A_1 \cos(\omega_n t) + A_2 \sin(\omega_n t). \quad (2.4)$$

Here $\omega_n = \sqrt{\frac{k}{m}}$ is defined as the *undamped circular natural frequency*. Make special notice that this parameter is dependant on the relation of stiffness to mass. The constants A_1 and A_2 can be found with the use of the initial conditions $u(0) = u_0$ and $\dot{u}(0) = v_0$ which gives $A_1 = u_0$ and $A_2 = \frac{v_0}{\omega_n}$. A simple case to study is with initial conditions consisting of a prescribed displacement of $u_0 \neq 0$ and no initial velocity $v_0 = 0$. Inserting the initial conditions into Equation 2.4 and its derivative \dot{u} gives

$$u(t) = u_0 \cos(\omega_n t). \quad (2.5)$$

The system will oscillate with an amplitude of u_0 over a period $T_n = \frac{2\pi}{\omega_n}$. The *undamped natural frequency* $f = \frac{\omega_n}{2\pi}$ gives the cycles per second. Figure 2.4 shows the sinusoidal behaviour of Equation 2.5, it can also be seen that the motion continues

¹In structural dynamics the homogeneous solution of a differential equation is denoted *complementary solution*, by convention.

with the same amplitude indefinitely. No realistic structural system will behave this way, since energy will dissipate from the system. The dissipation of energy is called damping.

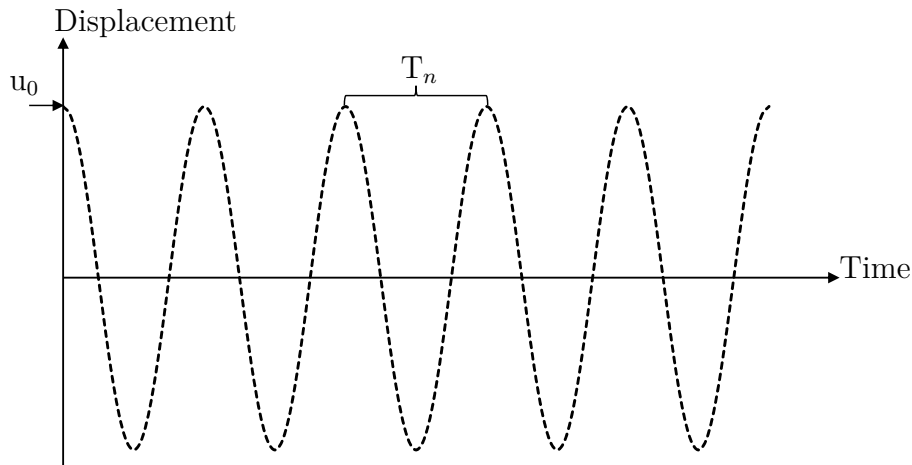


Figure 2.4: Graph of $u(t) = u_0 \cos(\omega_n t)$ starting from u_0 with period time $T_n = \frac{2\pi}{\omega_n}$.

2.2.3.4 Damping

A structure subjected to an excitation will vibrate with decreasing amplitude for a period of time. The progressively decreasing magnitude of the vibration is the result of dissipation of energy from the structure during the vibration. Many processes are involved in the energy dissipation, an example of which is friction. In structural dynamics the dissipation of energy is referred to as *damping*. The damping of a structure depend on many different factors that are difficult to consider, it is therefore generally impossible to predict the exact damping properties of a structure. It can be measured when the structure is completed, but the behaviour is very difficult to predict. Thus, taking damping into account is problematic, but several methods to model it exist. The most common way to handle damping in structural dynamics is the linear viscous dashpot model (Craig and Kurdila, 2006). The linear viscous damping model describes the damping force as $f_d = c(\dot{u}_2 - \dot{u}_1)$ where c is the coefficient of viscous damping and $(\dot{u}_2 - \dot{u}_1)$ is the relative velocity of the two points on each end of the dashpot, see Figure 2.5.

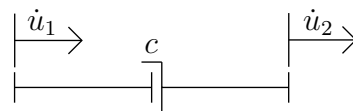


Figure 2.5: Linear viscous dashpot damping element.

The viscous dashpot model with the coefficient of viscous damping is handled similarly to the linear spring model. The difference is that the spring acts by storing

energy while the damping dashpot dissipates energy. In addition to c , the damping model introduces the critical damping coefficient $c_{cr} = 2\sqrt{km}$ and the damping ratio $\zeta = \frac{c}{c_{cr}}$, Section 2.3.2 illustrates the use of these coefficients in equations. The damping ratio ζ has the property that it states which of the three different damping behaviours a system will have.

- The system is underdamped: $\zeta < 1$
- The system is overdamped: $\zeta > 1$
- The system is critically damped: $\zeta = 1$

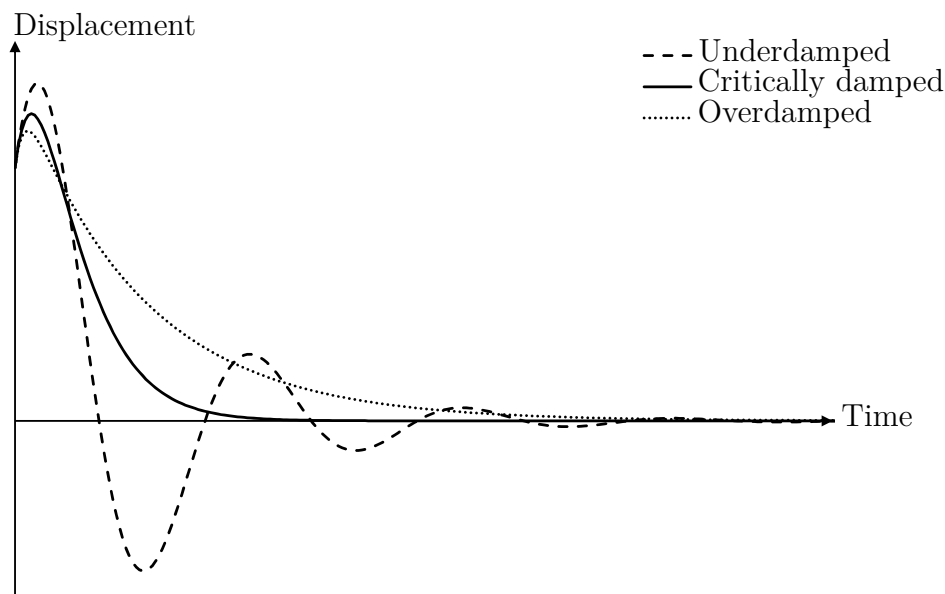


Figure 2.6: The three different cases of damping: underdamped ($\zeta < 1$), critically damped ($\zeta = 1$) and overdamped ($\zeta > 1$).

2.2.3.5 Resonance

The natural frequency, ω_n , is an important parameter when studying dynamics. When a system is subjected to an external dynamic force where the frequency of the force is the same as the natural frequency of the system, it will cause the system to resonate. Resonance will increase the amplitude of the motion continuously, theoretically until the displacement approaches infinity. For real structures this is obviously not the case, as a brittle structure would eventually fail when deformations become large enough and a ductile structure would start to yield, changing the stiffness properties and thus the natural frequency which would cause the resonant behaviour to cease. Nevertheless, avoiding resonance behaviour is a very important aspect of structural design (Chopra, 2014). Figure 2.7 shows the resonance behaviour in a simple manner.

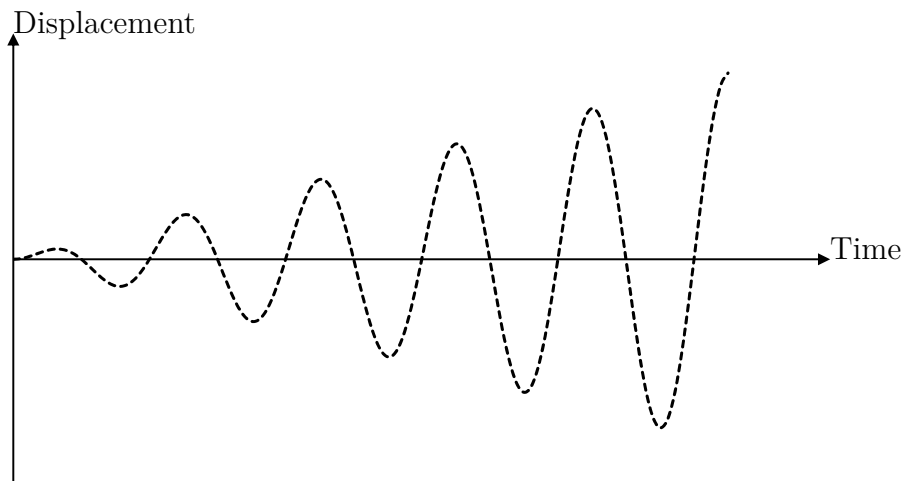


Figure 2.7: Resonance behaviour, when the frequency of an external load $\Omega = \omega_n$

2.2.4 Relative and absolute response

When a system has a moving base it becomes important to distinguish between relative response and absolute response. The principle is shown in Figure 2.8, where the displacement of the tip of a cantilever beam is illustrated. The relative displacement d_{rel} is the displacement of the tip of the beam relative to its base, the ground displacement d_g is the displacement of the base with regard to its original position and the absolute displacement is the total sum $d_{abs} = d_g + d_{rel}$. For comfort vibrations it's important to examine the absolute response, since the absolute response of a vibration is the one a person feels when standing on a floor in a vibrating structure, for example.

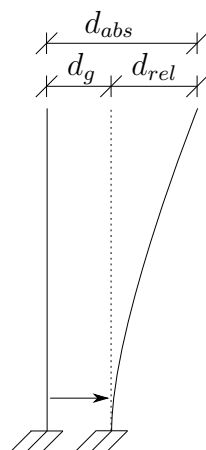


Figure 2.8: Ground motion, relative motion and absolute motion.

2.2.5 Comfort vibration

Comfort vibration has to do with the experience of vibrations. The human body's reaction when subjected to vibration is complicated. Different parts of the body have different frequency ranges that it is sensitive to and the sensitivity also varies between individuals. To be able to assess the vibration of a building with regards to discomfort for the users, frequency weightings curves has been developed by the International Standards Organisation (ISO). The weighting curves consider the direction of the vibration and the frequency (Brüel and Kjaer, 1989). Frequencies which the human body is more sensitive to are given a higher weighting factor and in this way a transformation of measured vibration into experienced discomfort is obtained. A human inside a vibrating building will experience the absolute response of the vibration and therefore it is the absolute response that are of most interest when it comes to comfort vibration.

2.3 Basic equations for dynamic systems

2.3.1 Orientation

This section covers the basic equations used for SDOF and MDOF systems. It will include the concepts of forced vibration, damping and moving base introduced in Section 2.2 into the equations. This section also includes a description of the numerical integration method Newmark- β , which for this thesis is the method used to solve the differential equations.

2.3.2 Basic equations for SDOF-systems

Analogously to Section 2.2.3.3, a mass-spring-damper system with a moving base is used to illustrate the SDOF system, as seen in Figure 2.9a. Here m is mass, k is the spring constant, c is the coefficient of viscous damping, $p(t)$ is the time dependent external force acting on the mass. Since the mass only moves in the lateral direction with one displacement coordinate defined it is a SDOF system. The total displacement is defined as $u(t)$ but denoted u in equations. Figure 2.9b shows a free body diagram of the system.

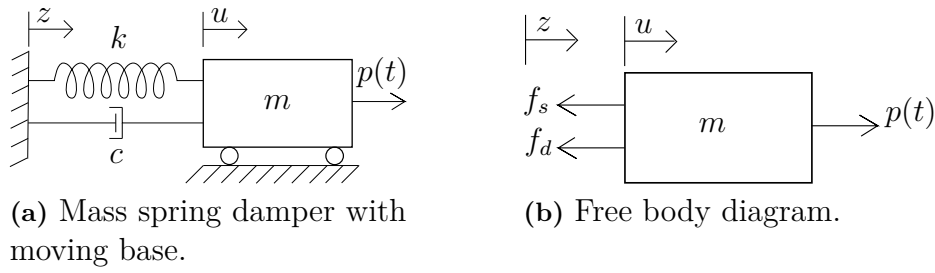


Figure 2.9: Mass-spring-damper with moving base and the free body diagram.

Using the force-displacement relationship with assumed linear relationship for the spring (Equation 2.8), the damping (Equation 2.9) together with Newton's second law (Equation 2.6), the equation of motion (Equation 2.10) is obtained.

$$\sum F_x = p(t) - f_s - f_d = ma \quad (2.6)$$

$$a = \ddot{u} \quad (2.7)$$

$$f_s = ku \quad (2.8)$$

$$f_d = c\dot{u} \quad (2.9)$$

$$m\ddot{u} + c\dot{u} + ku = p(t) \quad (2.10)$$

Dividing both sides of the equation with m and introducing the undamped circular natural frequency $\omega_n = \sqrt{\frac{k}{m}}$, viscous damping factor $\zeta = \frac{c}{c_{cr}}$ and the critical damping coefficient $c_{cr} = 2\sqrt{km}$, Equation 2.10 can be expressed as Equation 2.11

$$\ddot{u} + 2\zeta\omega_n\dot{u} + \omega_n^2u = \frac{p(t)}{m} \quad (2.11)$$

If the system has a moving base, denoted $z(t)$, the same procedure instead gives:

$$m\ddot{u} + c\dot{u} + ku = c\dot{z} + kz + p(t) \quad (2.12)$$

Defining the displacement relative to the mass as $w = u - z$ gives:

$$m(\ddot{w} + \ddot{z}) + c\dot{w} + kw = p(t) \quad (2.13)$$

Subtracting $m\ddot{z}$ from both sides gives:

$$m\ddot{w} + c\dot{w} + kw = p(t) - m\ddot{z} \quad (2.14)$$

dividing with m on both sides gives:

$$\ddot{w} + 2\zeta\omega_n\dot{w} + \omega_n^2w = \frac{p(t)}{m} - \ddot{z} \quad (2.15)$$

2.3.3 Basic equations for MDOF-systems

To be able to perform adequate analyses of a system it is typically insufficient to look at only one degree of freedom. Again the use of a simple mass-spring-damper-system is used to illustrate the principles for a MDOF-system, see Figure 2.10. The difference from a SDOF system is that Newton's second law now is implemented for each degree-of-freedom resulting in the same number of equations of motion as degrees of freedom. Figure 2.11 shows the free body diagram and Equations 2.16 and 2.17 show the resulting force summation.

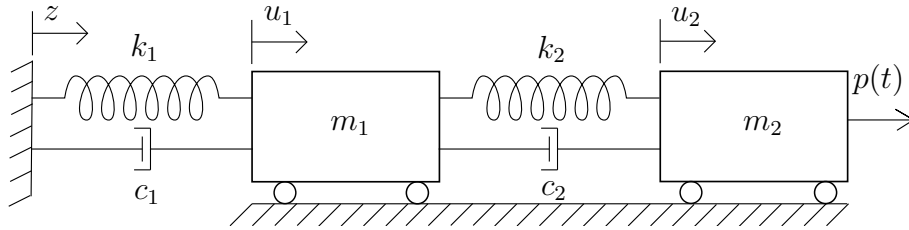


Figure 2.10: Mass-spring-damper system with external force and moving base.

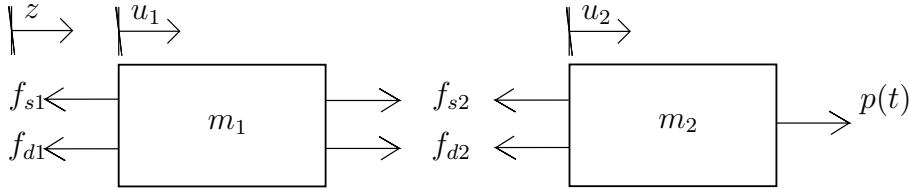


Figure 2.11: Free body diagram of the MDOF mass-spring-damper system.

$$\sum F_1 = -f_{s1} - f_{d1} + f_{s2} + f_{d2} = m_1 \ddot{u}_1 = m_1(\ddot{z} + \ddot{w}_1) \quad (2.16)$$

$$\sum F_2 = -f_{s2} - f_{d2} + p(t) = m_2 \ddot{u}_2 = m_2(\ddot{z} + \ddot{w}_2) \quad (2.17)$$

Using the following force-displacement relation with assumption of linear elastic spring force

$$f_{s1} = k_1(u_1 - z) = k_1 w_1 \quad (2.18)$$

$$f_{s2} = k_2(u_2 - u_1) = k_2(w_2 - w_1) \quad (2.19)$$

$$f_{d1} = c_1(\dot{u}_1 - \dot{z}) = c_1 \dot{w}_1 \quad (2.20)$$

$$f_{d2} = c_2(\dot{u}_2 - \dot{u}_1) = c_2(\dot{w}_2 - \dot{w}_1) \quad (2.21)$$

combined with the Newtons second law give two equation of motions as

$$m_1 \ddot{w}_1 + c_1 \dot{w}_1 + k_1 w_1 - c_2(\dot{w}_2 - \dot{w}_1) - k_2(w_2 - w_1) = -m_1 \ddot{z} \quad (2.22)$$

$$m_2 \ddot{w}_2 + c_2(\dot{w}_2 - \dot{w}_1) + k_2(w_2 - w_1) = p(t) - m_2 \ddot{z} \quad (2.23)$$

Writing Equation 2.22 and 2.23 on matrix form result in Equation 2.24

$$\mathbf{M}\ddot{\mathbf{w}} + \mathbf{C}\dot{\mathbf{w}} + \mathbf{K}\mathbf{w} = \mathbf{p}(t) + \mathbf{p}_{eff}(t), \quad (2.24)$$

where \mathbf{M} is the mass matrix, \mathbf{K} is the stiffness matrix, \mathbf{C} is the viscous damping matrix, $\mathbf{p}_{eff}(t)$ is the effective force vector, $\mathbf{p}(t)$ is the load vector, \mathbf{w} is the relative displacement vector, $\dot{\mathbf{w}}$ is the relative velocity vector and $\ddot{\mathbf{w}}$ is the relative acceleration vector.

$$\mathbf{M} = \begin{bmatrix} m_1 & 0 \\ 0 & m_2 \end{bmatrix} \quad \mathbf{K} = \begin{bmatrix} k_1 + k_2 & -k_2 \\ -k_2 & k_2 \end{bmatrix} \quad \mathbf{C} = \begin{bmatrix} c_1 + c_2 & -c_2 \\ -c_2 & c_2 \end{bmatrix} \quad (2.25)$$

$$\mathbf{p}_{eff}(t) = \begin{Bmatrix} -m_1\ddot{z} \\ -m_2\ddot{z} \end{Bmatrix} \quad \mathbf{p}(t) = \begin{Bmatrix} 0 \\ pt \end{Bmatrix} \quad \mathbf{w} = \begin{Bmatrix} w_1 \\ w_2 \end{Bmatrix} \quad \dot{\mathbf{w}} = \begin{Bmatrix} \dot{w}_1 \\ \dot{w}_2 \end{Bmatrix} \quad \ddot{\mathbf{w}} = \begin{Bmatrix} \ddot{w}_1 \\ \ddot{w}_2 \end{Bmatrix} \quad (2.26)$$

If the base motion is zero the equation of motion in the same manner as shown above becomes

$$\mathbf{M}\ddot{\mathbf{u}} + \mathbf{C}\dot{\mathbf{u}} + \mathbf{K}\mathbf{u} = \mathbf{p}(t). \quad (2.27)$$

2.3.4 Plate elements

There are several ways to model plates in the finite element method. The underlying plate equation can for example be based on Kirchhoff plate theory or Mindlin plate theory. The main difference between the two theories is that Kirchhoff theory makes the assumption that plane sections normal to the mid plane remain plane and normal to the mid-plane during deformation. This is a simplification that correlates well for thin plates at low frequencies and makes the Kirchhoff plate theory rather easy to use and is therefore also the most commonly used plate theory. For thicker plates Mindlin theory, which is a more precise theory, is to prefer (Ottosen and Petersson, 1992).

Several different element types can be used for plate analysis, which one to use depends on the type of analysis concluded. For example, one can use solid elements, shell elements, plates with plain stress or plain strain assumptions and so on.

2.3.5 Mode superposition

The natural eigenfrequencies are solved by looking at an undamped system of free vibration, i.e where $\mathbf{p}(t) = \mathbf{0}$. An example of an equation for such a system is shown in Equation 2.28

$$\mathbf{M}\ddot{\mathbf{u}} + \mathbf{K}\mathbf{u} = \mathbf{0}. \quad (2.28)$$

Assuming harmonic motion $\mathbf{u} = \mathbf{U} \cos(\omega t)$ in Equation 2.28 results in an eigenvalue problem as

$$(\mathbf{K} - \omega^2 \mathbf{M})\mathbf{U} = \mathbf{0} \quad (2.29)$$

where the nontrivial solution, i.e $\mathbf{U} \neq \mathbf{0}$, allows calculation of ω by solving $\det(\mathbf{K} - \omega^2 \mathbf{M}) = 0$. The number of natural eigenfrequencies is the same as the number of free DOF. For each eigenfrequency ω_r there exists an eigenvector ϕ_r with the same length as the number of DOF.

$$\phi_{r,j} = \left\{ \begin{array}{c} \phi_1 \\ \phi_2 \\ \vdots \\ \phi_i \\ \vdots \\ \phi_n \end{array} \right\} \quad (2.30)$$

where $i = 1, 2, \dots, n$ is the number of DOF and $j = 1, 2, \dots, m$ is the mode number. All the eigenvectors creates the eigenmatrix Φ .

$$\Phi = \begin{bmatrix} \phi_{1.1} & \phi_{1.2} & \cdots & \phi_{1.j} & \cdots & \phi_{1.m} \\ \phi_{2.1} & \phi_{2.2} & \cdots & \phi_{2.j} & \cdots & \phi_{2.m} \\ \vdots & \vdots & \ddots & \vdots & \vdots & \vdots \\ \phi_{i.1} & \phi_{i.2} & \cdots & \phi_{i.j} & \cdots & \phi_{i.m} \\ \vdots & \vdots & \vdots & \vdots & \ddots & \vdots \\ \phi_{n.1} & \phi_{n.2} & \cdots & \phi_{n.i} & \cdots & \phi_{n.m} \end{bmatrix} \quad (2.31)$$

To solve the equation of motion for a MDOF-system as Equation 2.27 the whole system needs to be solved simultaneously since the coupled equations are dependant of each other (Craig and Kurdila, 2006). That means that Equations 2.22 and 2.23 needs to be solved simultaneously since they are coupled. If a system consists of a large number of DOF this can be problematic. The mode superposition method is a method which transforms the coupled equations to uncoupled equations by utilising the orthogonality property of the eigenvectors. Introducing the definition of modal mass M_r and modal stiffness K_r , with r and s being natural modes $r \neq s$, as

$$M_r = \phi_r^T \mathbf{M} \phi_r, \quad K_r = \phi_r^T \mathbf{K} \phi_r. \quad (2.32)$$

When $r \neq s$ the modes r and s are orthogonal with respect to the mass and stiffness matrix if $\omega_r \neq \omega_s$, which implies the relation

$$\phi_r^T \mathbf{M} \phi_s = 0, \quad \phi_r^T \mathbf{K} \phi_s = 0. \quad (2.33)$$

Combining the relations of Equations 2.32 and 2.33 can be used to form diagonal mass and stiffness matrices, called the modal mass and modal stiffness matrices as

$$\begin{aligned} \mathbf{M}_m &= \Phi^T \mathbf{M} \Phi = \text{diag}(M_1, M_2, \dots, M_N), \\ \mathbf{K}_m &= \Phi^T \mathbf{K} \Phi = \text{diag}(K_1, K_2, \dots, K_N). \end{aligned} \quad (2.34)$$

The generalised damping matrix C is not necessarily diagonal. However, in order to simplify the damping model it is often times assumed to be diagonal, in which case the modal damping matrix can be formed as

$$\mathbf{C}_m = \mathbf{\Phi}^T \mathbf{C} \mathbf{\Phi} = \text{diag}(C_1, C_2, \dots, C_N). \quad (2.35)$$

The modal mass, stiffness and damping matrices are advantageous due to being diagonal, as the use of them uncouples the equations of motion. In order to use these properties, the principle coordinates $\boldsymbol{\eta}(t)$ are introduced and defined as

$$\mathbf{u}(t) = \mathbf{\Phi} \boldsymbol{\eta}(t). \quad (2.36)$$

Multiplication from the left of $\mathbf{\Phi}^T$ to Equation 2.27 gives

$$\mathbf{\Phi}^T \mathbf{M} \ddot{\mathbf{u}} + \mathbf{\Phi}^T \mathbf{C} \dot{\mathbf{u}} + \mathbf{\Phi}^T \mathbf{K} \mathbf{u} = \mathbf{\Phi}^T \mathbf{p}(t). \quad (2.37)$$

Introducing Equation 2.36 in 2.37 gives

$$\mathbf{M}_m \ddot{\boldsymbol{\eta}} + \mathbf{C}_m \dot{\boldsymbol{\eta}} + \mathbf{K}_m \boldsymbol{\eta} = \mathbf{f}_m \quad (2.38)$$

where \mathbf{M}_m is the modal mass matrix, \mathbf{K}_m is the modal stiffness matrix and \mathbf{C}_m is the generalised damping matrix defined as in Equations 2.34 and 2.35. The vector \mathbf{f}_m is defined as the modal force vector as

$$\mathbf{f}_m = \mathbf{\Phi}^T \mathbf{p}(t), \quad (2.39)$$

2.3.6 Direct integration methods

To obtain the response of an SDOF or MDOF system exposed to more complex loads, numerical solutions are required (Chopra, 2014). Both linear and nonlinear systems can be solved with a time-stepping scheme using time-step Δt . In such a scheme the derivatives appearing in the equation of motion are approximated by numerical integration. There are several different numerical integration methods where this procedure is used, one of which is the Newmark- β method. Newmark- β is an implicit method, meaning that the discretised displacement field u_{i+1} is expressed by the velocity (\dot{u}_{i+1}) and acceleration (\ddot{u}_{i+1}) fields at present times and earlier times. The resulting time scheme at time step $i + 1$ for an SDOF linear system is expressed as

$$m\ddot{u}_{i+1} + c\dot{u}_{i+1} + ku_{i+1} = p_{i+1}. \quad (2.40)$$

In the Newmark β method it is assumed that the displacement vector u_{i+1} and its derivative \dot{u}_{i+1} can be expressed according to Equation 2.41 and 2.42 (Chopra, 2014), the approximately equal sign is used to signify the approximation.

$$\dot{u}_{i+1} \approx \dot{u}_i + (1 - \gamma)\Delta t \ddot{u}_i + (\gamma \Delta t) \ddot{u}_{i+1} \quad (2.41)$$

$$u_{i+1} \approx u_i + \Delta t \dot{u}_i + \left(\frac{1}{2} - \beta\right)(\Delta t)^2 \ddot{u}_i + (\beta(\Delta t)^2) \ddot{u}_{i+1} \quad (2.42)$$

Applying Equation 2.41 and 2.42 in 2.40 gives an equation for \ddot{u}_{i+1} expressed in terms of u_i , \dot{u}_i , \ddot{u}_i and p_{i+1} as

$$\ddot{u}_{i+1} \approx \frac{p_{i+1} - c(\dot{u}_i + ((1 - \gamma)\Delta t)\ddot{u}_i - k(u_i + \Delta t\dot{u}_i + ((0.5 - \beta)(\Delta t)^2)\ddot{u}_i))}{m + c\gamma\Delta t + k\beta(\Delta t)^2} \quad (2.43)$$

With initial conditions $u(0) = u_0$ and $v(0) = \dot{u}_0$ the initial acceleration can be calculated according as

$$\ddot{u}_0 = \frac{p_0 - c\dot{u}_0 - ku_0}{m}. \quad (2.44)$$

With a known force the acceleration can now be solved for $i = 0$ with Equation 2.43. Thereafter the velocity can be calculated with Equation 2.41 and finally the displacement is calculated with Equation 2.42. Then the same calculations are performed iteratively for $i = 1, 2, 3, \dots$

The parameters β and γ control the stability and accuracy. Throughout the study the constant average method, which is a special case of the Newmark- β method with $\beta = \frac{1}{4}$ and $\gamma = \frac{1}{2}$, will be used. This gives an unconditionally stable system, which means that the system will provide a solution independent of the size of the time step used. The results of a unconditionally stable analysis may still be inaccurate if the time step is too large, but there is no stability constraint on the time step which is the case for a conditionally stable analysis. For the constant average method Equations 2.41 and 2.42 become

$$\dot{u}_{i+1} \approx \dot{u}_i + \frac{\Delta t}{2}(\ddot{u}_i + \ddot{u}_{i+1}) \quad (2.45)$$

$$u_{i+1} \approx u_i + \frac{(\Delta t)^2}{4}(\ddot{u}_i + \ddot{u}_{i+1}) \quad (2.46)$$

With initial conditions as described above \ddot{u}_{i+1} can be expressed in terms of u_i , \dot{u}_i , \ddot{u}_i and p_{i+1} as

$$\ddot{u}_{i+1} \approx \frac{p_{i+1} - c(\dot{u}_i + \frac{\Delta t}{2}\ddot{u}_i) - k(u_i + \Delta t\dot{u}_i + \frac{(\Delta t)^2}{4}\ddot{u}_i)}{m + c\frac{\Delta t}{2} + k\frac{(\Delta t)^2}{4}}. \quad (2.47)$$

2.4 Applications of structural dynamics

2.4.1 Orientation

In this section two different types of analyses, THA and RSA are introduced. Additionally, the theory that enables analyses of MDOF-system through the use of modal participation factors and modal combination rules is presented. In the analysis of a structure subjected to vibration, both the total and relative response in terms of

displacement, velocity or acceleration could be of interest depending on the type of structure and type of analysis. It is usually not important in which direction the response maximum will take place, hence the sign preceding the response output is regularly disregarded. Thus the outputs are given as absolute values. Therefore it is the peak values, i.e the absolute maximum values that is of special interest.

2.4.2 Time History Analysis

A SDOF-system subjected to a ground motion will have a response that is dependant on the natural frequency, or natural vibration period, and the damping ratio (Chopra, 2014). In a THA the response for each natural frequency and damping ratio of interest, at each time step over a time period, is calculated. The result is the response as a function of time. To obtain accurate results a sufficiently short time step is required. If an MDOF system is to be analysed a method for modal analysis such as mode superposition, which was described in Chapter 2.3.5, is necessary. Generally a THA results in large quantities of output data and is therefore time consuming to perform. Figure 2.12 shows an example of a ground motion and the associated THA for the vertical DOF of the middle node in a plate. Figure 2.12a shows the ground motion that the plate is subjected to and Figure 2.12b the corresponding THA in form of relative acceleration.

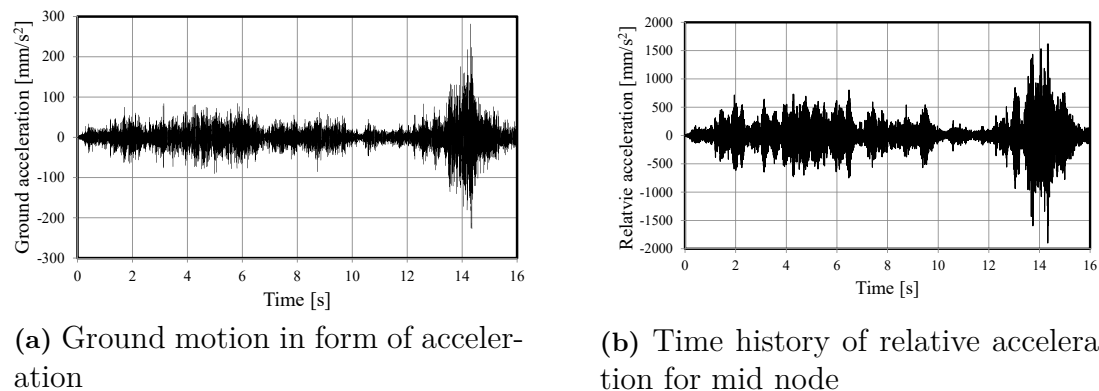


Figure 2.12: Example of ground motion and the associated THA.

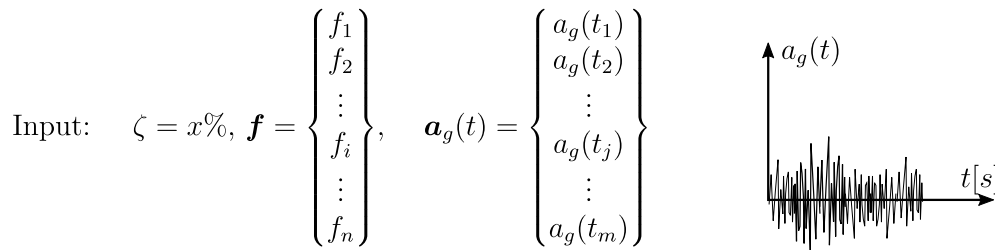
2.4.3 Response Spectrum Analysis

2.4.3.1 Orientation

The following section explains how to perform a complete RSA. It explains calculation of response spectra, calculation of MPF and how to combine the results of the response spectra and MPF using modal combination rules.

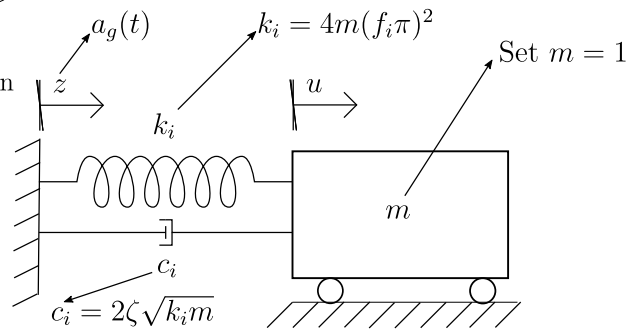
2.4.3.2 Calculation of response spectrum

As mentioned previously, a THA of an MDOF system is time consuming and computationally heavy. In order to save time, one can perform a RSA instead. In order to do a RSA one first needs to create response spectra for acceleration, velocity and displacement. Basically, the procedure is to perform a THA for a SDOF system for one specific natural frequency, a damping ratio ζ and a ground motion signal. From the resulting time history of the relative acceleration, velocity and displacement, the absolute maximum values are extracted and inserted into frequency-response graphs. This procedure is then repeated for a second natural frequency, then a third etc. The iterations continue until the responses have been calculated for the entire frequency range of interest. The basic method is described as a flowchart in Figure 2.13.

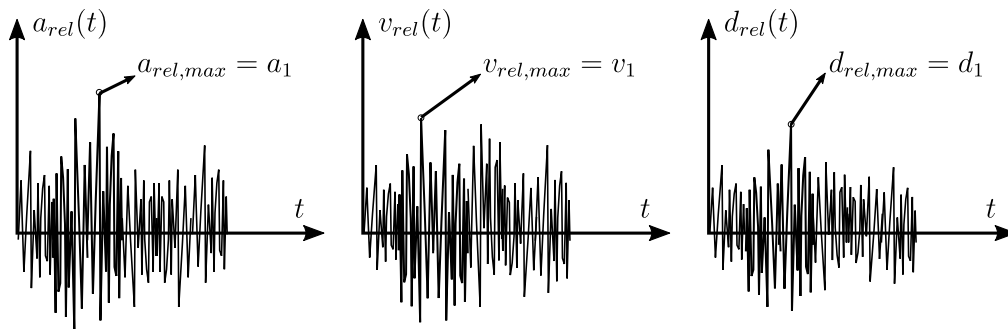


① For $i = 1$

For a SDOF system, solve the equation of motion $m\ddot{w} + c_i\dot{w} + k_iw = -m\ddot{z}$ through numerical integration using Newmark- β



Output from step ① is the relative response for frequency f_1 , extract absolute max values for the response



② Plot the responses against frequency, and repeat from ① for $i = 2 \rightarrow n$

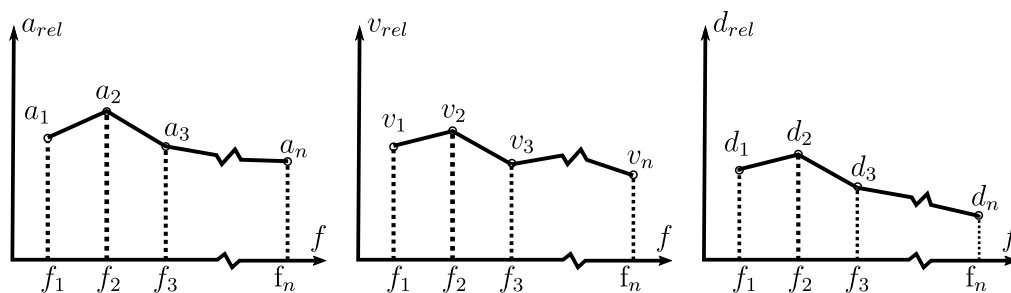


Figure 2.13: Procedure for calculation of response spectra.

The end result of the calculations are the response spectra for acceleration, velocity and displacement. A graph of an acceleration response spectrum can be seen in Figure 2.14

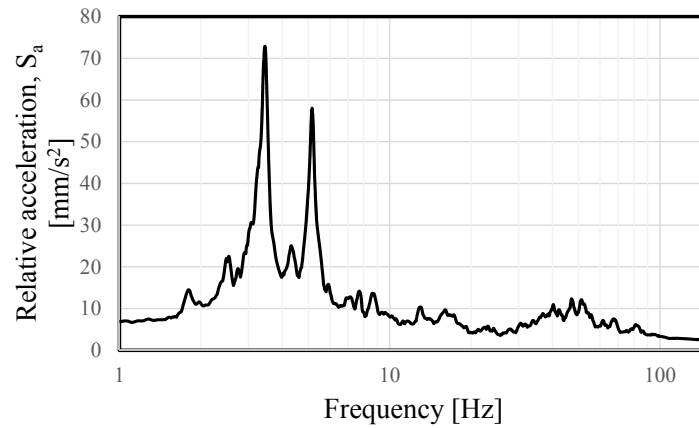


Figure 2.14: Graph of response spectrum with the relative acceleration response for the frequency range 1-200 [Hz].

From a RSA, it is possible to calculate both relative and absolute response, see Section 2.2.4. To distinguish between the values from the response spectrum and the actual response in a MDOF system it is convenient to introduce a notation for the response spectrum values. According to Chopra (2014), the relative displacement spectrum, S_d , the relative velocity spectrum, S_v , and the relative acceleration spectrum, S_a , from the RSA are commonly defined as

$$S_d = u_o(\omega, \zeta) \equiv \max | u(t, \omega, \zeta) |, \quad (2.48a)$$

$$S_v = \dot{u}_o(\omega, \zeta) \equiv \max | \dot{u}(t, \omega, \zeta) |, \quad (2.48b)$$

$$S_a = \ddot{u}_o(\omega, \zeta) \equiv \max | \ddot{u}(t, \omega, \zeta) |, \quad (2.48c)$$

where u , \dot{u} and \ddot{u} is the relative displacement, velocity and acceleration respectively. The absolute response spectra are defined as

$$S_{d.abs} = u_o^t(\omega, \zeta) = \max | u(t, \omega, \zeta) + u_g(t, \omega, \zeta) |, \quad (2.49a)$$

$$S_{v.abs} = \dot{u}_o^t(\omega, \zeta) = \max | \dot{u}(t, \omega, \zeta) + \dot{u}_g(t, \omega, \zeta) |, \quad (2.49b)$$

$$S_{a.abs} = \ddot{u}_o^t(\omega, \zeta) = \max | \ddot{u}(t, \omega, \zeta) + \ddot{u}_g(t, \omega, \zeta) |, \quad (2.49c)$$

where u_g , \dot{u}_g and \ddot{u}_g is the ground displacement, velocity and acceleration respectively. As can be seen in Equations 2.48 to 2.49 the response spectra are independent of time.

2.4.3.3 Spectral displacement, pseudovelocity and pseudoacceleration

In earthquake analysis with response spectra, it is often useful to look at *spectral displacement*, *spectral pseudovelocity* and *spectral pseudoacceleration* (Craig and

Kurdila, 2006). These are defined as

$$S_d(T, \zeta) = w_{max} = \frac{1}{\omega_n} W(t_m), \quad (2.50a)$$

$$S_v(T, \zeta) = W(t_m) = \omega_n S_d, \quad (2.50b)$$

$$S_a(T, \zeta) = \omega_n^2 S_d = \omega_n S_v, \quad (2.50c)$$

$$W(t) = \int_0^t \ddot{z}(\tau) e^{-\zeta \omega_n (t-\tau)} \sin \omega_n (t-\tau) d\tau. \quad (2.50d)$$

Equation 2.50d is the Duhamel integral solution of

$$m\ddot{w} + c\dot{w} + kw = -m\ddot{z} \quad (2.51)$$

which is Equation 2.14 when there is no external force. The study will not utilise this method, but as will be mentioned in the method chapter, ADINA converts between physical quantities using the relations of Equations 2.50a, 2.50b and 2.50c.

2.4.3.4 Modal participation factor

As explained in Section 2.3.5, the superposition method can be used to uncouple the equations of a MDOF-system by introducing principle coordinates and modal matrices. In a similar way the *modal participation factor* is used together with the eigenvectors to obtain the response from all the modes in the MDOF-system. For a system, subjected to a ground motion in form of a single-support excitation and no external force, Equation 2.38 in Section 2.3.5 can be written as

$$\mathbf{M}_m \ddot{\boldsymbol{\eta}} + \mathbf{C}_m \dot{\boldsymbol{\eta}} + \mathbf{K}_m \boldsymbol{\eta} = -\boldsymbol{\phi}^T \mathbf{M} \mathbf{r} \ddot{u}_g \quad (2.52)$$

where \mathbf{r} is the *influence coefficient vector* that relate the relative displacement of a DOF to the base motion (Datta, 2010). The calculation of the influence coefficient vector is explained in Section 2.4.3.5. The influence coefficient vector has the same amount of rows as the number of DOF of the analysed system. The DOF that are in the same direction as the ground motion will cause the corresponding rows of the influence coefficient vector to be equal to one, with all other rows being zero. The influence coefficient vector helps to transform the response of a SDOF-system to the response of a MDOF-system (Pozzi and Der Kiureghian, 2015). The principle coordinates, $\boldsymbol{\eta}$, also called the modal displacement response, allows the relative displacement to be expressed as Equation 2.36. Assuming modal damping, dividing Equation 2.52 with modal mass results in

$$\ddot{\eta}_j + 2\zeta_j \omega_j \dot{\eta}_j + \omega_j^2 \eta_j = -\Gamma_j \ddot{u}_g. \quad (2.53)$$

Γ_j is defined as the modal participation factor (MPF). One MPF exist for each mode j , where $j = 1, 2, \dots, m$. The MPF can be calculated as

$$\Gamma_j = \frac{\boldsymbol{\phi}_j^T \mathbf{M} \mathbf{r}}{\boldsymbol{\phi}_j^T \mathbf{M} \boldsymbol{\phi}_j}. \quad (2.54)$$

Each unique mode has one specific MPF tied to it. The MPF for all modes can be collected in a column vector $\mathbf{\Gamma}$,

$$\mathbf{\Gamma} = \begin{pmatrix} \Gamma_1 \\ \Gamma_2 \\ \vdots \\ \Gamma_j \\ \vdots \\ \Gamma_m \end{pmatrix} \quad (2.55)$$

Equation 2.53 is an uncoupled equation and can be solved as a SDOF-system. The maximum modal displacement for mode j is calculated as

$$\eta_{j.max} = \Gamma_j S_d(\omega_j, \zeta_j). \quad (2.56)$$

Combining Equations 2.56 and 2.36, the relative displacement for a specific mode j and DOF i can be expressed as

$$u_{i.j} = \phi_{i.j} \Gamma_j S_d(\omega_j, \zeta_j). \quad (2.57)$$

In the same way other spectral values can be used to obtain the maximum response for a specific mode and DOF in a MDOF-system. To complete the RSA and get the total response, the response of all the modes in the analysis needs to be combined. This is accomplished with the use of one of the modal combination rules, described in Section 2.4.3.7.

2.4.3.5 Calculation of the influence coefficient vector

The influence coefficient vector was briefly introduced in Section 2.4.3.4. As mentioned, the number of rows of the vector are the same as number of DOF in the system. A common way to reduce the system is to remove the DOFs that are prescribed to zero, most commonly these are the boundary conditions. If so, only the free DOFs are left and the size of the influence coefficient vector is reduced to have the same number of rows as free DOFs. For small systems, the influence coefficient vector can manually be set to one for rows corresponding to DOF that are in the same direction as the ground motion, and zero for the rest. For larger system, manual creation of the influence coefficient vector becomes unmanageable.

Datta (2010) proposes a method to calculate the influence coefficient vector using the stiffness matrix \mathbf{K} . The first step is to decide if some of the DOFs can be condensed out of the analysis. If that is the case, the stiffness matrix is rearranged so that values belonging to the DOFs that should be removed, i.e condensed out, are placed in the lower right. Let c be the notation for condensed-DOFs, d is the notation for number of dynamic-DOFs, equal to the number of remaining DOFs. The rearranged and partitioned stiffness matrix takes the form

$$\mathbf{K} = \begin{bmatrix} \mathbf{K}_{dd} & \mathbf{K}_{dc} \\ \mathbf{K}_{cd} & \mathbf{K}_{cc} \end{bmatrix}. \quad (2.58)$$

\mathbf{K}_{cc} is the matrix consisting of values connected to the DOFs that are condensed out. The condensed stiffness matrix \mathbf{K}_d is then calculated as

$$\mathbf{K}_d = \mathbf{K}_{dd} - \mathbf{K}_{dc}\mathbf{K}_{cc}^{-1}\mathbf{K}_{cd}. \quad (2.59)$$

When the condensed stiffness matrix \mathbf{K}_d is calculated a new rearrangement is performed. The matrix \mathbf{K}_d is rearranged, so the prescribed DOF are at the bottom and free DOF at the top. Let n be equal to the number of free DOF and s equal to the number of prescribed DOF. The values belonging to the prescribed DOF should be placed in the lower right and the partitioning should be

$$\mathbf{K}_d = \begin{bmatrix} \mathbf{K}_{nnd} & \mathbf{K}_{nsd} \\ \mathbf{K}_{snd} & \mathbf{K}_{ssd} \end{bmatrix}. \quad (2.60)$$

\mathbf{K}_{ssd} is the matrix consisting of values belonging to the prescribed DOF and \mathbf{K}_{nnd} is the matrix consisting of values belonging to the remaining free DOF. Now the influence coefficient matrix can be calculated as

$$\mathbf{R} = -\mathbf{K}_{nnd}^{-1}\mathbf{K}_{nsd}. \quad (2.61)$$

The influence coefficient matrix will be of the size $n \times s$, where each row is representing one free DOF. Hence, the number of rows is equal to the number of free DOF. By the same logic, each column is connected to one of the s prescribed DOF. It is now possible to create the influence coefficient vector \mathbf{r} from the influence coefficient matrix \mathbf{R} . By choosing the columns corresponding to prescribed DOF, that are in the same direction as the ground motion that the system is subjected to, and adding them together one obtains the influence coefficient vector.

2.4.3.6 Product of MPF and eigenvector

As explained in Section 2.4.3.4 the MPF is calculated using the influence coefficient vector, mass and stiffness matrix and the eigenvector. Since the MPF is calculated using the eigenvector, the vector norm of the eigenvector will decide the value of the MPF. Effectively this means that the MPF alone can not be compared directly unless the comparison entails MPFs calculated using the same eigenvector norm. For calculations of the actual response the MPF must be multiplied with the eigenvector value corresponding to the node of interest, as can be seen in Equation 2.57. When all the factors have been multiplied the normalisation of the eigenvector does not have an effect on the end result. It should be the same regardless of how the vector is normalised.

2.4.3.7 Modal combination rules

The individual modal responses shown in Section 2.4.3.4 are combined into a total response using one of the modal combination rules (Datta, 2010). There are three

main modal combination rules which are ABSSUM, SRSS and CQC. ABSSUM is short for *absolute sum of maximum values of response*, and as the name indicates the method takes the absolute value for each mode and sums it to get the total response. This results in an upper bound solution since neither the time at which the peak values occur or whether it is a positive or negative value is taken into account in the spectral values as explained in Section 2.4.3. To calculate the total displacement of a certain DOF i , with influence from all m modes, the equation when using ABSSUM is

$$u_{i.max} = \sum_{j=1}^m |u_{i.j}|. \quad (2.62)$$

SRSS is short for *square root of sum of squares* and the method is well suited for structures with outspread natural frequencies (Datta, 2010). Again, assuming response in form of displacement the total displacement for DOF i is

$$u_{i.max} = \sqrt{\sum_{j=1}^m u_{i.j}^2}. \quad (2.63)$$

As can be seen in Equation 2.63 the spectral values are squared before summation and the square root is taken for the summed response to result in the total absolute response.

If the structures has natural frequencies which are not well spread out the CQC rule, *complete quadratic combination*, is better to use (Datta, 2010). CQC is a variant of the SRSS rule, where a second term is added under the square root, compare Equation 2.63 and Equation 2.64. The CQC is calculated as

$$u_{i.max} = \sqrt{\sum_{j=1}^m u_{i.j}^2 + \sum_{j=1}^m \sum_{k=1}^m p_{jk} u_{i.j} u_{i.k}}. \quad (2.64)$$

where both j and k represent the mode number. The second term is only valid for when $j \neq k$. p_{jk} is the correlation coefficient and has a value between 0-1 and Equation 2.65 shows a common definition (Datta, 2010). Through the second term in Equation 2.64, the CQC consider how well the spectral response for different modes correlate, where

$$p_{jk} = \frac{\zeta^2(1 + \beta_{jk})^2}{(1 - \beta_{jk})^2 + 4\zeta^2\beta_{jk}}, \quad \beta = \frac{\omega_j}{\omega_k}. \quad (2.65)$$

According to Chopra (2014), the SRSS and CQC results should be interpreted as a mean of the peak values and are most accurate for ground motion with a smooth response spectrum.

3

Method

3.1 Calculation tools

3.1.1 Orientation

This section describes the functionality and general properties of the tools that is used in the thesis work. The tools consist of MATLAB scripts with functions from the CALFEM package and the commercial software ADINA FEM. For brevity, the MATLAB and CALFEM scripts are referred to as *the MATLAB script*, *the MATLAB program*, *MATLAB* or simply *the script* in the thesis. For the purpose of this thesis a key assumption is that the results from the THA in ADINA is considered as the correct answer in comparisons. Furthermore, a distinction is made between a full RSA and the parts that comprise the RSA. The RSA is the combined results of a MPF analysis and a response spectrum. Some analyses are done on the response spectrum or the MPF separately, while others are done on a full RSA. Hence, when only MPF or response spectra are mentioned, it does not refer to the full RSA, which is the combined results.

3.1.2 MATLAB

3.1.2.1 Description of general properties

The MATLAB script performs dynamic FEM analysis of Kirchhoff plate elements. Some functions from the CALFEM package are used in this script. The plate stiffness and mass matrices used for the analysis were taken explicitly from Szilard (2004). The element type used is *plain stress* 4 node quadrilateral elements with 12 DOF per element. The specifics of the setup is shown in Figure 3.1.

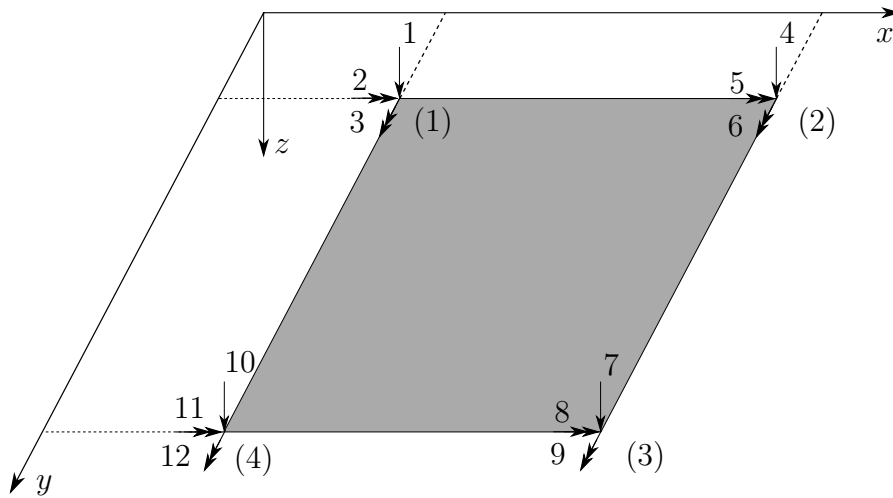


Figure 3.1: Four node rectangular quadrilateral element with three DOF per node, vertical displacement and $x - y$ rotations.

3.1.2.2 Purpose and function of the script

The script serves two primary functions. The first pertaining to calculation of the MPF's and natural frequencies of plates, and the second being calculation of a response spectrum using a ground motion signal as input. The results of these two calculations can then be combined, achieving a RSA for a plate. The MPF calculation is done in accordance with the theory explained in Section 2.4.3.4. This analysis is possible for rectangular plates of any length-width ratio, with three types of boundary conditions in any configuration. The boundary conditions are simply supported (SS), fixed (clamped) and free (unsupported). Element density can be changed, but only functions for an equal number of elements in x and y direction. The output from this calculation are the natural frequencies, eigenvectors and MPFs. Since the complete eigenvectors are calculated and stored in the output, it is possible to study any node of choice.

The calculation of the response spectrum is done in accordance with the Newmark- β method explained in Section 2.3.6. The input consist of a ground motion signal as acceleration, a chosen frequency range to study and general properties such as initial conditions and damping ratio. The output consist of the peak response at each frequency in the provided frequency range, which is the response spectrum as explained in theory Section 2.4.3.

Finally, the script combines the output of the two analysis into the relative response for each mode as per Equation 2.57 and then combine these into the total relative response according to the modal combination rule SRSS, see Equation 2.63.

3.1.3 ADINA

3.1.3.1 Description of general properties

All types of analysis in ADINA are done using four node quadrilateral shell elements with 24 DOF per element. The ADINA shell elements are based on Mindlin plate theory (*ADINA, Theory and Modeling Guide* 2012), which implies that it provides a better description of thick plate behaviour than the MATLAB script. However, for slender plates the results should be similar. The plates are modelled using isotropic linear elastic materials. The analyses that ADINA is used for is development of response spectra, MPF analysis, RSA and THA. For all the analyses in ADINA a damping ratio of 0.02 (2%) is used.

3.1.3.2 Horizontal modes

As mentioned in the previous section ADINA has 24 DOF per four-node element, this includes DOF in-plane of the plate. Consequently, some vibrational modes from ADINA analysis are horizontal/in plane vibration. As the MATLAB script is modelled without in-plane DOF it does not have any horizontal modes. This study omits horizontal vibrations, but the presence of horizontal modes in ADINA has the consequence that its mode numbers are shifted upwards each time a horizontal mode appear. However, this does not affect the vertical response.

3.1.3.3 Generation of response spectrum with ADINA

To generate a response spectrum with ADINA a SDOF system is created by modelling a massless cantilever beam with a large point mass at the free end, see Figure 3.2. The beam model is then subjected to a mass proportional load as a ground acceleration. The model is simulated using a dynamic implicit analysis where the displacement, velocity and acceleration of the point mass as a function of the frequency comprise the response spectra. The response spectra generated in ADINA is used for verification of the response spectra generated in MATLAB.



Figure 3.2: Cantilever beam with point mass, model used for generation of response spectrum in ADINA.

3.1.3.4 MPF with ADINA

A MPF analysis in ADINA is done by choosing *modal participation factors* as analysis type on the model of choice. It calculates the natural frequencies, eigenvectors and MPFs.

3.1.3.5 RSA with ADINA

The RSA in ADINA is done the same way as the MPF analysis, with the difference that a response spectrum needs to be loaded into the post-processing file. Due to how ADINA converts the physical quantities of the output into *pseudoresponse* the inserted response spectrum is required to have the same unit as the desired output. For example, if the response spectrum has the physical quantity acceleration, the relative acceleration output will be calculated numerically. However, the relative velocity and displacement is in fact the *spectral pseudovelocity* and *spectral displacement*, as explained in Section 2.4.3.3. For ADINA RSA, the modal combination rule SRSS (Equation 2.63) is used unless otherwise specified.

3.1.3.6 THA with ADINA

For the THA the ground response as acceleration is inserted as a time function into ADINA. To run a THA in ADINA there are three options: dynamic explicit, dynamic implicit and mode superposition. The mode superposition method, see Section 2.3.5, carries the advantage that the number of modes accounted for in the analysis can be chosen. Since the higher modes have negligible contribution to the total response the mode superposition method is used, which is beneficial for computation time. The results of ADINA THA is the primary tool used to analyse the accuracy of RSA.

3.1.4 Number of elements and convergence

As will be shown in the results in Chapter 4 the mesh size and convergence is a complex matter in this study. Due to this there is no general choice with regards to mesh size and convergence in the method chapter.

3.2 General properties and information with regard to the plate analysis

3.2.1 Orientation

This chapter explains the notations, definitions and general parameters that are used in the plate analyses and the results in Chapter 4. It contains information on the location and names of specific nodes, how plate sides are named, plate properties that are used in all analyses and the ground motions used as loads.

3.2.1.1 Names of the plate sides

For all the plates in the study, the plate sides are denoted as a and b , where a is the length and b is the width, as shown in Figure 3.3.

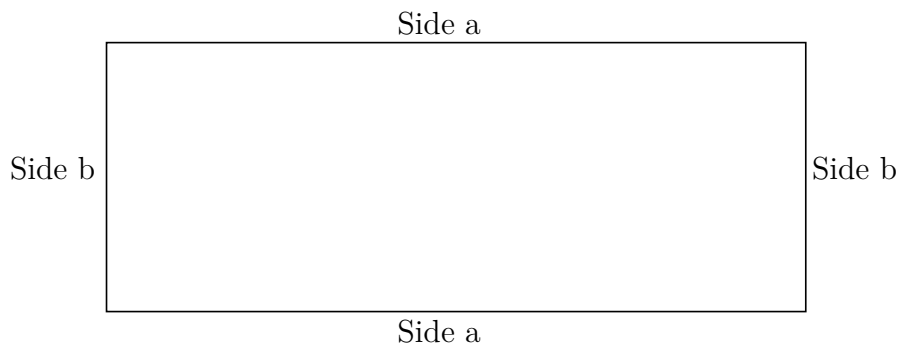


Figure 3.3: Name of the sides of the studied plates.

3.2.1.2 Nodal map and introduction to terminology used in the following chapters

The study is for all cases done for vertical response and unless otherwise specified done by analysis of the response in the centre node, denoted d . The location of the nodes checked and their nomenclature can be seen in Figure 3.4. Many of the analyses includes the product $\phi\Gamma$, where Γ is the MPF and ϕ is a single value from the eigenmatrix which corresponds to a specific DOF and a specific mode. As this factor will be referred to frequently in the thesis, it is given the name *modal contribution*. As an example, the *modal contribution of mode 2 in node c* means the factor $\phi\Gamma$ where Γ is the MPF of Mode 2 and ϕ is the value from the eigenmatrix corresponding to Mode 2 and the vertical DOF in Node c. Graphs with $\phi\Gamma$ on the y -axis will mean vertical modal contribution for centre node, unless otherwise specified.

As will be seen further on in the thesis, there are many natural modes which do not activate when a plate is subjected to a uniform ground motion of the entire plate. This means that for both analyses types there are many modes which will have zero contribution to the response. In order to make for a better reading experience, the term *contributing mode* will be used with reference to modes that have a contribution to the response. For example, when the *second contributing mode* of a plate is mentioned, it will refer to the second natural mode which contributes to the total vertical response. If the plate in question receives contribution to the total response from the natural modes 1, 4, 8 and 16, the first contributing mode is mode 1, the second contributing mode refers to mode 4, and so on.

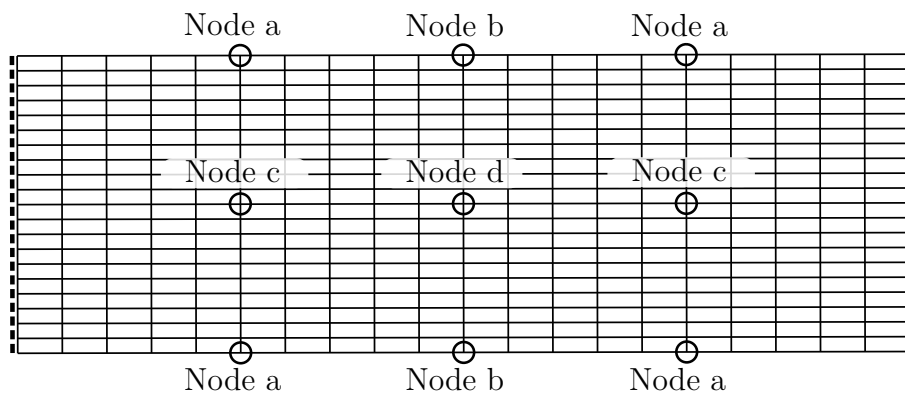


Figure 3.4: Rectangular plate with the node names and positions.

3.2.1.3 Properties in common for all plates

The study entails both quadratic and rectangular plates, which have variable side lengths and in some cases variable thickness. However, all the plates in the study share the properties in Table 3.1. The properties chosen are typical concrete properties.

Table 3.1: Properties used for all the studied plates.

Density [kg/m ³]	Young's modulus [GPa]	Poisson's ratio [-]
2500	30	0.2

3.2.2 Ground motions used as input for the analysis

3.2.2.1 Traffic load 1

The bulk of the analyses are done using the same ground motion. The ground motion is a measurement from a construction site in Halmstad, Sweden. It is the measured ground velocity with respect to time, and the origin of the ground motion is a train

passing near the measurement site. The indata obtained from the measurement is the velocity measured 65000 times in a 16 second period. This signal is converted to acceleration by numerical derivation, due to easier compatibility with the Newmark- β method. The ground motion converted into acceleration can be seen in Figure 3.5. Unless otherwise specified this is the ground motion used for the analyses.

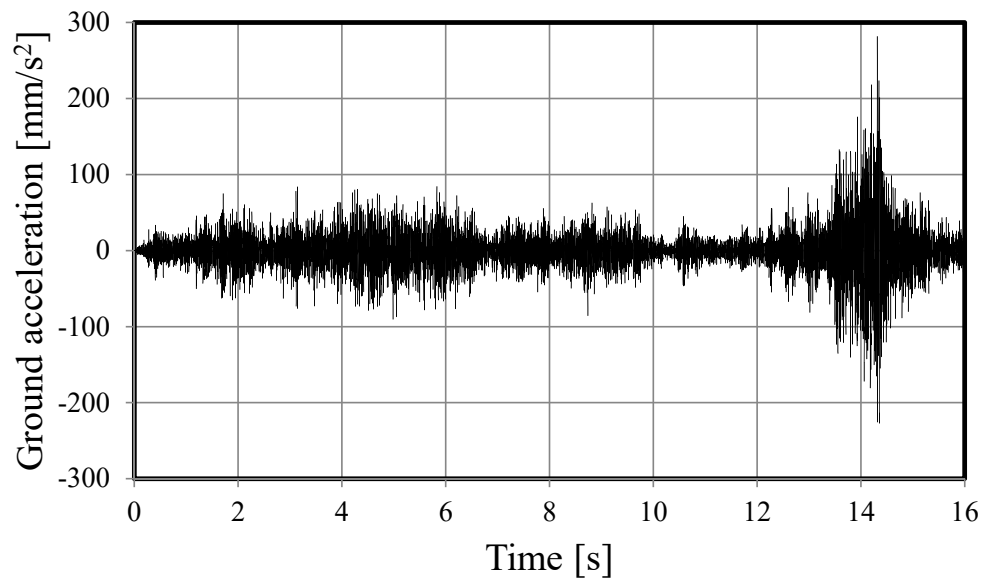


Figure 3.5: Ground acceleration 1. Vibration is the result of a train passage.

3.2.2.2 Traffic load 2

Some plates are analysed with a second ground motion input. The second ground motion is the same as the one used in (Fagerström and Lindorsson, 2017), shown in Figure 3.6.

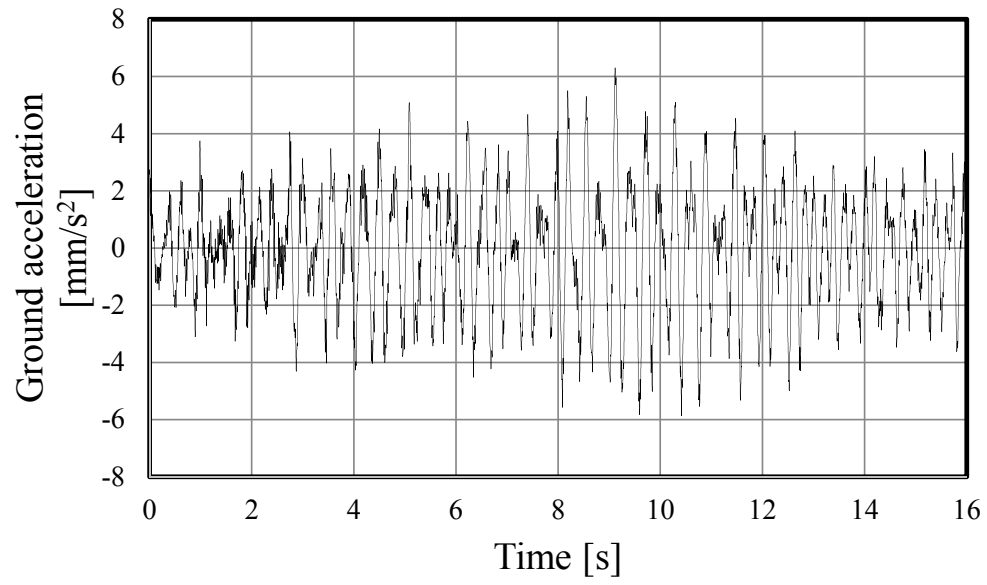


Figure 3.6: Ground acceleration 2.

4

Results

4.1 Orientation

This chapter presents the results of the modal contribution study and the comparative study of RSA and THA for various plates. As will become evident in this chapter the conformity of results between THA and RSA was poor for a handful of plates. For this reason an in-depth analysis of two plates were made and the results are presented in this chapter. Modal contribution was explained in Section 3.2.1.2.

4.2 Study of modal contribution

4.2.1 Orientation

In this section modal contributions calculated with MATLAB are compared with modal contributions calculated with ADINA. This was done in order to verify the results from the MATLAB script with ADINA. An investigation of the relation between plate geometry and modal contribution is performed by studying several quadratic plates with different side lengths and rectangular plates with varying length/width-ratios. The section also includes an investigation into the viability of interpolating modal contribution and eigenfrequencies from data of other plates. Section 4.3 covers a large parameter study of plates with respect to RSA and THA, but parts of that study pertain specifically to the modal contribution, which is presented in this section.

4.2.2 Plates analysed in modal contribution study

4.2.2.1 Geometry of studied quadratic plates

To investigate how the modal contribution correlates with the size of the plate, the modal contribution for seven simply supported quadratic plates was studied. The only difference between the plates is the length of their sides. The Young's modulus, density and Poisson's ratio for the plates are shown in Table 3.1, and the geometry of the plates in Table 4.1. Two analyses were performed for the plates. Analysis 1 was performed with a constant thickness. This led to plate Q1 and Q2 being very thick in relation to their width and length. Analysis 2 was performed with variable thickness of the plates so that the first mode frequency was the same for all plates. The chosen frequency is the first mode frequency for a $5 \times 5 \text{ m}^2$ simply supported plate with thickness 0.2 m , i.e plate Q4 from Table 4.1.

Table 4.1: Geometry of the studied quadratic plates.

Plate	Width [m]	Length [m]	Analysis 1	Analysis 2
			Thickness [m]	Thickness [m]
Q1	1	1	0.2	0.0080
Q2	2	2	0.2	0.0320
Q3	4	4	0.2	0.1280
Q4	5	5	0.2	0.2000
Q5	8	8	0.2	0.5120
Q6	16	16	0.2	2.0480
Q7	32	32	0.2	8.1920

4.2.2.2 Geometry of studied rectangular plates

The modal contribution for six simply supported plates, with varying ratio between the width and length but constant thickness of 0.2 m , was studied to investigate the relation between the modal contribution and the geometry of the plate. Table 4.2 shows the geometry of the plate. The Young's modulus, density and Poisson's ratio for the plates are shown in Table 3.1. The ratios were chosen partly so that there would be considerable difference in stiffness between the smallest and the largest plate, but also so that the plates are mirrored so that the long side is ten, five and two times the length of the short side.

Table 4.2: Geometry of the studied rectangular plates.

Plate	Width [m]	Length [m]	Ratio width/length
R1	5	50	0.1
R2	5	25	0.2
R3	5	10	0.5
R4	5	2.5	2
R5	5	1	5
R6	5	0.5	10

4.2.2.3 Geometry of plates in parameter study

To limit the amount of variables of the studied plates, several properties were kept constant through the parameter study. The Young's modulus, density and Poisson's ratio for the plates are shown in Table 3.1. The thickness of all plates are 0.2 m. Table 4.3 shows the boundary conditions and geometry of the studied plates. Notations for the side of the plates are described in Figure 3.3. All the studied plates have symmetric boundary conditions, i.e opposite sides have the same boundary conditions. The plates are named so that the letter indicates the boundary condition and the number indicates the geometry. Five different boundary conditions and geometries were studied, resulting in a total of 25 plates. However, due to plate type A and B having the same boundary conditions along the entire rim there are 21 unique plates. A schematic figure of the plate types can be seen in Figure 4.1 and the dimensions and BC's of all the plates are shown in Table 4.3.

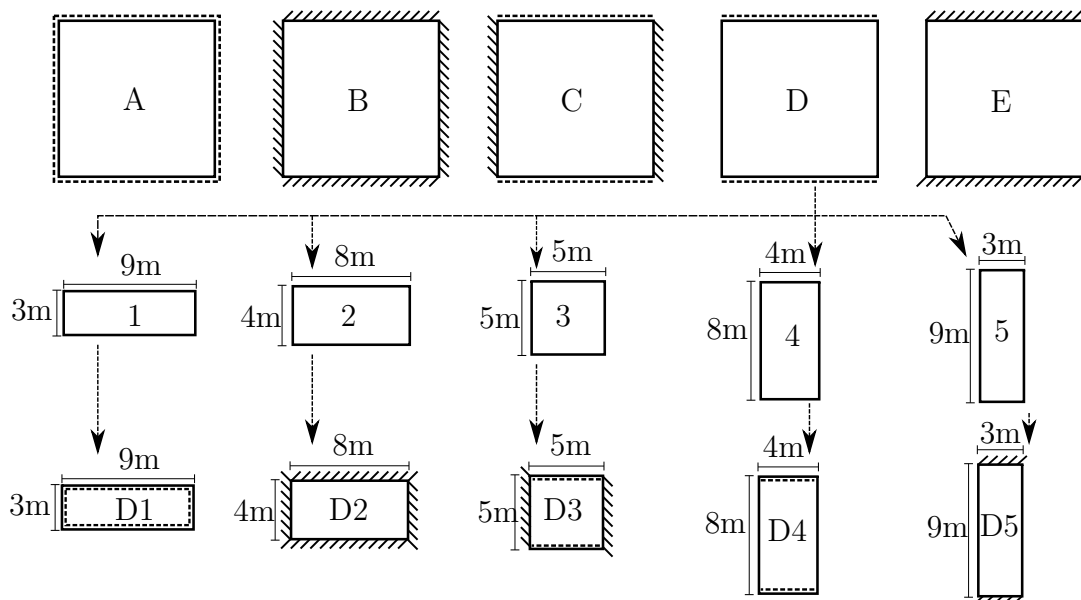


Figure 4.1: Schematic of the different plate types, exemplifying with the dimensions and BCs of plate type D.

Table 4.3: Name and geometry of plates in parameter study. SS is short for simply supported.

Plate	BC		Length [m]	
	Side a	Side b	Side a	Side b
A1	SS	SS	9	3
A2	SS	SS	8	4
A3	SS	SS	5	5
A4	SS	SS	4	8
A5	SS	SS	3	9
B1	Fixed	Fixed	9	3
B2	Fixed	Fixed	8	4
B3	Fixed	Fixed	5	5
B4	Fixed	Fixed	4	8
B5	Fixed	Fixed	3	9
C1	SS	Fixed	9	3
C2	SS	Fixed	8	4
C3	SS	Fixed	5	5
C4	SS	Fixed	4	8
C5	SS	Fixed	3	9
D1	SS	Free	9	3
D2	SS	Free	8	4
D3	SS	Free	5	5
D4	SS	Free	4	8
D5	SS	Free	3	9
E1	Fixed	Free	9	3
E2	Fixed	Free	8	4
E3	Fixed	Free	5	5
E4	Fixed	Free	4	8
E5	Fixed	Free	3	9

4.2.3 Number of elements used in modal contribution study

To verify that the mesh is sufficiently fine in the modal contribution study, a convergence study was performed. As explained in Section 2.4.3.4, the modal contribution is calculated using the influence coefficient vector, mass- and stiffness matrix and the eigenvector. At this stage of the study, it was assumed that the convergence of the modal contribution is closely linked with the convergence of the natural frequencies. Figure 4.2 shows the convergence of the first mode frequency calculated with the MATLAB script. With analytical calculation, using Equation 2.1, the first mode frequency for plate A3/Q4 becomes 25.6 Hz. It can be observed that at around 100 elements the first mode frequency is rather accurate.

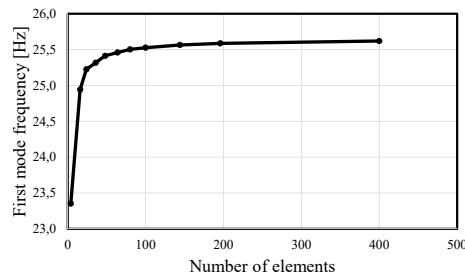


Figure 4.2: Graph of how the first mode frequency of plate A3/Q4 calculated with the MATLAB program converges depending on number of elements.

Figure 4.3 displays how the frequencies for the first 65 modes of plate Q4 calculated with ADINA varies depending on number of elements. Here it can be observed that a 10×10 mesh deviates noticeably from a 20×20 mesh for modes above the tenth mode.

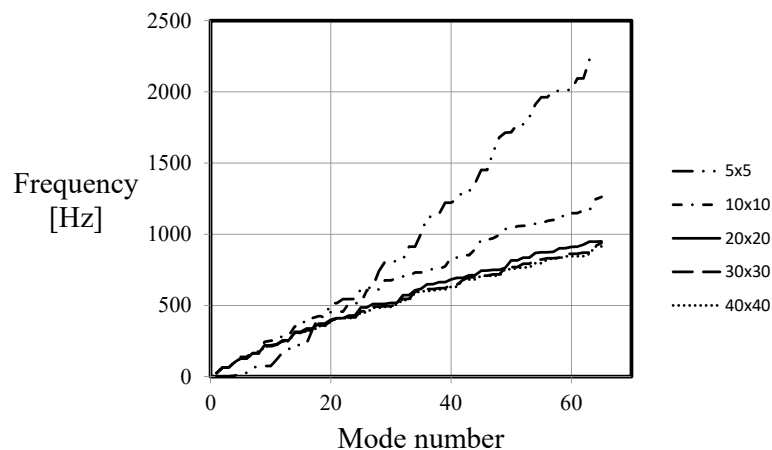


Figure 4.3: Convergence of frequencies calculated with ADINA.

It was decided that for the purpose of the modal contribution study a mesh of 20×20 elements was a fine enough mesh for all the plates in the modal contribution study. Figure 4.4a shows the modal contribution on the vertical mid DOF for plate A1 calculated with a mesh of 20×20 elements and with 30×90 elements. The results are very similar for the first three contributing modes but deviations on the frequency starts to appear after the third contributing mode.

Figure 4.4b shows how the accumulated contribution on the vertical mid DOF is increasing when more modes are included in the analysis. The accumulated contribution is normalised with respect to total contribution, i.e when the graph approaches 1 on the y -axis the total contribution has been reached. The total contribution is referring to the response when all modes used in the plate analysis are included. The two sets of meshes give a slightly different result. With a finer mesh the later modes have slightly more influence, but for both meshes the 15 first modes represent over 95 % of the total contribution. Due to closely spaced frequencies for some modes,

4. Results

the order of where certain modes appear differs between the two sets of meshes, which is the reason the curves in Figure 4.4b increase at different number of modes.

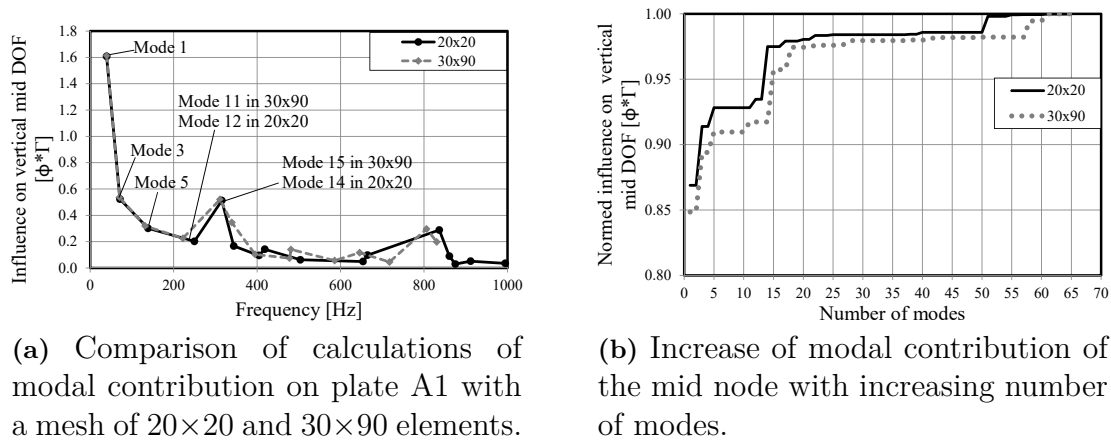


Figure 4.4: Study of the impact on modal contribution with different element sizes

4.2.4 Modal contribution in MATLAB verified with modal contribution in ADINA

Verification of the calculations of the modal contribution obtained with MATLAB was done by comparison with ADINA modal contribution. Figure 4.5 shows the modal contribution for the first 13 contributing modes for the centre node in plate Q4 with a thickness of 0.2 m.

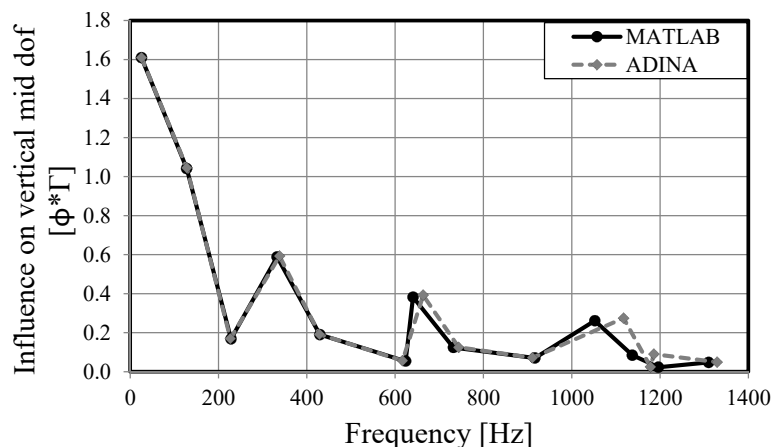


Figure 4.5: Comparison of modal contribution calculated with MATLAB and ADINA for plate Q4 with thickness of 0.2 m and 400 elements.

The results conform well between MATLAB and ADINA for the first 5 contributing modes. For the higher modes a frequency difference start to appear, but the modal contribution is similar. In Table 4.4 the numerical values from the same comparison

as shown in Figure 4.5 are displayed. The modal contribution is described quite well up to frequencies of 600 Hz, and is comparatively low for frequencies exceeding that value. Consequently, the results were considered to be of sufficient accuracy since the principal load used for this thesis has a negligible response for frequencies that high.

Table 4.4: Comparison of frequency and modal contribution from MATLAB and ADINA for plate Q4 with thickness of 0.2 m and 400 elements.

ADINA Frequency	MATLAB Frequency	Difference [%] Frequency	ADINA $\phi\Gamma$	MATLAB $\phi\Gamma$	Difference [%] $\phi\Gamma$
25.57	25.62	-0.20	1.61	1.61	0.06
128.38	127.98	0.31	-1.04	-1.04	0.28
227.06	228.40	-0.59	0.17	0.17	0.63
338.26	332.79	1.62	0.59	0.59	0.74
428.87	429.52	-0.15	-0.19	-0.19	0.54
616.75	623.69	-1.12	0.06	0.05	3.96
663.64	640.47	3.49	-0.39	-0.38	2.42
743.97	732.02	1.61	0.13	0.12	0.88
911.05	916.54	-0.60	-0.07	-0.07	1.93
1117.44	1052.18	5.84	0.27	0.26	4.89
1178.29	1137.38	3.47	0.02	-0.08	439.05
1185.98	1196.34	-0.87	-0.09	0.02	125.55
1329.32	1310.16	1.44	0.05	0.05	2.17

4.2.5 Results from the study of modal contribution

4.2.5.1 Study of modal contribution for quadratic plates

To further verify the modal contribution calculated with MATLAB, the first mode frequency and the modal contribution for the seven quadratic plates were calculated in ADINA and compared with MATLAB.

The geometry of the studied plates are described in Table 4.1. The first frequency mode was calculated with analytic formulas, see Equation 2.1, and with ADINA and MATLAB. As described in Section 4.2.2.1 an analysis using constant thickness for the seven plates was performed. Table 4.5 shows the first mode frequency and Table 4.6 shows the modal contribution for Analysis 1.

Table 4.5: Comparison of the first mode frequency calculated analytically, and with ADINA and MATLAB.

Analysis 1	First mode frequency [Hz]			Difference [%] ADINA vs MATLAB
	Analytical value	ADINA	MATLAB	
Q1	640.95	580.17	640.49	-10.40
Q2	160.24	155.99	160.12	-2.65
Q3	40.06	39.84	40.03	-0.48
Q4	25.64	25.57	25.62	-0.20
Q5	10.01	10.02	10.01	0.14
Q6	2.50	2.51	2.50	0.33
Q7	0.63	0.63	0.63	0.38

Table 4.6: Comparison of modal contribution of the first mode calculated with ADINA and MATLAB.

Analysis 1	$\phi\Gamma$		Difference [%]
	ADINA	MATLAB	
Q1	1.5380	1.6092	-4.63
Q2	1.5900	1.6092	-1.21
Q3	1.6078	1.6092	-0.09
Q4	1.6101	1.6092	0.06
Q5	1.6127	1.6092	0.22
Q6	1.6140	1.6092	0.30
Q7	1.6144	1.6092	0.32

The results for plate Q3-Q7 present similar values but for plate Q2 and especially Q1 the difference is larger. Since the thickness for the plates are kept constant, plates with short sides, as Q1 and Q2, are thicker relative to their sides which is likely to be the cause of the discrepancy. Both MATLAB and the analytical formula applies Kirchhoff (slender) plate theory, while ADINA shell elements apply Mindlin plate theory, which is more suitable for thick plates. It is likely that plates Q1 and Q2 fell into the region of thick plates, and should therefore be calculated with Mindlin theory.

To avoid the thick plates resulting from the constant thickness, a second analysis was performed. For Analysis 2 the plate thicknesses are varied so the first mode frequency is constant. The chosen frequency is the first mode frequency for plate Q4. Table 4.1 shows the thicknesses of the plates for Analysis 2 and Table 4.7 shows the frequencies calculated analytically, with ADINA and with MATLAB. Table 4.8 shows the modal contribution for the first mode in the centre node for Analysis 2.

Table 4.7: Comparison of the first mode frequency calculated analytically, and with ADINA and MATLAB.

Analysis 2	First mode frequency [Hz]			Difference [%] ADINA vs MATLAB
	Analytical value	Adina	MATLAB	
Q1	25.6380	25.7147	25.6195	0.37
Q2	25.6380	25.6932	25.6195	0.29
Q3	25.6380	25.6190	25.6195	0.00
Q4	25.6380	25.5695	25.6195	-0.20
Q5	25.6380	25.3749	25.6195	-0.96
Q6	25.6380	24.5419	25.6195	-4.39
Q7	25.6380	22.0250	25.6195	-16.32

Table 4.8: Comparison of the modal contribution calculated with ADINA and MATLAB.

Analysis 2	$\phi\Gamma$		Difference [%]
Plate	ADINA	MATLAB	
Q1	1.6143	1.6092	0.32
Q2	1.6138	1.6092	0.28
Q3	1.6117	1.6092	0.15
Q4	1.6101	1.6092	0.06
Q5	1.6038	1.6092	-0.34
Q6	1.5766	1.6092	-2.07
Q7	1.5092	1.6092	-6.63

As can be seen in Tables 4.7 and 4.8 the frequencies and modal contributions for plate Q1 to Q7 are practically constant for MATLAB and the analytical frequency calculation. ADINA has a small difference that increases for the thicker plates. Again, the reason could be that ADINA applies Mindlin theory, since plates Q6 and Q7 which have the largest divergence are very thick.

From the two analyses of the square plates it seems as if the frequencies and modal contribution calculated with MATLAB are reliable, assuming that the calculations are limited to slender plates. Plates Q1 and Q2 for Analysis 1, and plates Q6 and Q7 for analysis 2 have extreme geometries that are very unlikely to appear in a real plate in a building. The rest of the study analyses plates that can comfortably be categorised as slender plates, hence Kirchhoff plate theory should suffice well.

If the thick plates are disregarded from both analyses, the results of the quadratic plate analysis indicate that the modal contribution is independent of the size of the plate as long as the boundary conditions are constant.

4.2.5.2 Study of modal contribution for rectangular plates

To further investigate the relation between modal contribution and the geometry of the plate, six simply supported rectangular plates with varying ratio between the length and width were studied. Table 4.2 shows the geometry of the plates and Table 4.9 shows the modal contribution of the first five contributing modes calculated with MATLAB.

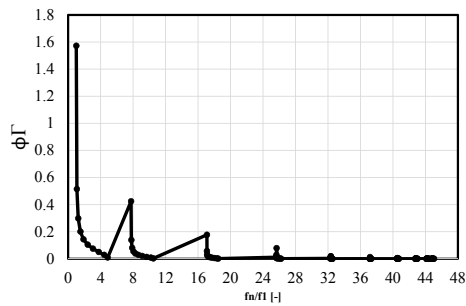
Table 4.9: Modal contribution of the first five contributing modes on the centre node for 6 rectangular plates calculated with MATLAB.

Plate	$\phi\Gamma_1$	$\phi\Gamma_2$	$\phi\Gamma_3$	$\phi\Gamma_4$	$\phi\Gamma_5$
R1	1.57	0.51	0.30	0.20	0.14
R2	1.60	0.52	0.30	0.20	0.14
R3	1.61	0.52	0.30	0.51	0.17
R4	1.61	0.52	0.30	0.51	0.17
R5	1.60	0.52	0.30	0.20	0.14
R6	1.57	0.51	0.30	0.20	0.14

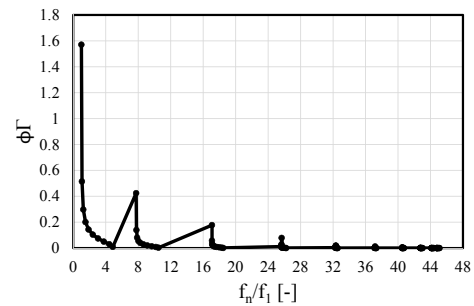
The modal contribution changes marginally with changing length/width ratio, but

the mirrored plates have the same modal contribution. Since the natural frequencies are different for the mirrored plates, it implies that the natural frequencies does not affect the modal contribution.

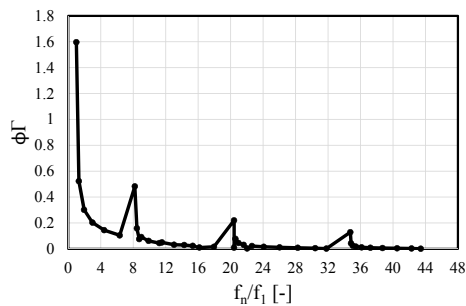
In Figure 4.6 the modal contribution for the plates in Table 4.2 have been plotted against frequency normalised with respect to the first mode frequency. Modes with up to 45 times as high frequency as the first mode frequency have been included. Again, it can be observed that the value of the modal contributions are the same for the mirrored plates and that the modes are located at the same normalised frequency. In other words, two plates with the same boundary conditions along the entire rim will have identical looking graphs if the plates have the same length/width ratio and the frequency axis is normalised with respect to the first mode frequency. Another important observation is that for plates that do not have the same length/width ratio the natural frequencies of certain modes can change significantly.



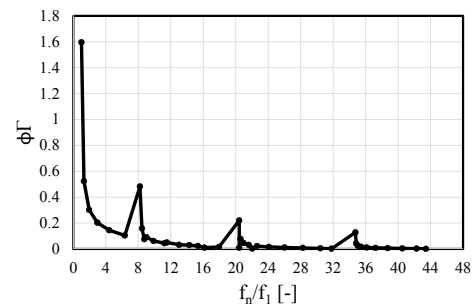
(a) Plate R1, with ratio 0.1.



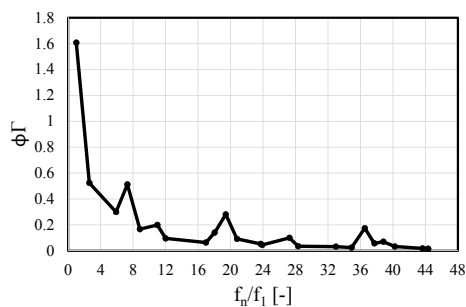
(b) Plate R6, with ratio 10.



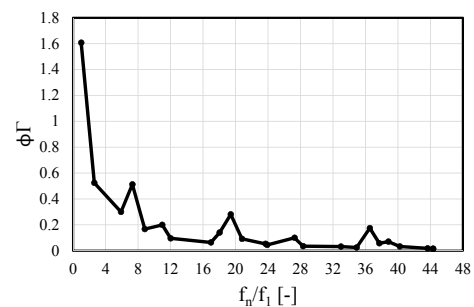
(c) Plate R2, with ratio 0.2.



(d) Plate R5, with ratio 5.



(e) Plate R3, with ratio 0.5.



(f) Plate R4, with ratio 2.

Figure 4.6: Modal contribution plotted in relation to frequency which has been normalised with the first mode frequency of the plate. For clarity, modal contributions smaller than 10^{-9} are not shown in the graph. Calculations were performed with MATLAB

4.2.5.3 Study of possibilities for interpolation of modal contribution for different plates

To investigate if the modal contributions for a plate can be interpolated from the modal contribution for similar plates, plate A1 was used. Two additional plates based on A1 were added, with the same length but the width was changed from 3 to 4 and 5 m respectively, resulting in three plates with the same length and fairly close width. The modal contribution for the three plates were studied. Figure 4.7 shows the modal contribution on the vertical centre node for the three plates plotted against the frequency normalised with respect to the first mode frequency.

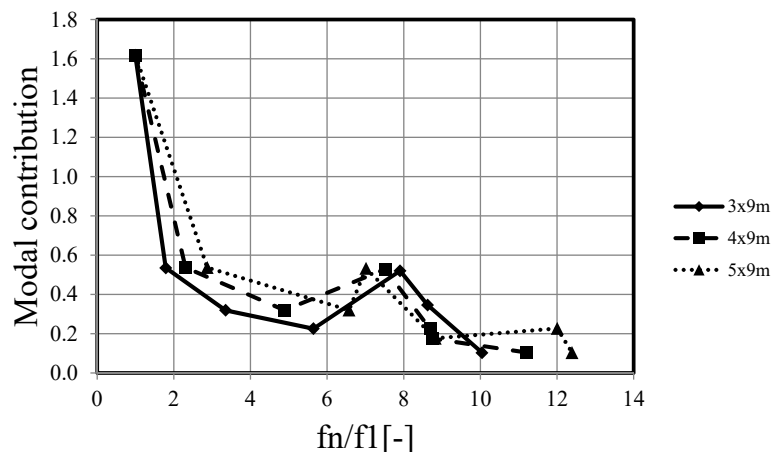


Figure 4.7: Modal contribution on vertical mid DOF plotted in relation to normalised frequency.

There is a clear pattern and regularity in the behaviour for the first three contributing modes. For these modes the modal contribution is of the same magnitude, and the normalised frequency for the plate with dimension $4 \times 9 \text{ m}^2$ lies between the two other plates. For higher modes the plates start to behave differently, and as was observed in Section 4.2.4, this can be caused by insufficient mesh density. However, the discrepancy that appears on the higher modes can also be a result of modes "switching" place when the stiffness and mass conditions change. This phenomenon makes interpolation risky, because the difference in stiffness and mass between two plates can significantly change at which frequency a mode with large modal contribution appears. Interpolating the first few contributing modes between plates that are more or less identical with only one geometric parameter differing slightly will probably result in a decent approximation, but the usefulness of that option is fairly limited.

4.2.5.4 Study of modal contribution for plates in Parameter study

The modal contributions were calculated for the plates presented in Section 4.2.2.3. The results are presented in form of graphs similar to the one in Figure 4.5 and

are found in Appendix A. The study shows that there are similarities to be found for the modal contribution between similar plate geometries and BC's. The modal contributions of the first mode for plates with the same boundary conditions typically have similar magnitude. However, the similarities beyond that are few, and its clearly difficult to recognise patterns.

4.3 Comparison of THA and RSA

4.3.1 Orientation

In this section the comparative study of THA and RSA is presented. It includes comparison of response spectra calculated in ADINA and MATLAB and comparison of a complete RSA performed in ADINA and MATLAB. The parameter study of 21 plates where the maximum responses were calculated with RSA and then compared with THA is also covered here. The maximum response was calculated in terms of relative acceleration, velocity and displacement. During the parameter study it was discovered that the RSA for some plates needed a rather fine mesh resulting in MATLAB calculations being very time consuming. Therefore it was decided to perform the RSA with ADINA in the parameter study to be able to obtain converged results quicker than what would have been possible with MATLAB. However, the parameter study from the coarse mesh provided interesting insight into the convergence behaviour when compared with the parameter study using fine mesh, which is why it is kept here.

4.3.2 Geometry of studied plates in parameter study

The parameter study with comparison between RSA and THA are performed for the plates described in Section 4.2.2.3. A modal damping of 2 % was used when calculating the response spectrum in all analyses.

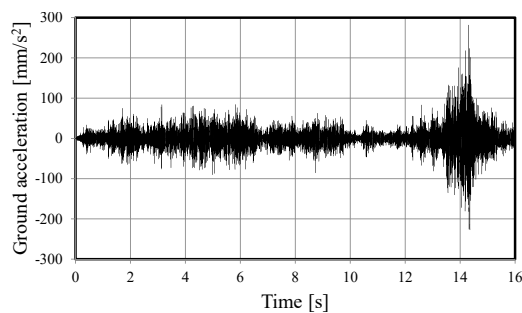
4.3.3 Initial number of elements used in parameter study

Performing a THA is very time consuming, and the time required to complete an analysis increases dramatically as the number of elements increase. The aim of the comparison is to investigate how well the results of the RSA match the results of the THA. Hence, the actual magnitudes of the calculated responses are of lesser importance. After consideration of the time required to perform a THA and the number of plates which would be analysed, it was decided that the 20×20 mesh used for the modal contribution study would be sufficient, see Section 4.2.3.

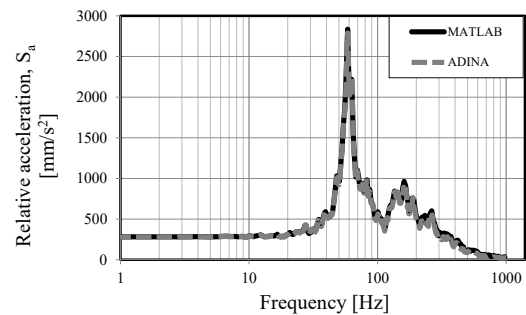
4.3.4 Verification of response spectrum calculated with ground motion from Traffic load 1

To verify the response spectrum calculated with MATLAB a response spectrum was created with ADINA as described in Section 3.1.3.3. Figure 4.8 shows the response spectra calculated with ADINA and MATLAB. The two different spectra show good conformity, thus the calculation of the response spectra are considered reliable.

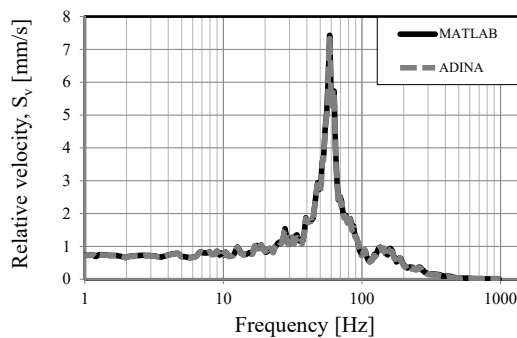
In Figure 4.8a Traffic load 1 is shown. The original time step for the measured traffic load was 2.44×10^{-4} seconds and with time period of about 16 seconds resulting in over 65600 time steps. To decrease the time required for the calculations it was decided to remove two thirds of the original time history and thereby reduce the amount of time steps to 21870, with a time step of 7.32×10^{-4} seconds. A THA and RSA were performed with both the original and the reduced traffic load for a plate. The results obtained were the same for the two traffic loads and therefore the reduced traffic load was assumed to be reliable.



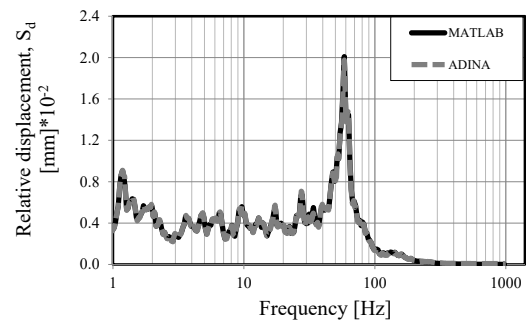
(a) Input data for the response spectrum in form of ground acceleration.



(b) Response spectrum, relative acceleration.



(c) Response spectrum, relative velocity.



(d) Response spectrum, relative displacement.

Figure 4.8: Response spectrum calculated with ADINA and MATLAB in form of relative responses based on ground acceleration.

4.3.5 RSA with MATLAB verified through RSA with ADINA

In Section 4.2.5.1 and 4.2.5.2 the results of the modal contribution calculated with MATLAB conform well with modal contribution calculated with ADINA. The next step in a RSA is to combine the modal contribution with the response spectrum as shown in Equation 2.57. To obtain the total response, the single responses are combined into the total response using one of the modal combination rules described in Chapter 2.4.3.7, for the parameter study SRSS (Equation 2.63) was used.

To verify the RSA calculated with MATLAB, plates A3 and D5 from Table 4.3 were studied. The response spectrum calculated with MATLAB was loaded into the post-processing file of a Modal participation analysis in ADINA, and the total response is the result. The modal damping used was set to 2 % and the modal combination rule SRSS was used in both ADINA and MATLAB. Since the purpose of this study was to confirm the RSA calculations, a mesh of 20x20 elements was used to limit the calculation time with the MATLAB program. Table 4.10 shows the total relative acceleration, velocity, displacement and first mode frequency calculated with both MATLAB and ADINA. The results conform well and the largest deviation is 1.87 %. The results indicate that the calculations done in MATLAB are reliable. The small deviation could be explained by the small frequency offset that was observed in Section 4.2.4.

Table 4.10: Comparison of RSA calculated with MATLAB and ADINA. The responses at the centre of the plates is compared.

	Plate A3			Plate D5		
	MATLAB	ADINA	Difference [%]	MATLAB	ADINA	Difference [%]
a_{rel} [mm/s ²]	922	909	-1.42	431	423	-1.87
v_{rel} [mm/s] $\times 10^{-1}$	19.77	19.80	0.13	10.48	10.47	-0.05
d_{rel} [mm] $\times 10^{-4}$	77.98	77.21	-1.00	51.45	52.22	1.47
First mode frequency [Hz]	25.62	25.57	-0.20	3.89	3.90	0.10

4.3.6 Parameter study of THA compared with RSA using coarse mesh

The differences between the relative acceleration, relative velocity and relative displacement from THA and RSA for the plates in the parameter study using a coarse mesh are displayed in Table 4.11. The complete results from the comparison of THA and RSA using a coarse mesh can be seen in Appendix B.

Table 4.11: Comparison of responses with RSA and THA with coarse mesh

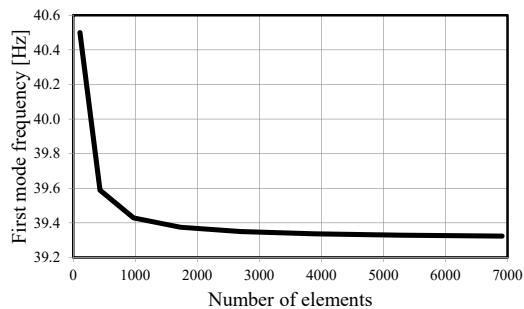
Plate	Difference [%]		
	a_{rel}	v_{rel}	d_{rel}
A1/A5	16.46	2.44	12.38
A2/A4	16.71	18.26	21.26
A3	6.39	17.75	-1.78
B1/B5	7.97	4.03	6.34
B2/B4	8.05	9.42	4.80
B3	-4.35	1.41	-1.86
C1	23.83	18.65	19.73
C2	-0.22	18.79	0.10
C3	3.36	15.96	5.23
C4	10.41	14.41	13.09
C5	-0.72	-4.34	-2.76
D1	3.09	10.18	2.78
D2	-1.18	3.65	5.08
D3	8.87	7.64	4.95
D4	-64.43	-86.32	-24.35
D5	-72.17	-89.60	-16.07
E1	21.82	26.64	29.24
E2	22.35	20.73	19.16
E3	21.95	13.66	7.54
E4	18.75	16.95	22.65
E5	-57.04	-48.24	-10.60

There is a large spread in difference between THA and RSA for the three responses in all plates. For the relative displacement the difference varies from THA being 29.24 % larger than the RSA to 24.24 % smaller. For the relative velocity the same spread is from 28.73 % greater to 89.60 % smaller and for the relative acceleration 22.35 % greater to 72.17 % smaller. Due to the large spread and the substantial inaccuracy of some plates it was decided to perform another convergence study.

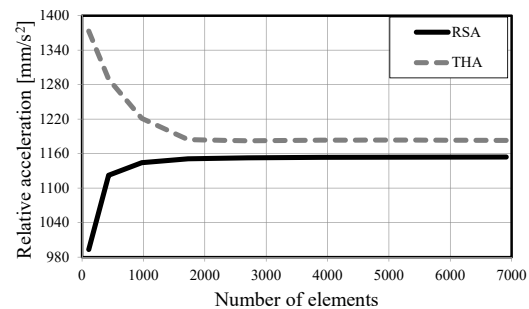
4.3.7 Refined mesh in parameter study

The parameter study covered in Section 4.3.6 revealed a large spread in the conformity between THA and RSA. The only obvious observation that could be made was that the beam-like plates D4, D5 and E5 stood out with significant deviation between the analysis types. Some sample analyses with finer meshes were done for a few plates at this point, including D5. Some plates changed significantly with finer mesh, while others did not. It was decided to perform a convergence study for one of the plates that seemed to be very sensitive with respect to mesh refinement. The plate of choice was A1, which has the dimensions 3×9 m and is simply supported on all edges. The convergence study started at a mesh of 6×18 elements for the short and long side, respectively. Each subsequent analysis added 6 and 18 elements up until a mesh of 48×144 elements for the last analysis. The convergence of the first

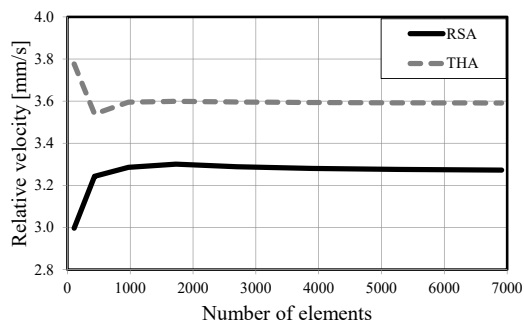
mode frequency and the response in form of the relative acceleration, velocity and displacement were studied and are shown in Figure 4.9.



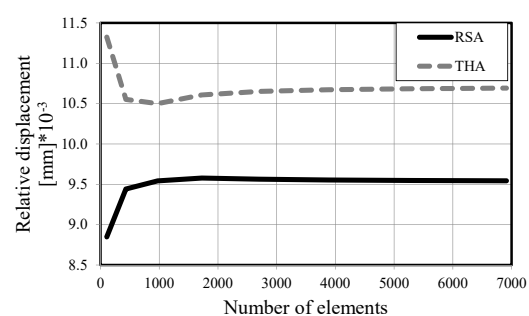
(a) Convergence of first mode frequency.



(b) Convergence of relative acceleration.



(c) Convergence of relative velocity.



(d) Convergence of relative displacement.

Figure 4.9: Convergence study of the first mode frequency and responses with RSA and THA for plate A1/A5.

Unlike the 5×5 simply supported plate in Section 4.2, plate A1 needs more than 400 elements to reach convergence for all four studied quantities, especially for THA and particularly for acceleration in THA. However, it can also be noted that the difference between the converged and non-converged results are rather small with respect to frequency. The first mode frequency only differs about 0.2 Hz and therefore a modal contribution study seems not to be as sensitive to the mesh size.

It can be observed that the convergence differs slightly between the different responses, and displacement seems to require more elements. From Figure 4.9 it becomes clear that the THA and RSA does not converge towards the same value. RSA is an approximate method and therefore it is not expected that the THA and RSA will yield the exact same response. Furthermore, THA and RSA converge from different directions, and also seems to change direction slightly as more elements are added.

As mentioned previously, a THA is very time consuming when using a large number of elements. Therefore, it was decided that a mesh of 30×90 elements, i.e 2700 elements, gave a good enough result for plate A1 both with THA and RSA.

Plate A1 has the dimension of 3×9 meters and a mesh of 30×90 elements results in 10 cm^2 quadratic elements. This value was chosen as the updated mesh size for the parameter study. Since different plates seem to require very different mesh densities, it would have been preferable to complete convergence studies for each plate in the parameter study using both RSA and THA. However, such a convergence study would have been extremely time consuming to complete. Knowing that it might not be sufficient for all the plates in the parameter study, it was decided that an element size of 10 cm^2 should be used.

4.3.8 Parameter study of THA compared with RSA using refined mesh

4.3.8.1 Orientation

This sections covers the results from the parameter study of the 21 plates using the 10 cm^2 mesh mentioned in the previous section. The results for each type of plate A, B, C, D and E are handled in separate sections. The results are given as response of the vertical mid DOF in terms of relative acceleration, velocity and displacement, and the difference between the THA and RSA. In Section 4.3.8.7 the difference of all plates in the parameter study are shown and analysed.

4.3.8.2 Plate type A

Table 4.12 shows the responses of the vertical mid DOF for the plates of type A. Due to symmetry plate A1 is equal to A5 and A2 is equal to A4, which is why A4 and A5 are omitted. The responses obtained with RSA are consistently larger than the responses of THA. There is a noticeably large spread in results between THA and RSA, ranging from 2.49 % to 28.49 % difference.

Table 4.12: Comparison of response with THA and RSA in the plates of type A.

	$a_{rel} [\text{mm/s}^2]$		Difference	$v_{rel} [\text{mm/s}] \times 10^{-1}$		Difference	$d_{rel} [\text{mm}] \times 10^{-3}$		Difference
	RSA	THA	[%]	RSA	THA	[%]	RSA	THA	[%]
A1/A5	1153	1182	2.49	32.89	35.96	8.55	9.56	10.65	10.21
A2/A4	1117	1291	13.46	28.29	37.78	25.12	8.84	12.37	28.49
A3	931	970	3.96	19.55	24.19	19.21	7.75	8.08	4.13

4.3.8.3 Plate type B

Table 4.13 shows the responses of the vertical mid DOF for the plates of type B. Again, for symmetry reasons plates B4 and B5 are omitted. Overall, the plates of type B show fairly good conformity between the THA and RSA for all three

responses. The largest deviation is 8.08 %. The THA has larger responses than the RSA for plate B2/B4 and B3. For plate B1/B5 the relative acceleration is greater for THA while the relative velocity and relative displacement is larger with RSA.

Table 4.13: Comparison of response with THA and RSA in the plates of type B.

	a_{rel} [mm/s ²]		Difference	v_{rel} [mm/s] $\times 10^{-1}$		Difference	d_{rel} [mm] $\times 10^{-3}$		Difference
	RSA	THA	[%]	RSA	THA	[%]	RSA	THA	[%]
B1/B5	1697	1754	3.27	31.67	30.85	-2.68	6.73	6.31	-6.62
B2/B4	1802	1805	0.17	47.80	52.00	8.08	13.87	14.38	3.51
B3	1758	1897	7.31	42.96	45.54	5.67	12.72	13.14	3.25

4.3.8.4 Plate type C

Table 4.14 shows the responses of the vertical mid DOF for the plates of type C. The largest difference for plate type C is 13.89 %. Generally the conformity between the THA and RSA is fairly good for all three responses. The THA has higher response than RSA for plate C1 and C4. For plate C5 the relative displacement is the only quantity higher for THA than RSA. For plate C2 and C3 the relative velocity and relative acceleration is higher for THA.

Table 4.14: Comparison of response with THA and RSA in the plates of type C.

	a_{rel} [mm/s ²]		Difference	v_{rel} [mm/s] $\times 10^{-1}$		Difference	d_{rel} [mm] $\times 10^{-3}$		Difference
	RSA	THA	[%]	RSA	THA	[%]	RSA	THA	[%]
C1	1060	1195	11.26	30.92	34.93	11.49	9.07	10.40	12.80
C2	1038	1018	-2.01	27.20	29.20	6.87	11.34	13.17	13.89
C3	1080	1059	-1.95	21.04	23.68	11.16	6.74	6.90	2.32
C4	1783	2045	12.81	49.26	55.63	11.46	14.83	16.88	12.12
C5	1613	1557	-3.58	31.05	29.74	-4.39	6.78	6.30	-7.74

4.3.8.5 Plate type D

Table 4.15 shows the responses of the vertical mid DOF for the plates of type D. The plates of type D show a very large spread in conformity of results. Plates D1, D2 and D3 show good conformity while plate D4 and D5 present a very large disparity between THA and RSA. Besides the relative acceleration of plate D3, plates D1, D2 and D3 have higher responses with THA. The largest difference for plate D1, D2 and D3 is 14.60 %. For plate D4 and D5 all the responses are higher for RSA and the largest difference is 100 %.

Table 4.15: Comparison of response with THA and RSA in the plates of type D.

	a_{rel} [mm/s ²]		Difference	v_{rel} [mm/s] $\times 10^{-1}$		Difference	d_{rel} [mm] $\times 10^{-3}$		Difference
	RSA	THA	[%]	RSA	THA	[%]	RSA	THA	[%]
D1	585	611	4.22	14.60	16.64	12.26	5.06	5.11	0.99
D2	458	476	3.84	10.95	11.36	3.57	4.58	4.90	6.56
D3	409	405	-0.99	12.34	12.72	3.00	5.02	5.14	2.44
D4	459	308	-48.82	11.88	5.94	-100.01	6.21	5.33	-16.36
D5	449	235	-91.13	10.64	6.00	-77.22	5.34	4.53	-18.03

4.3.8.6 Plate type E

Table 4.16 shows the responses of the vertical mid DOF for the plates of type E. Plates E1-E4 all show a fairly good conformity with the largest difference at 13.85%. Besides the relative acceleration for plate E1 all responses for plates E1-E4 are higher for THA. Plate E5 show a significant difference between RSA and THA, with relative acceleration and velocity reaching 54.79 and 50.74 % difference, respectively. Similarly to plates D4 and D5, plate E5 has significantly smaller values of THA response compared to RSA response.

Table 4.16: Comparison of response with THA and RSA in the plates of type E.

	a_{rel} [mm/s ²]		Difference	v_{rel} [mm/s] $\times 10^{-1}$		Difference	d_{rel} [mm] $\times 10^{-3}$		Difference
	RSA	THA	[%]	RSA	THA	[%]	RSA	THA	[%]
E1	1068	1042	-2.43	22.04	22.39	1.54	4.81	4.82	0.19
E2	820	951	13.85	25.01	27.81	10.07	7.34	7.86	6.55
E3	582	660	11.75	17.08	18.54	7.87	6.17	6.65	7.20
E4	1170	1181	0.98	29.92	29.94	0.04	8.71	9.87	11.69
E5	642	415	-54.79	17.87	11.86	-50.74	6.54	6.03	-8.35

4.3.8.7 Summary of difference between THA and RSA from parameter study

In Table 4.17 a summary of the difference between THA and RSA for all the plates in the parameter study are displayed together with the first mode frequency of the plates.

Table 4.17: Comparison of responses, as percentage difference between RSA and THA with the fine mesh. Positive difference means the THA is larger than RSA.

	First mode frequency [Hz]	Difference [%]		
		a_{rel}	v_{rel}	d_{rel}
A1/A5	39.35	2.49	8.55	10.21
A2/A4	24.95	13.46	25.12	28.49
A3	25.54	3.96	19.21	4.13
B1/B5	81.88	3.27	-2.68	-6.62
B2/B4	49.23	0.17	8.08	3.51
B3	46.16	7.31	5.67	3.25
C1	40.72	11.26	11.49	12.80
C2	27.63	-2.01	6.87	13.89
C3	37.24	-1.95	11.16	2.32
C4	47.72	12.81	11.46	12.12
C5	81.18	-3.58	-4.39	-7.74
D1	35.31	4.22	12.26	0.99
D2	19.87	3.84	3.57	6.56
D3	12.67	-0.99	3.00	2.44
D4	4.93	-48.82	-100.01	-16.36
D5	3.89	-91.13	-77.22	-18.03
E1	78.94	-2.43	1.54	0.19
E2	44.78	13.85	10.07	6.55
E3	28.73	11.75	7.87	7.20
E4	11.24	0.98	0.04	11.69
E5	8.87	-54.79	-50.74	-8.35

There is a large spread in results between the responses in RSA and THA for all three motions. When studying the relative displacement the smallest difference is 0.19 % while the largest is as much as 28.49 %. When considering all responses, the largest difference is over 100 %. Evidently plate type B, which is fixed along all edges, has a relatively small deviation between the THA and RSA. The rectangular plates D4, D5 and E5, all with the long sides unsupported show large deviations and have a low first mode frequency. An interesting observation is that plate E4, which also has the long sides unsupported and a relatively low first mode frequency, has much better conformity than the other plates with similar boundary conditions and geometries.

For the large majority of the plates there is a positive sign in front of the percentage difference, which means that THA results are higher than the RSA. The highest positive difference is 28.49 % in relative displacement for plate A2/A4.

There seems to be a difference between THA and RSA that is fairly general, ranging from 0-30% which is most often with a positive sign. Aside from that general difference, there is another type of difference between RSA and THA which is unique to plates D4, D5 and E5. These plates have significantly higher percentage difference between THA and RSA. Unlike the other plates, the difference is concentrated primarily to acceleration and velocity, and the responses are all lower for THA than

for RSA. In order to understand the reasons behind these results, a more thorough study of plate D5 and B3 is made. The reasons these plates were chosen were that it seemed prudent to investigate a plate that had a very large difference between THA and RSA, and one which had a relatively small difference. These in-depth studies are covered in Sections 4.4.3 and 4.4.4.

4.3.9 Comparison of results from parameter study with fine and coarse mesh

For some plates, the percentage difference between THA and RSA changed noticeably between the coarse mesh, i.e the 20×20 mesh, and the fine mesh, i.e the 10 cm^2 mesh described in Section 4.3.7. Table 4.18 shows the percentage change in response between the coarse mesh and the fine mesh. As an example, looking at acceleration difference for plate A1, by increasing the amount of elements the RSA changed 2.52 % and the THA changed 13.78%.

Table 4.18: Percentage difference of responses between analyses with 20×20 mesh and 10 cm^2 mesh.

	$a_{rel}[\%]$		$v_{rel}[\%]$		$d_{rel}[\%]$	
	RSA	THA	RSA	THA	RSA	THA
A1	2.52	-13.78	0.74	6.95	0.34	-2.14
A2	11.19	7.73	10.31	17.84	5.45	14.13
A3	0.99	-1.57	-1.15	0.64	-0.64	5.19
B1	5.84	1.04	6.81	0.29	9.93	-2.54
B2	5.46	-2.64	3.43	2.00	3.58	2.27
B3	3.17	13.98	-4.56	-0.04	-7.89	-2.48
C1	-1.27	-17.97	1.34	-7.35	3.90	-4.40
C2	5.00	3.30	-1.99	-16.97	-4.68	9.77
C3	-0.92	-6.46	-0.09	-5.81	-1.13	-4.24
C4	-1.85	0.88	-2.00	-5.51	0.39	-0.72
C5	-4.95	-7.93	-0.44	-0.49	4.53	-0.10
D1	1.57	2.72	-1.95	0.41	2.67	0.88
D2	2.74	7.57	-1.22	-1.31	-2.40	-0.81
D3	-0.52	-11.40	-0.59	-5.64	1.65	-0.94
D4	-3.82	6.04	-4.10	-11.75	-1.87	4.68
D5	4.02	-6.55	1.54	7.97	3.68	2.05
E1	19.68	-5.23	22.97	-3.38	25.58	-4.97
E2	4.86	-5.55	6.46	-6.12	8.42	-5.86
E3	0.31	-12.71	2.40	-4.15	3.97	3.62
E4	2.06	-19.35	3.05	-16.69	2.66	-11.13
E5	-5.13	-3.63	-3.07	-4.80	-2.59	-0.50

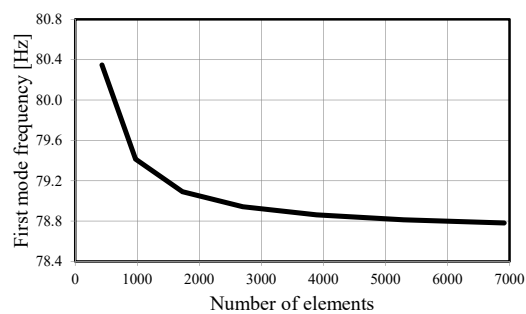
Table 4.18 underlines the complexity of convergence for the plates. The first convergence study, covered in Section 4.2.3, was unfortunately made for plate A3, which is one of the plates that converged with the fewest amount of elements for both RSA

and THA. Some plates, for example E1, changed considerably for RSA while having decent convergence in THA with the coarse mesh. In the opposite situation, plate E4 did not change much with respect to RSA but saw a large difference in THA. To summarise, it is evident that the convergence behaviour is erratic. One could very well end up in a situation where a chosen mesh results in a situation where the RSA is converged while the THA is not for one plate, with the opposite being true for another plate.

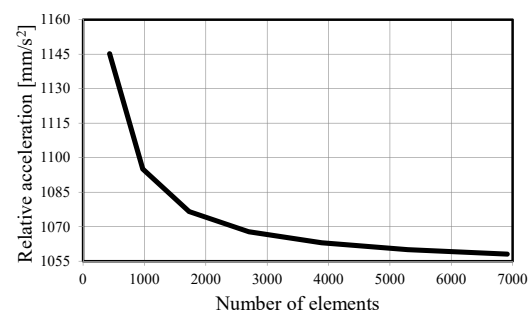
4.3.10 Convergence study of a plate sensitive to mesh size

Initially it was assumed that the RSA needed approximately the same mesh as the plates in the modal contribution study, i.e. 20×20 elements, see Section 4.2.3.

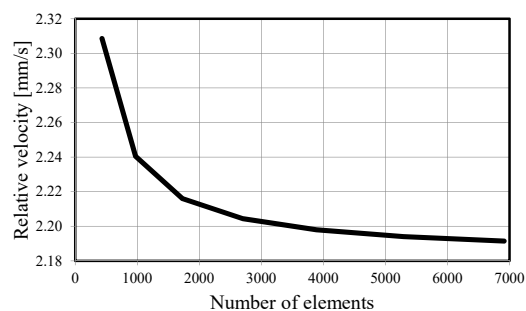
The comparison of the parameter study using both the coarse mesh and fine mesh, see Section 4.3.9, revealed that the sensitivity for the element size varies both between plate and analysis type. Especially plate E1 was discovered to be sensitive to the number of elements needed for the RSA. Another convergence study of the RSA response for plate E1 was performed. The geometry of plate E1, which has a first mode frequency of approximately 79 Hz, is shown in Table 4.3 and Figure 4.10 shows the result of the convergence study.



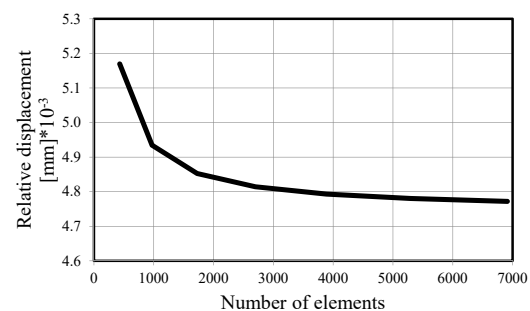
(a) Convergence of first mode frequency.



(b) Convergence of relative acceleration.



(c) Convergence of relative velocity.



(d) Convergence of relative displacement.

Figure 4.10: Convergence study of the first mode frequency and responses with RSA for plate E1.

Evidently, 30×90 elements, i.e 2700 elements, produce results that are not converged. However, the magnitude in the difference between 2700 elements and 7000 elements is relatively small. Thus, increasing the amount of elements for the RSA of plate E1 would not change the results dramatically.

4.3.11 RSA using modal combination rule ABSSUM

In Section 2.4.3.7 the different modal combination rules were described. All RSA analyses performed thus far has applied the modal combination rule SRSS, Equation 2.63. The results produced with RSA using SRSS have mostly resulted in responses with smaller values than THA, see Table 4.17. An alternative modal combination rule is the ABSSUM rule, Equation 2.62, which gives considerably more conservative results. Table 4.19 shows the difference between THA and RSA when ABSSUM is applied for the plates in the parameter study. Again, the studied responses are relative acceleration, relative velocity and relative displacement. The complete results from the comparison of THA and RSA using ABSSUM can be seen in Appendix C.

Table 4.19: Difference between the responses with THA and RSA using modal combination rule ABSSUM.

Plate	Difference[%]		
	a_{rel}	v_{rel}	d_{rel}
A1/A5	-87.12	-35.07	-19.51
A2/A4	-85.76	-25.59	-6.89
A3	-71.82	-14.45	-11.31
B1/B5	-55.65	-33.14	-23.75
B2/B4	-73.67	-19.26	-10.65
B3	-50.60	-18.87	-5.26
C1	-81.06	-29.31	-11.46
C2	-132.42	-51.80	-9.01
C3	-106.02	-36.01	-16.44
C4	-52.65	-16.56	-3.27
C5	-62.22	-33.22	-26.23
D1	-31.74	-4.38	-10.53
D2	-55.23	-26.12	-4.58
D3	-72.26	-28.41	-13.88
D4	-193.67	-238.57	-60.60
D5	-283.40	-197.86	-62.17
E1	-22.33	-7.26	-5.82
E2	-29.12	-8.69	-6.59
E3	-57.11	-27.36	-10.22
E4	-63.62	-43.24	-29.59
E5	-193.18	-138.33	-60.96

Applying the modal combination rule ABSSUM results in RSA consistently obtaining a higher response than THA for all the plates in the parameter study. However,

the spread in accuracy becomes even greater than with SRSS. Evidently, ABSSUM will result in a large overestimation for some plates. Relative velocity and relative acceleration in particular reach very high values with a significant difference with respect to THA. The largest difference is 283.40 %. For the relative displacement the differences between THA and RSA lies between 3 % and 63 %. Nevertheless, using ABSSUM seems to consistently produce conservative results.

4.4 In depth study of plates from parameter study

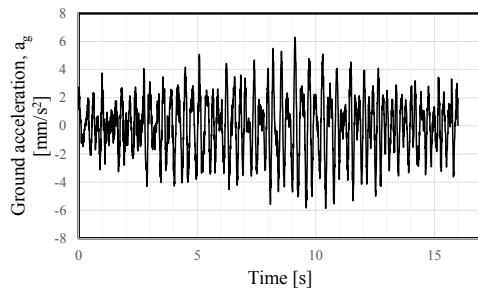
4.4.1 Orientation

Due to the spread of results between the RSA and THA that was observed in the parameter study covered in Section 4.3.8, a closer investigation of two plates of choice was performed. The chosen plates were plate D5 which had the largest deviation and plate B3 which had a small deviation between RSA and THA. These plates were chosen in order to study the difference which caused plate D5 to have low conformity and B3 to have high conformity. Furthermore, this section includes studies of the length of time-step used for THA and of how the number of modes used affect the RSA. The deformed shapes of D5 and B3 in THA at the time of maximum displacement will also be studied, with the purpose of understanding their behaviour. This section will also cover analyses of plates D5 and B3, when subjected to Traffic Load 2, further described in Section 4.4.2. However, unless otherwise specified, ground motion from Traffic load 1 are used for the analyses in this section.

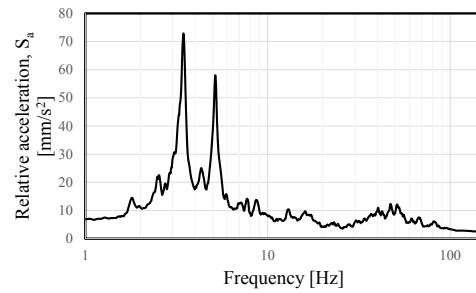
4.4.2 Response spectrum from Traffic load 2

To further examine the D5 and B3 plate, it was subjected to Traffic load 2. The traffic load was applied to a THA of the D5 and B3 plate. Response spectra of Traffic load 2 was calculated and used with the modal contributions from the D5 and D3 plate. The results of these analyses can be viewed in Sections 4.4.3.6 and 4.4.4.3. Traffic load 2 and its resulting response spectra can be seen in Figure 4.11.

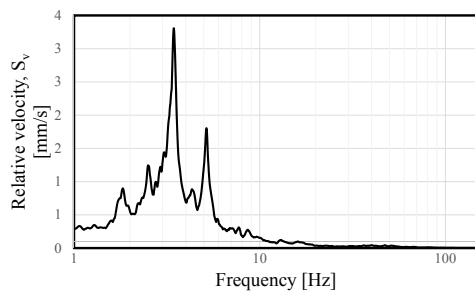
4. Results



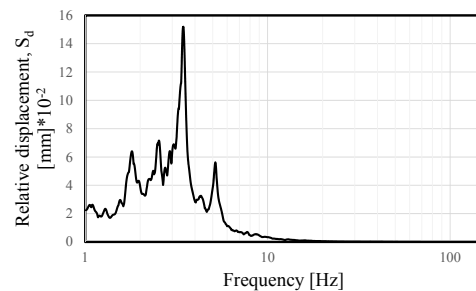
(a) Input data for the response spectrum in form of ground acceleration.



(b) Response spectrum, relative acceleration.



(c) Response spectrum, relative velocity.



(d) Response spectrum, relative displacement.

Figure 4.11: The ground acceleration for Traffic load 2 and the response spectra calculated from the ground acceleration.

In Figure 4.8 the response spectra of Traffic load 1 can be viewed for comparison. One major difference between the two traffic loads is the frequency range where the peak response is located. For Traffic load 1 the peak responses are in the range of approximately 58-130 Hz, see Figure 4.8, whereas Traffic load 2 has its major response in the 1-10 Hz region. The second difference is the amplitude, where for example the acceleration of Traffic load 1 produces a response spectrum that peaks close to 3000 mm/s², see Figure 4.8b, whereas the acceleration peaks below 80 mm/s² for Traffic load 2, see Figure 4.11b.

4.4.3 In depth analysis of plate with large deviation between THA and RSA, plate D5

4.4.3.1 Analysis of the entire time history

As was shown in Section 4.3.8, plate D5 had the largest deviation between the results of RSA and THA. Due to this, the behaviour of D5 in THA and RSA was analysed further. In the parameter study, the highest single response in the centre node was compared with THA and RSA. To get a better understanding of the plate

behaviour, the entire time history of the centre node was studied, see Figure 4.12.

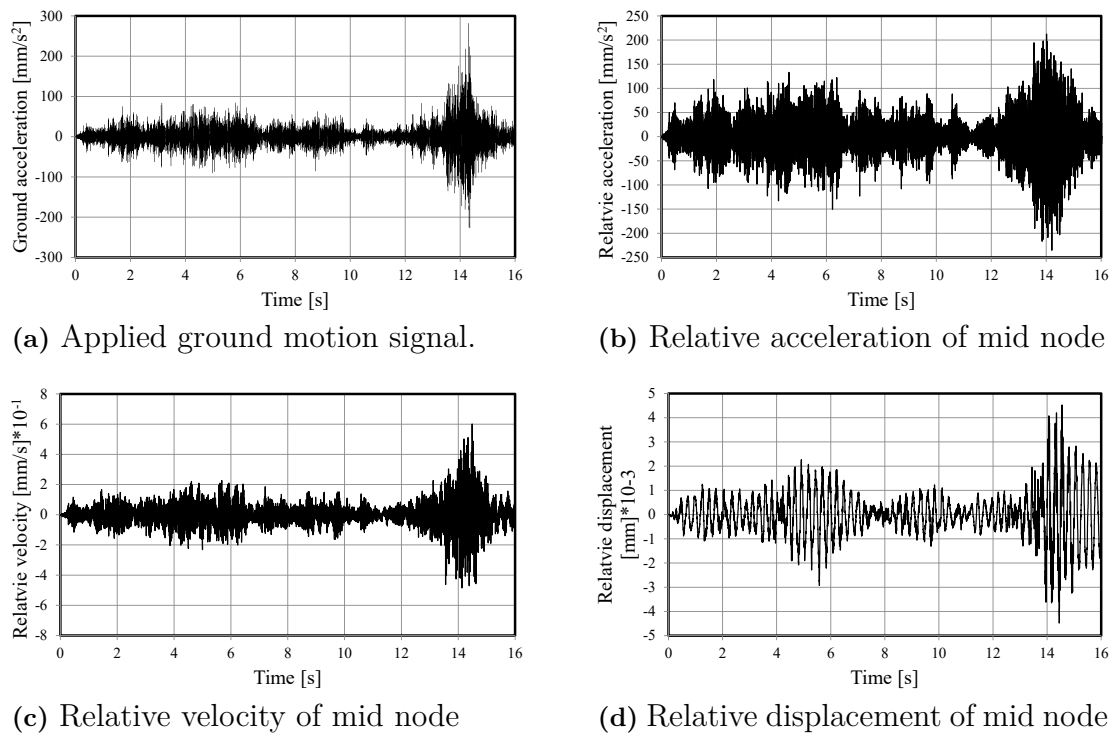


Figure 4.12: The applied ground motion signal and complete time history of the mid node in plate D5 for all three responses.

It is clear from the graphs in Figure 4.12 that all the maximum responses arise in close proximity to the maximum values of the ground motion signal, which occurs around the 14 second mark. After the maximum response has been reached, all the responses begin to subside, with displacement being the slowest to do so. Since the ground motion ends at the same time as the time period analysed, all three responses fail to subside down to zero before the end of the analysis, displacement in particular. However, it is clear from all three graphs that all the responses are moving towards zero and that no maximum values could be missed because of this. Furthermore, it can be noted that the displacement curve has a more sparse graph compared to the denser graphs of the velocity and acceleration. This indicates that the displacement is influenced more from the lower modes than acceleration and velocity

It can also be noted that both the maximum values of ground motion and the maximum responses are concentrated within a short space of time. Plate D5 has the lowest natural frequencies of all the plates in the parameter study, and consequently there is less chance of several modes reaching peak values simultaneously within a short space of time. The significance of this will be covered more in Section 4.4.3.5.

4.4.3.2 Study of general response in plate D5

To investigate the difference in general behaviour between RSA and THA, additional nodes in the plate were studied. Figure 3.4 shows the notations and location of the studied nodes, and Table 4.20 show the results of the comparison.

Table 4.20: Comparison of the relative response of plate D5 calculated with THA and RSA.

Plate D5 Node	a_{rel} [mm/s ²]		Difference	v_{rel} [mm/s] $\times 10^{-1}$		Difference	d_{rel} [mm] $\times 10^{-3}$		Difference
	RSA	THA	%	RSA	THA	%	RSA	THA	%
a	336.34	411.81	18.33	7.89	11.75	32.84	3.94	4.96	20.55
b	477.12	386.62	-23.41	11.14	10.68	-4.30	5.52	4.73	-16.63
c	317.27	253.63	-25.09	7.55	6.46	-16.83	3.82	4.78	20.23
d	449.069	234.95	-91.13	10.64	6.00	-77.22	5.34	4.53	-18.03

There is a significant difference in the response between RSA and THA for all four nodes. Notably, the location of the largest responses are different in the two analyses. In the THA the largest response is found at node a and in the RSA at node b. Another observation is that the maximum response occur at the plate edge, rather than the centre line.

4.4.3.3 Investigation on how the time-step length influence THA response

The accuracy of THA can depend significantly on the length of the time-step used for the analysis. A suitable length of the time-step depends on the highest frequency that should be included in the analysis. A suitable guideline is to use a time-step, Δt , shorter than 1/20 of the period of the highest eigenfrequency, i.e $\Delta t < T/20$ where $T = 1/f$. In the study of plate D5 a time-step of 7.32×10^{-4} seconds and 200 modes have been used. The eigenfrequency for mode 200 is approximately 1850 Hz. To describe such a high frequency it would require a time-step of about 2.7×10^{-5} seconds, which is a considerably smaller value than the one used in the analyses. Following the guideline, a time-step of 7.32×10^{-4} seconds should permit study of modes up to a frequency of about 68 Hz.

To investigate if the difference of the THA and RSA was a result of insufficiently short time-steps a comparison of the response including only the first few modes was performed. Two analyses were done each for THA and RSA, the first using only the first mode and the second using the first four modes. The reason for including four modes in the second analysis was that modes one and four are contributing modes for both THA and RSA, whereas modes two and three are not. The fourth mode of plate D5 has a natural frequency of approximately 36 Hz, which indicates that it should be described well with the time-step 7.32×10^{-4} . The results of the analyses are shown in Table 4.21. The first mode analysis shows well corresponding results

Table 4.21: Comparison of RSA and THA in the centre of the plates, i.e node d, including 1 and 4 modes.

Plate D5	1 mode			4 modes		
	RSA	THA	Difference %	RSA	THA	Difference %
a_{rel} [mm/s ²]	358.49	356.27	-0.62	408.48	172.05	-137.42
v_{rel} [mm/s] $\times 10^{-1}$	9.14	9.07	-0.79	10.38	5.45	-90.43
d_{rel} [mm] $\times 10^{-3}$	5.03	4.93	-1.97	5.33	4.70	-13.41

between THA and RSA, whereas the four mode analysis result in markedly different responses. The relative acceleration deviates 133%, even though the frequency of this mode is well below the limit according to the time-step guideline.

4.4.3.4 Investigation on how the number of modes influence the response of RSA

An additional control that the fourth mode was correctly described with the time-step is to compare the modal contribution of MATLAB with ADINA. Figure 4.13 show the influence of the modal contribution on the middle node of plate D5 calculated both with ADINA and MATLAB.

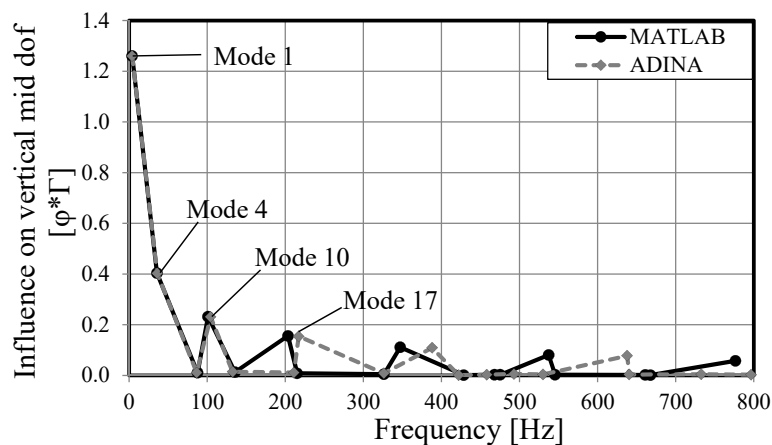


Figure 4.13: Influence on the response of the mid DOF according RSA with MATLAB and ADINA.

The modal contribution and its corresponding frequency matches well up until the 17th mode, from then and upwards the frequency differs increasingly but the value of the modal contribution matches well between MATLAB and ADINA. This is an expected result and was observed already in Section 4.2.4. It can be argued that the difference in frequency above the 17th mode has small influence on the response. In part because the modal contribution is low, but also because the response spectrum of Traffic Load 1 has very low response at frequencies above 200 Hz. The second data point in Figure 4.13 represents the fourth mode and has a natural frequency of approximately 36 Hz, evidently mode four is very similar between MATLAB and

ADINA. However, as was shown in Table 4.21 the THA and RSA begin to deviate significantly when Mode 4 is added. This implies the THA and RSA deviate even at low frequencies that correlate well between MATLAB and ADINA.

To show that the higher modes contribute negligibly to the total response for Traffic load 1, Figure 4.14 displays how the response of the RSA is increasing when more modes are included in the analysis. The accumulated response is normed with respect to total response, i.e when the graph approaches 1 on the Y axis the total response is approached. The total response is referring to the response of the plate with 200 modes included in the analysis. As can be observed the relative displacement nearly reaches its total response by inclusion of just four modes. Including modes 10 and 17 pushes all the responses above 99% of total response.

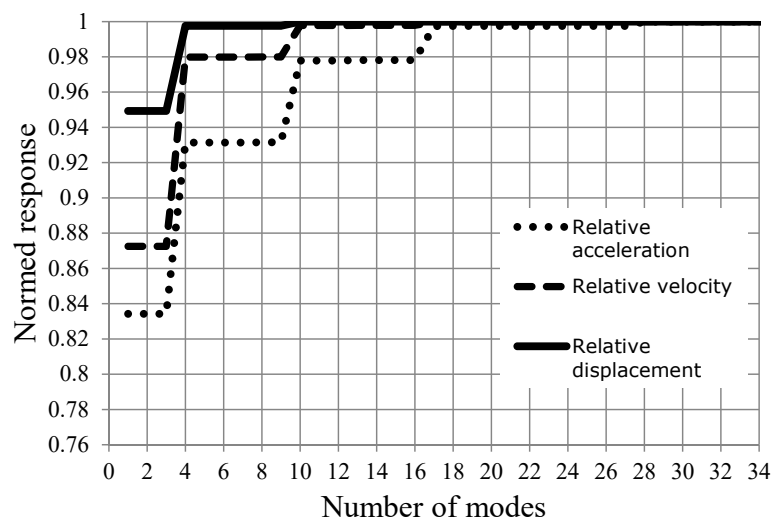


Figure 4.14: Increase of the response on the mid node with increasing number of modes calculated with MATLAB and a 20×20 mesh. The contributing modes are modes 1, 4, 10 and 17.

As mentioned in Section 4.2.3 a mesh of 20×20 was used for the MPF study. Since only a general behaviour is illustrated with the normed response data in Figure 4.14 the data is from calculation in MATLAB with a 20×20 mesh. Figure 4.15 displays the four modes that contributes to the majority of the total response of the midnode in plate D5, i.e mode 1, 4, 10 and 17 which was observed in Figure 4.14. A comparison with the displacements of the plate at the time for the largest response in the THA, see Figure 4.16, illustrates the difference of the plate displacements for the RSA and THA.

4.4.3.5 How mode interaction influences the difference of RSA and THA

Based on the results in Sections 4.4.3.3 and 4.4.3.4 it was concluded that neither the time-step of the THA nor the inclusion of too high modes were the source of the discrepancy of plate D5. At this point, the hypothesis was that in THA the modes

might not have sufficient time to reach full interaction during the brief window of peak ground motion from Traffic Load 1. A more hands-on approach was tried. The basic idea was to look at the displacement of the plate in the THA around the time of maximum response and see how the modes interacted at that point in the time history. As previously mentioned, the modes 1, 4, 10 and 17 provided nearly 100% of the total response for the RSA, with mode 1 and 4 having the largest contribution. These modes are shown in Figure 4.15, the deformed shape of plate D5 at the time of maximum displacement in the THA is shown in Figure 4.16.

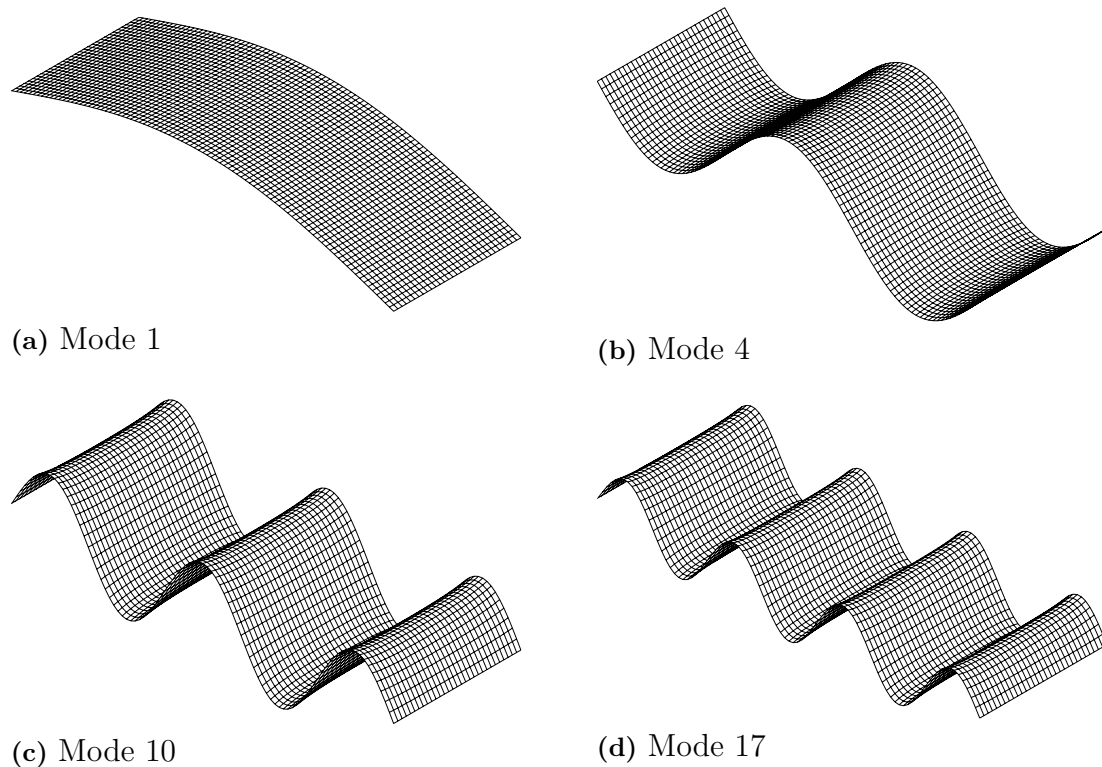


Figure 4.15: The four modes that contributes to the majority of the response for plate D5 according to RSA.

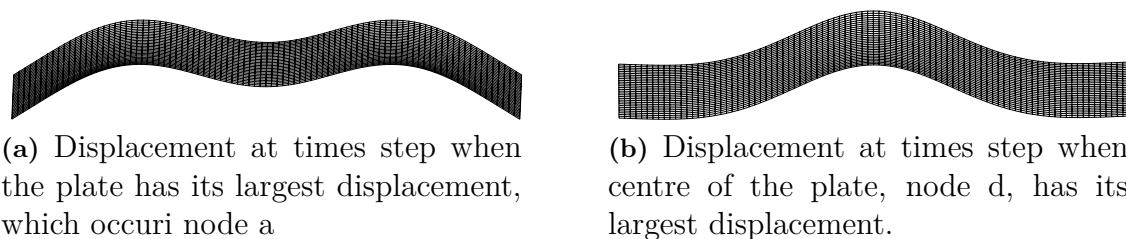


Figure 4.16: Displacements of plate D5 at time steps with largest displacements according to THA.

The deformed shape of D5 at the time of maximum displacement in THA, Figure 4.16a, clearly shows significant presence of Mode 1 and 4, moreover it can be seen

that the modes are counteracting each other with respect to displacement in the centre node, but interacting with respect to displacement in nodes a and c. For RSA, contribution of all modes are stacked for all three modal combination rules. THA describes how the specific plate reacts to a specific load for each individual time-step. Consequently, in THA it is possible that the modes do not interact fully. The possibility of low interaction is increased if the mode frequencies are low and the duration of maximum ground motion is short, which both are true for plate D5 with Traffic load 1. Figure 4.17 attempts to illustrate the basic principle behind the large difference between THA and RSA for plate D5.

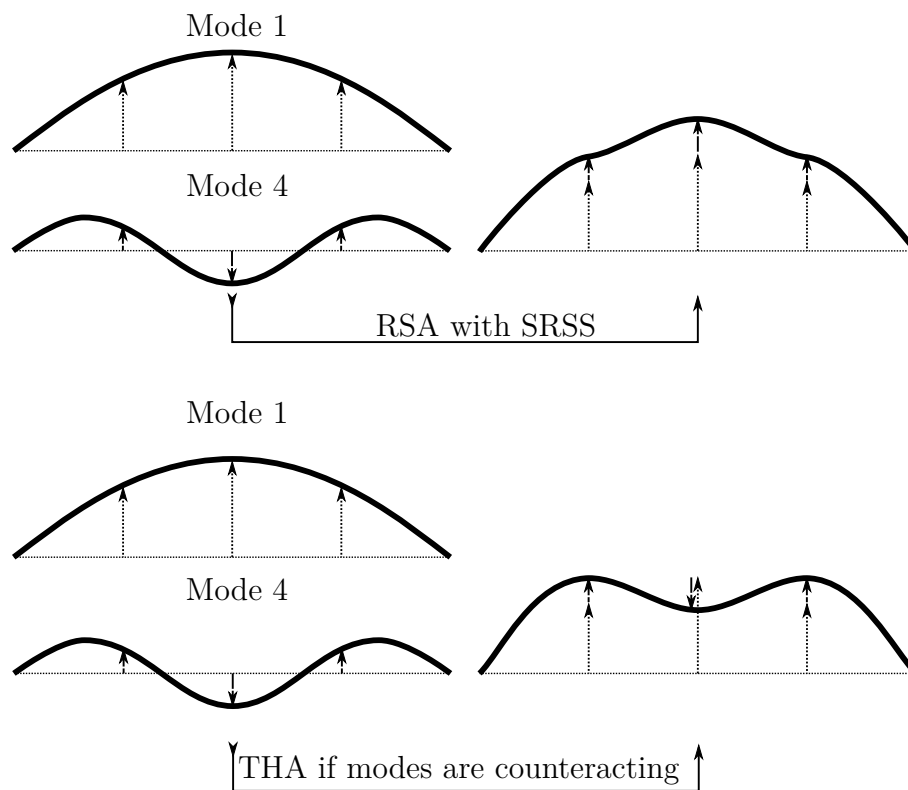


Figure 4.17: Illustration of how responses from modes are combined to a total response in RSA and THA.

As is shown in Table 4.20, the RSA reaches its maximum values of displacement at nodes b and THA at nodes a and c, which are nodes located on the free edges. The reason for the free edges having slightly higher response is because modes 1, 4, 10 and 17 all have a very slight concavity perpendicular to the main direction. In addition, there is a small contribution from modes 8 and 13, which can be seen in Figure 4.18. These two modes have a rather small modal contribution, but their natural frequencies are 87.7 and 135.6 Hz, which both are in regions of high response in the Response spectrum for Traffic load 1. Due to the modal contribution being so low for these modes, they have a low contribution to the total response, but their contributions are largest along the free edge.

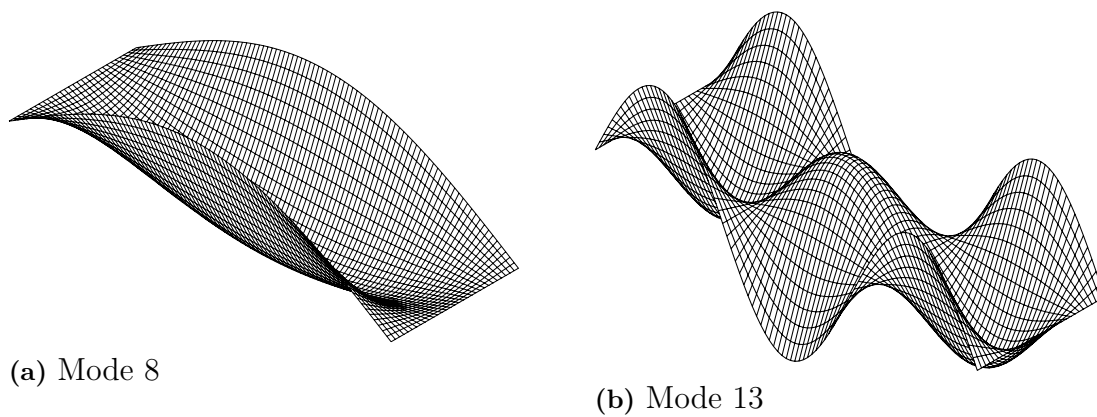


Figure 4.18: Modes 8 and 13 for plate D5, which contributes to the response at the free edge.

4.4.3.6 Analysis with Traffic load 2

The results of the THA and RSA of plate D5 with Traffic load 2 can be seen in Table 4.22. The results of the comparison of THA and RSA of plate D5 for Traffic load 2 show significantly better conformity compared to Traffic load 1. With Traffic load 1 the difference is 16%, 90% and 72 % for displacement, velocity and acceleration, respectively. For Traffic load 2 all three responses differ less than 2 % between the THA and RSA, see Table 4.22

Table 4.22: Comparison of THA and RSA of plate D5 calculated with Traffic load 2.

Plate D5	RSA	THA	Difference [%]
a_{rel} [mm/s ²]	24.64	25.10	1.83
v_{rel} [mm/s] × 10 ⁻¹	10.51	10.48	-0.27
d_{rel} [mm] × 10 ⁻³	43.87	43.85	-0.05

The good correspondence here is reasonable considering that the response spectra of Traffic load 2, see Figure 4.11, all have very low response above 10 Hz. This means that of the contributing modes in D5, only mode one will see significant activation. Hence, there is no situation with modes counteracting each other for this load. The displacement and velocity spectra are both practically zero above 10 Hz, whereas there is a small value of acceleration past that point. Acceleration is the parameter deviating the most between RSA and THA for this ground motion.

4.4.3.7 Maximum response of plate D4, E4 and E5.

Based on the observations made in Section 4.4.3.5, plates D4 and E5 were studied with respect to the deformed shape at the time of maximum response in THA. Plate

E4 was also studied, to see why it had so much better conformity of results between THA and RSA.

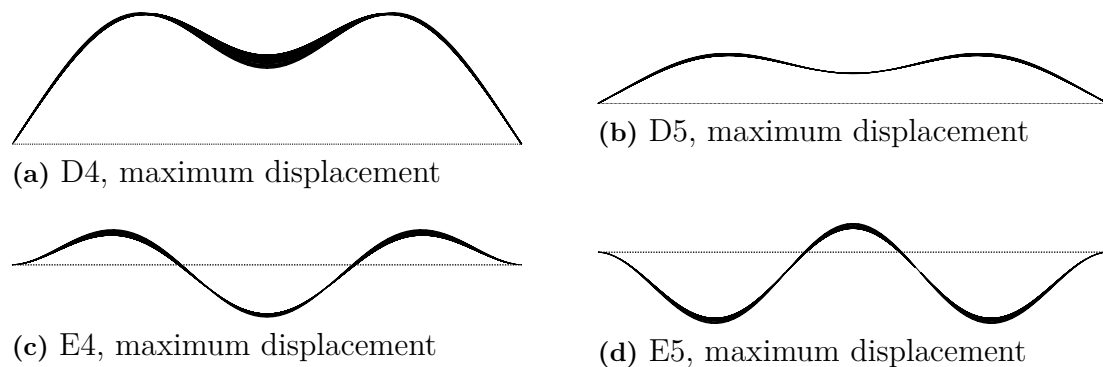


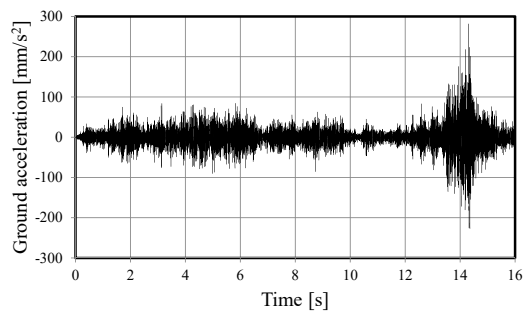
Figure 4.19: Plates D4, D5, E4 and E5 at the time of maximum displacement in THA.

As can be seen in Figure 4.19a, plate D4 has a response very similar to D5 with the first two contributing modes counteracting each other. The same can be seen for plate E5 in Figure 4.19d, but with much higher influence from the second contributing mode. Plate E4, Figure 4.19c, receives a majority of its response from the second contributing mode. In fact it is hard to even distinguish the contribution of the first mode in the figure. For plate E4, the first contributing mode is Mode 1 with a natural frequency of 11.24 Hz. The second contributing mode, which is Mode 6, has a natural frequency of 60.31 Hz. Consulting the graphs of the response spectra of Traffic load 1 in Figure 4.8, one can see that the first mode of plate E4 is in a region of very low response. On the other hand, Mode 6 is very close to highest peak of the response spectra. Furthermore, it is evident that for plate E4 in THA, the first and second contributing mode are interacting in the plate center, which explains the good conformity between THA and RSA for this plate.

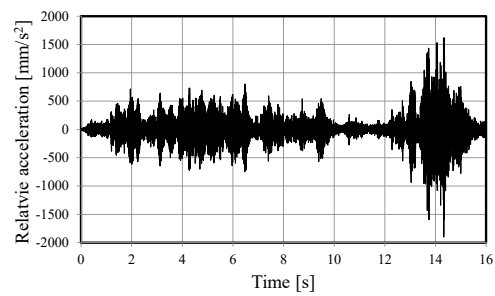
4.4.4 In depth analysis of plate with small deviation between THA and RSA, plate B3

4.4.4.1 Analysis of the entire time story

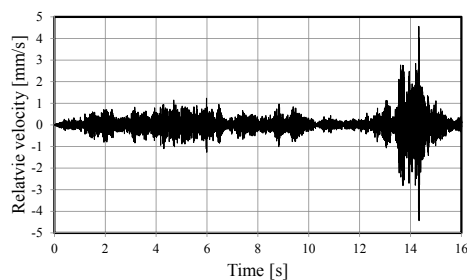
Plate B3 in the parameter study described in Chapter 4.3.8 showed a relative small deviation between the THA and RSA. To investigate why the results in a THA and RSA were similar a deeper study of the plate was made. Figure 4.20 shows the complete THA of the mid node of plate B3 and the ground acceleration that was used as input data.



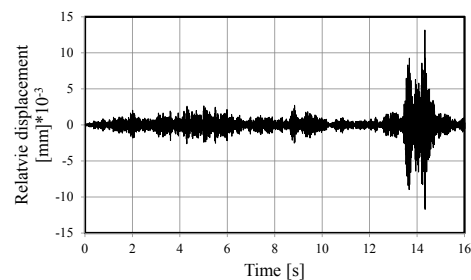
(a) Input data for the THA in form of ground acceleration.



(b) Relative acceleration of mid node in plate B3 from THA.



(c) Relative velocity of mid node in plate B3 from THA.



(d) Relative displacement of mid node in plate B3 from THA.

Figure 4.20: Complete THA of the mid node in plate B3.

Comparing Figure 4.20d with Figure 4.12d, it is evident that the displacement time history of the mid node for B3 is denser than for plate D5. Since plate B3 has higher natural frequencies than D5, it is an expected result.

Looking at the modal contribution graph for plate B3, Figure 4.21, it is observed that modes 1 and 6 have the largest modal contributions. Comparing the frequency of mode 1 and 6, see Figure 4.21 with the response spectrum, see Figure 4.8 only mode 1 is residing in a region of high response in the response spectra. Mode 6 is still within the active region of the response spectra, but should have significantly lower contribution to total response than Mode 1. It is expected then, that for plate B3 a significant portion of the contribution to the response should come from Mode 1, and considerably smaller contributions coming from Mode 6 and later modes.

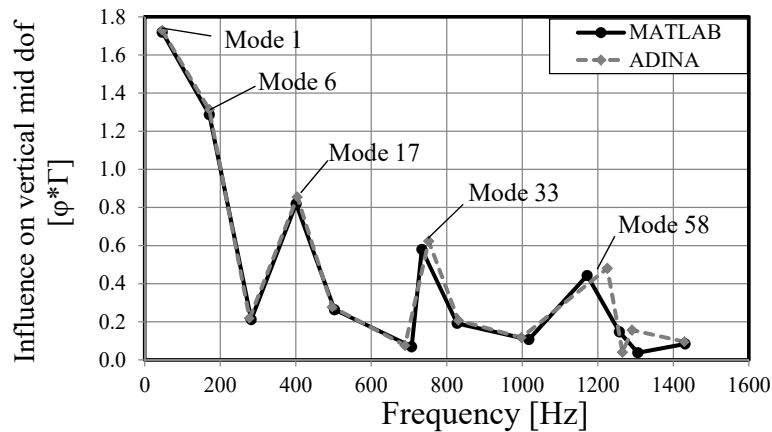


Figure 4.21: Influence on the response of the mid DOF according to RSA with MATLAB and ADINA.

4.4.4.2 Investigation on how the modes influence the response

Figure 4.22 displays how the responses are increasing with more modes included in the analysis similarly to Figure 4.15 and as was explained in Section 4.4.3.

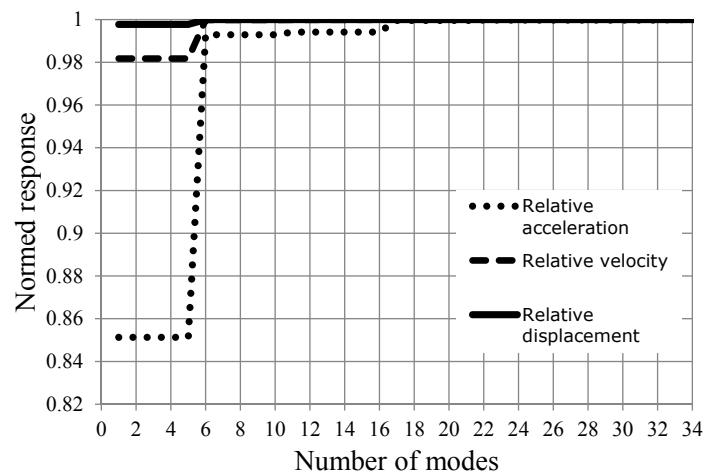


Figure 4.22: Increase of the response on the mid node with increasing number of modes.

In accordance with the predictions made from Figure 4.21, the response is influenced mostly from Mode 1. So much so, that by including only Mode 1 the relative displacement practically reaches its total response. Relative velocity is also close to its total with Mode 1, but relative acceleration receives a relative large contribution from Mode 6.

Table 4.23 shows the response of THA and RSA with inclusion of Mode 1, and when including Modes 1 and 6. The first and sixth mode have natural frequencies

of approximately 46 and 166 Hz, respectively. The RSA and THA show conforming results both when only the response from the first mode is included and when the response from the first six modes are included.

Table 4.23: Comparison of RSA and THA including 1 and 6 modes.

Plate B3	1 mode			6 modes		
	RSA	THA	Difference[%]	RSA	THA	Difference [%]
$a_{rel}[\text{mm/s}^2]$	1333.37	1344.50	0.75	1741.39	1867.67	0.68
$v_{rel}[\text{mm/s}] \times 10^{-1}$	41.57	41.31	-0.63	42.94	46.16	0.70
$d_{rel}[\text{mm}] \times 10^{-3}$	12.67	12.87	1.54	12.72	13.16	0.34

Figure 4.23 shows the shapes of Modes 1 and 6 for plate B3, Figure 4.24 shows the deformed shape of B3 at the time of maximum displacement in THA. As was shown in Figure 4.22, the displacement receives more than 99% of its total response from Mode 1, which can be observed from the deformed shape of B3 at the time of maximum displacement in THA. Since Mode 6 receives contribution for acceleration and velocity, but not displacement, it is not visible at all.

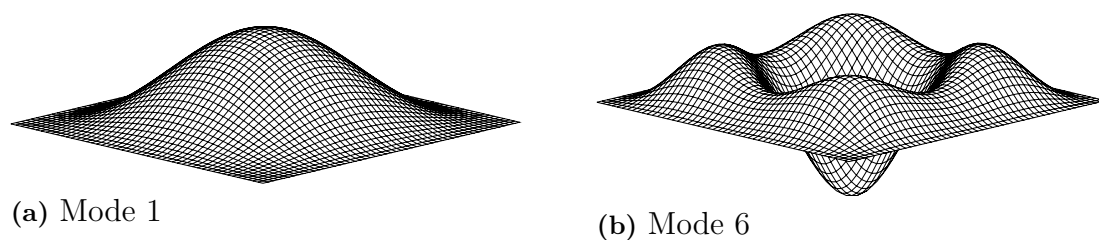


Figure 4.23: The two modes that contributes to the majority of the response for plate B3 according to RSA.

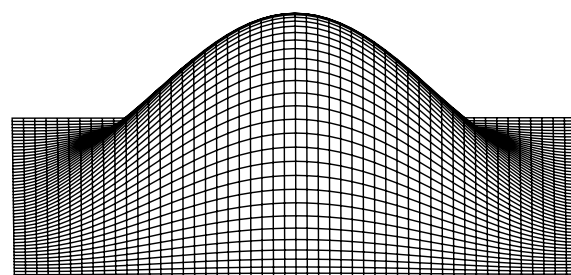


Figure 4.24: Displacements at the time of largest response in plate B3 in THA.

The good conformity for displacement is readily explained by the fact that displacement is in practice only affected by mode 1, so there is no case of modes counter-acting each other for displacement, as was seen with plate D5 in Section 4.4.3.5. However, D5 saw a smaller deviation for displacement which was fairly in tune with many other plates, again due to mode 1 having such a dominating influence on the displacement. The largest discrepancies were seen with velocity and acceleration,

which for B3 conforms fairly well between RSA and THA. This is believed to be due to B3 having so much higher natural frequencies for its first two contributing modes that they achieve full interaction for velocity and acceleration whereas D5 did not.

4.4.4.3 Analysis with Traffic load 2

The results of the THA and RSA of plate B3 with Traffic load 2 can be seen in Table 4.24. Just as was observed for plate D5 in Chapter 4.4.3.6 plate B3 shows better conformity between THA and RSA with Traffic load 2 compared to Traffic load 1. With Traffic load 1 the difference is 7.31 %, 5.67 % and 3.25 % for the relative displacement, velocity and acceleration, respectively. For Traffic load 2 the largest difference is 3.20 % for plate B3.

Table 4.24: Comparison of THA and RSA of plate B3 calculated with Traffic load 2.

Plate B3	RSA	THA	Difference [%]
$a_{rel} [mm/s^2]$	16.98	17.54	3.20
$v_{rel} [mm/s] \times 10^{-2}$	5.77	5.73	-0.67
$d_{rel} [mm] \times 10^{-4}$	2.20	2.16	-1.89

For plate B3 only the first mode is within the frequency range to be affected by the response spectrum for Traffic load 2. Hence no case of modes counteracting each other in THA is present. Thus the conformity of THA and RSA is expected in this case.

5

Conclusion

5.1 Orientation

This chapter includes a summary of the general and specific observations made based on the results in Chapter 4. Here the results are analysed and discussed. It includes the topics of convergence, influence of the load applied and the general accuracy of the method. Free discussion about the results and the understanding of them are also covered. Advice on how to approach the RSA method for plates, how to avoid different pitfalls and how to interpret results correctly are also made here. The chapter closes with a recommendation on further studies for the method.

5.2 Interpretation and analysis of results

5.2.1 Plates with large differences between results of THA and RSA, plates D4, D5 and E5.

As was shown in Chapter 4, there were three plates with substantial difference between THA and RSA, they are plates D4, D5 and E5. These plates, when subjected to Traffic load 1, exhibit a behaviour that is unique to them, which at first sight produced large errors that initially called into question if the method is reliable or not. The conclusion is that these three plates show significant discrepancies between RSA and THA because of how the contributing modes interact with each other when subjected to Traffic load 1. All three plates exhibit peak responses around the short time period when the ground excitation of Traffic Load 1 is at its largest, but the RSA show significantly higher response by large percentages. Figure 4.17 shows the principle of what is happening for these plates. The RSA always stacks all modal contribution, while in the THA it is possible that two contributing modes can counteract each other in a certain position of the plate. When studying the deformed shape of plates D4, D5 and E5 at the time of the peak response in THA (Figure 4.19) the first two contributing modes are clearly visible and counteracting each other in the centre node. One thing in common for all three plates is that the first contribut-

ing mode is located in a region of low response, while the second contributing mode is in a region of higher response. When the first and second contributing modes are the most dominant, with fairly low natural frequencies, they have lower probability of achieving maximum contribution at the same time. A very interesting special case is Plate E4, which has good conformity between THA and RSA. As was explained in Section 4.4.3.7, plate E4's second contributing mode has a natural frequency that is very close to the largest peak of the response spectrum. Its first contributing mode is in a low response region of the spectra. As a result, the second contributing mode dominates the behaviour of E4 at the time of maximum response. In Figure 4.19c, it is also visible that the small influence of the first contributing mode is working in the same direction as the second contributing mode. Hence the good conformity between RSA and THA for this plate.

One can argue that from a designer perspective, the results of the RSA are in these circumstances preferable. While the THA gives a more realistic response for this exact particular ground motion, it is very far from the worst case scenario which could happen for a similar ground response that has a slightly longer time window of peak motion. The discrepancy of these plates could therefore be considered to be an advantage for the RSA, since the worst case scenario could be a possible outcome for another slightly different ground motion. Regardless if it is considered an advantage or not, the large differences in response for the three plates are not a result of the method being inaccurate, as was feared at first.

5.2.2 General accuracy of results

As Fagerström and Lindorsson (2017) showed, the conformity between RSA and THA was very good for beam elements. The initial hypothesis was that plates would show similar conformity. This proved to be a false assumption, as the plates of the parameter study can diverge significantly between RSA and THA. However, as was shown in Section 4.4.3.5 and explained in the previous section, the largest differences between RSA and THA was a result of the THA not reaching maximum mode interaction during the short time period of maximum ground motion for three plates. The rest of the plates of the parameter study show a fairly good conformity, which for all but one single response fall within the expected margin of error for the method. The reason for the general difference of 1 – 30% between THA and RSA is believed to be caused by the modal combination rules not being ideal for jagged response spectra. If the response spectrum is jagged, which was the case in this study, a fairly small shift in the natural frequency of a dominant contributing mode can have a significant impact on the calculated response. As an example, the acceleration response spectrum of Traffic Load 1 has its maximum response of 2830 mm/s² at 58.44 Hz. If the studied plate has a significant mode around 58.44 Hz an error of 2-3 % for the frequency can result in a difference of more than 30 % for the acceleration response for that mode. If the mode in the example has a large modal contribution, the error in calculated response can become substantial. Consequently, all modes with high modal contribution, which have natural frequencies within the

dominant frequency range of the response spectrum, needs to be calculated with great precision.

Another reason for the large difference between RSA and THA can be because of convergence error, which is covered in the following section.

5.2.3 Convergence

The convergence studies were fairly complicated in the work on this thesis. There are many different parameters that can be studied in the convergence, such as mode frequencies, the modal contribution and the total response. Evidently, when having all the results of the study at hand, different plate types have different requirements on the mesh density. There is also a difference between how many elements that were needed for convergence for the RSA and THA, and it varied between plates. There is no discernible pattern or general rule that plates of a certain geometry and boundary conditions require a more or less dense mesh. It is also highly erratic which one of RSA and THA that require the more dense mesh. As there was not enough time to complete convergence studies on all 21 plates for both RSA and THA it is possible that there are plates which have not converged fully for the mesh used in the parameter study. This is a potential error source for the final results of the parameter study. However, the difference in results between the parameter study with 20×20 elements and the one with 10 cm^2 elements, as well as a few sample cases studied, both indicate that the results would not change notably with even finer meshes.

5.2.4 Interpolation of modal contribution

The investigation of interpolation of modal contribution from plates with similar geometries indicated that it cannot be done easily. For the low frequency contributing modes with precisely calculated frequencies and eigenvectors, there is a relationship between the geometry, the modal contribution and the frequency. In the study only one parameter was changed, the width of the plate. Even with such a small difference, the study showed that only the first three contributing modes could be used for interpolation. For contributing modes beyond the third, modes started appearing in different order. This might have to do with the convergence of higher mode frequencies, which is a problem that can be circumvented with a denser mesh. However, a more crucial problem is that if the stiffness and mass proportions of a plate changes enough, the modes will not appear in the same order or with the same frequency. The point where this mode shift happens would need to be investigated thoroughly to enable accurate interpolation. To produce tables that include enough material to be of use would require a very large parameter study which should have very dense meshes to ensure convergence. In this thesis the first few contributing modes have been the most influential on the total response. It could be argued that

you would only need the first 1-4 contributing modes, which could enable interpolation. However, since the RSA method produce results that differ up to 30 % from THA for relative response, it is presumably not a prudent choice. The results that are of interest for a designer is the comfort weighted total response. Both absolute response and comfort weighting adds to the potential error. Risking bad results for the relative response by interpolation could eventually be compounding to a large error.

5.2.5 Natural modes activated with uniform vibration

One surprising result with both RSA and THA was that many natural modes were not activated by the applied ground motion. In RSA it manifested in that the modal contribution of modes that were assumed to have a large contribution to vertical motion were in fact close to zero. As can be observed from the graphs of modal contribution in Appendix A, all plates have a large quantity of modes with no modal contribution. When looking at the response in the centre node this was not noticed, since most of the lower modes with zero modal contribution are modes that have no response in the centre because of their mode shape. The issue was noticed when the response in other nodes than the centre node was studied. It seemed very odd that, for example mode 2, would have no influence on vertical motion in the quarter points of the plates. This, in combination with the large difference between THA and RSA initially caused concern about whether the method itself was faulty. It seemed obvious at the time that mode 2 should have a large influence on the vertical motion. However, in THA no trace of these modes could be seen when studying the deformed plate in ADINA. In Figure 4.15 the largest contributing modes of plate D5 are shown. It is evident that the most influential contributing modes for D5 are the typical beam modes, but only beam mode 1, 3, 5 and 7, which are equivalent to D5's mode 1, 4, 10 and 17, contribute to the vertical response. After going back and reviewing the results of Fagerström and Lindorsson (2017), it was noticed that the beams studied in their report exhibited similar behaviour. The conclusion drawn from this was that uniform shaking of a beam or a plate only activates the modes with an odd number of half sine waves. This find also resulted in the introduction of the term *contributing mode*, which was introduced in Chapter 3 and has been used throughout the thesis.

5.3 Advice and options when using the method

5.3.1 Importance of conservative results and use of the modal combination rules

As was explained in Section 5.2.2 the results of the parameter study is within the expected margin of error for the method. Since the method is supposed to give a

fast method of obtaining approximate results, relatively small errors could be acceptable as long as the results are conservative. Hence, the largest problem with the results is that they are in many cases not conservative. One way to make sure that RSA produce conservative results is to apply the modal combination rule ABSSUM, Equation 2.62. The comparison between THA and RSA consistently resulted in larger response with RSA using ABSSUM. ABSSUM is generally considered to produce insufficiently accurate results, due to large overestimation of response. However, even though the study showed some large differences, using ABSSUM could be a useful alternative from a designer's point of view to get a worst case scenario of the expected response. Possibly the two modal combination rules could be combined to obtain a mean value of the response to obtain conservative results with less overestimation. As has been mentioned previously, all three modal combination rules presented in this thesis are developed to work for smoother response spectra. Ideally, continued work on this method should try to incorporate smooth response spectra. This can be done by so called widening of the response spectrum. This is not covered in the thesis, but is an option worth exploring further.

5.3.2 Optimisation of MATLAB script

As the thesis progressed, it was discovered that a much denser element mesh was required than what was originally anticipated. At this point, MATLAB had to be abandoned when performing the second parameter study. Due to the initial assumption of a much coarser mesh requirement, no substantial effort went into the optimisation of the MATLAB code. MATLAB is definitely a great tool to use for an analysis such as this, and it provided several advantages with respect to ease of obtaining results. However, if MATLAB is to be used the code needs to be well optimised to run the analyses with dense meshes effectively. In this study, it was decided that a switch to ADINA would be a more efficient use of time.

5.3.3 Application of symmetry conditions to reduce model size

Again, the initial assumption at the outset of the work on this thesis was that the element mesh would not need to be very dense. This assumption was partly based on the results of Fagerström and Lindorsson (2017). In their study good convergence was obtained for models with just 16 beam elements. This had the consequence that the work was initiated with the assumption that the plates would not need very dense meshes to converge well, which proved to be false. Since the element mesh density turned out to be very important, it is worth exploring the use of plate symmetry conditions to cut the model size in half, or even to one quarter. That could save immensely on the calculation time when going forward with this method.

5.3.4 Relationship between boundary conditions and accuracy of results

The parameter study included plates with five different sets of boundary conditions (BC), these are shown in Figure 4.1. Naturally, there are far more compositions of BC that could be studied. Each plate type was studied with five different geometries. There is some indication that some BC compositions provide better conformity of results than others between RSA and THA. Plate type B and C had better conformity between THA and RSA compared to plate type A, D and E. However, it is likely that the accuracy of results greatly depend on the the dominant frequencies of the ground motion and the natural frequencies of the plates, so one should not draw general conclusions on how the BC affect the accuracy of the method.

5.4 Further studies

5.4.1 Modal combination rules and widening of response spectra

In this thesis, the modal combination rules ABSSUM and SRSS were used. These two and CQC are the most frequently used modal combination rules when performing RSA for earthquake response. As has been mentioned earlier in the chapter, all three modal combination rules are best used with smooth response spectra. A literature study on an alternative modal combination rule better suited for ground motion caused by train or heavy road traffic could result in improvement of the conformity between THA and RSA for plates. Another option to explore is to widen the response spectra in order to smoothen the spectra used for the analysis, which would increase the accuracy of the modal combination rules.

5.4.2 Absolute response

While our study ended up focusing exclusively on relative response, the simple method to calculate comfort vibrations builds upon comfort weighting of the absolute response. Fagerström and Lindorsson (2017) recommended further studies into a general method to combine the modal contribution with the absolute response in a manner that produce accurate results.

5.4.3 Comfort weighting

The subject of comfort weighting is crucial to the usefulness of the method. Again, Fagerström and Lindorsson (2017) recommended further studies into how to apply comfort weighting to the absolute response in a satisfying manner.

5.5 Final conclusions

The most important lesson learned during the work on this thesis was that plates are significantly more complicated than beams with respect to dynamic effects. Hence, some precautions must be taken when analysing plates, both in RSA and THA. RSA for plates can be significantly affected by the dominant modes of the plate with respect to the dominant frequency range of the response spectra. Convergence studies are crucial both when doing RSA and THA. If possible, convergence studies should be done for both analysis types if the methods are compared with each other. In the case of THA, it is good to remember that the results obtained might not be the worst case scenario, as was the case with a few of the plates in this study. If there are large discrepancies in results, it's good to study the deformed shape in THA to better understand what is happening.

Throughout the analysis in the thesis it has been shown that RSA does not necessarily provide a conservative result. Before choosing which modal combination rule to use in the RSA it is important to consider the intention of the analysis. If results on the safe side are desirable, then ABSSUM could be considered. If a more precise result is desirable SRSS could be the better choice, but one should know that SRSS might result in an underestimation of the response.

Regardless of the choice of modal combination rule, to be able to interpret the results correctly it is necessary to have a good understanding of the interplay between the response spectra and the plate behaviour, and make sure that results have converged.

Bibliography

- Brüel and Kjaer (1989). *Brüel and Kjaer, Human Vibration* (cit. on p. 12).
- Ottosen, Niels Saabye and Hans Petersson (1992). *Introduction to the finite element method*. Prentice-Hall (cit. on p. 15).
- Szilard, Rudolph (2004). *Theories and Applications of Plate Analysis*. Classical, Numerical and Engineering Methods. John Wiley & Sons, Inc. ISBN: 0-471-42989-9 (cit. on p. 27).
- Craig, Roy R. and Andrew J. Kurdila (2006). *Fundamentals of structural dynamics*. John Wiley & Sons, Inc. ISBN: 978-0-471-43044-5 (cit. on pp. 9, 16, 22).
- Feldmann, M, Ch Heinemeyer, and B Völling (2007). *Design guide for floor vibrations, ArcelorMittal, Commercial Sections* (cit. on p. 7).
- Datta, Tushar Kanti (2010). *Seismic analysis of structures*. John Wiley & Sons, Inc. ISBN: 978-0-470-82461-0 (cit. on pp. 23, 24, 25, 26).
- ADINA, Theory and Modeling Guide* (2012). ADINA R & D. Watertown, MA (cit. on p. 29).
- Chopra, Anil K. (2014). *Dynamics of structures*. Theory and applications to earthquake engineering. Pearson Education Limited. ISBN: 978-0132858038 (cit. on pp. 10, 17, 19, 22, 26).
- Pozzi, Matteo and Armen Der Kiureghian (2015). “Response spectrum analysis for floor acceleration”. In: *Earthquake Engineering & Structural Dynamics* 44(12), pp. 2111–2127 (cit. on p. 23).
- Fagerström, Linnea and Philip Lindorsson (2017). “Calculation of vibrations in the early design phase”. MA thesis. Chalmers University of Technology (cit. on pp. v, vii, xix, 1, 2, 33, 74, 76, 77, 78, 79).
- Merriam-Webster (2018). *Merriam-Webster Online Dictionary*. URL: <https://www.merriam-webster.com/dictionary/vibration> (visited on 02/05/2018) (cit. on p. 5).

A

Graphs from the parameter study of modal contribution

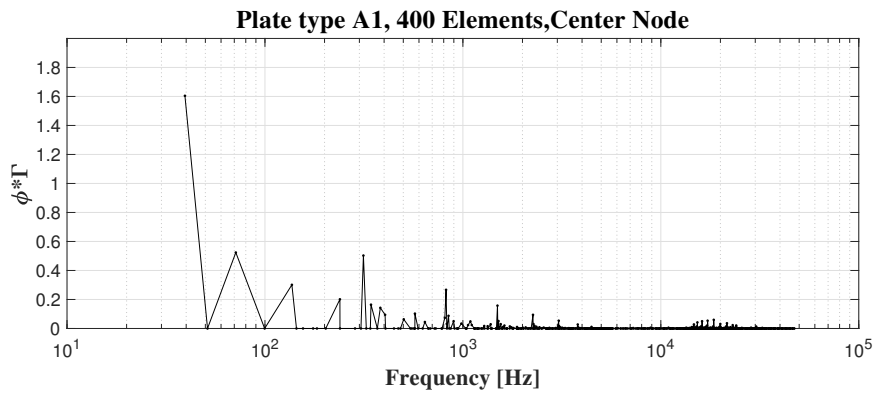


Figure A.1: Modal contribution on the vertical mid DOF of plate A1.

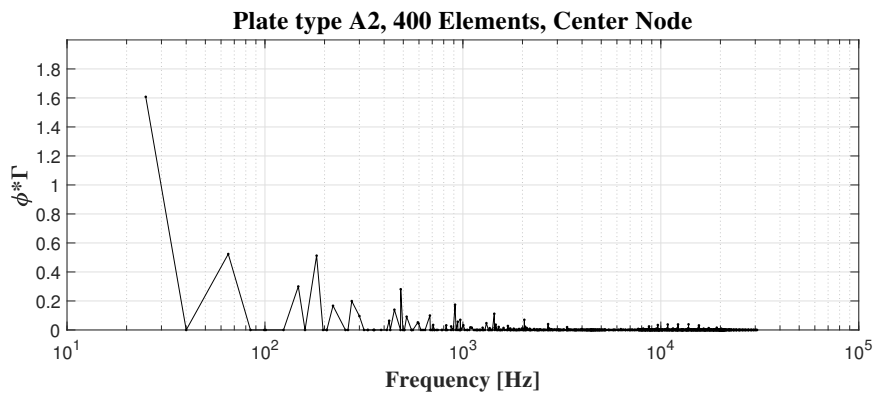


Figure A.2: Modal contribution on the vertical mid DOF of plate A2.

A. Graphs from the parameter study of modal contribution

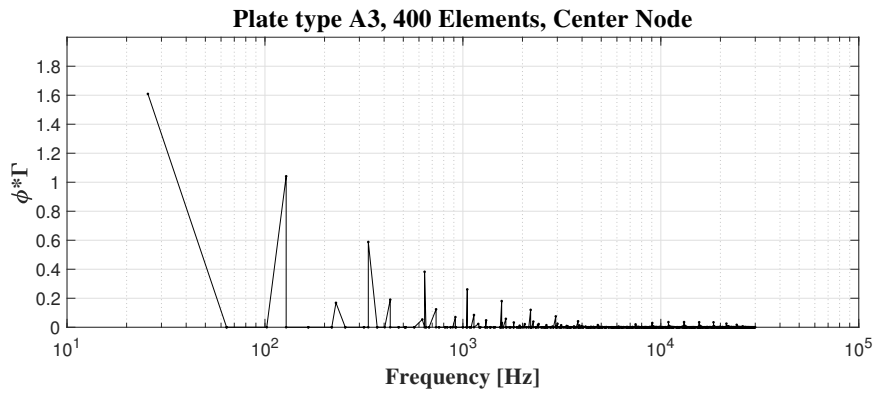


Figure A.3: Modal contribution on the vertical mid DOF of plate A3.

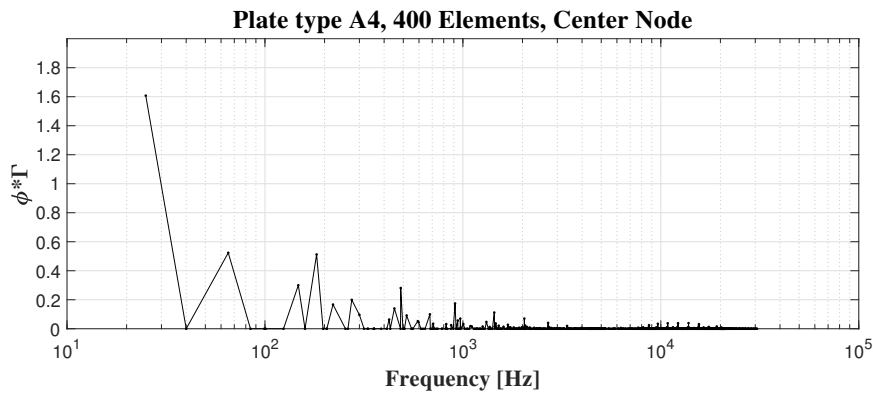


Figure A.4: Modal contribution on the vertical mid DOF of plate A4.

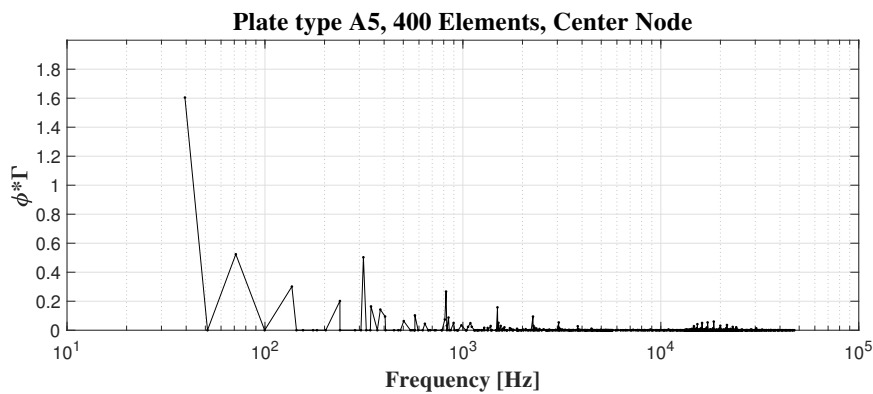


Figure A.5: Modal contribution on the vertical mid DOF of plate A5.

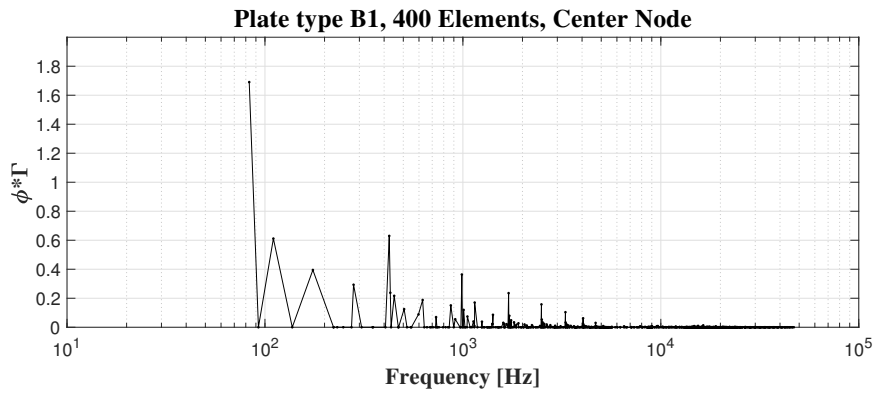


Figure A.6: Modal contribution on the vertical mid DOF of plate B1.

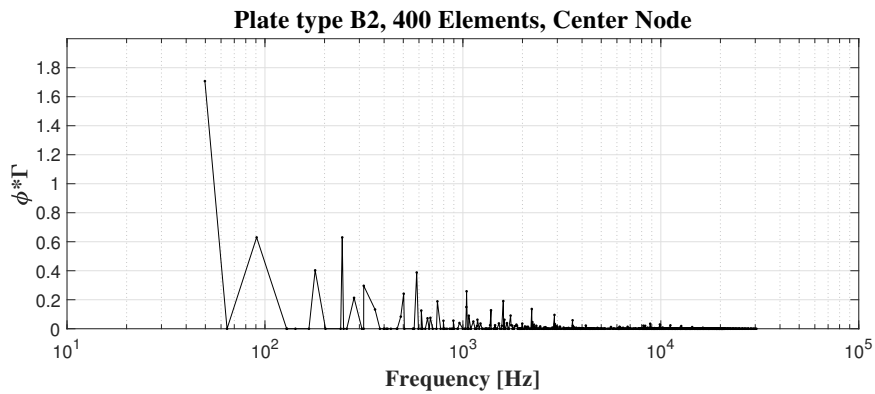


Figure A.7: Modal contribution on the vertical mid DOF of plate B2.

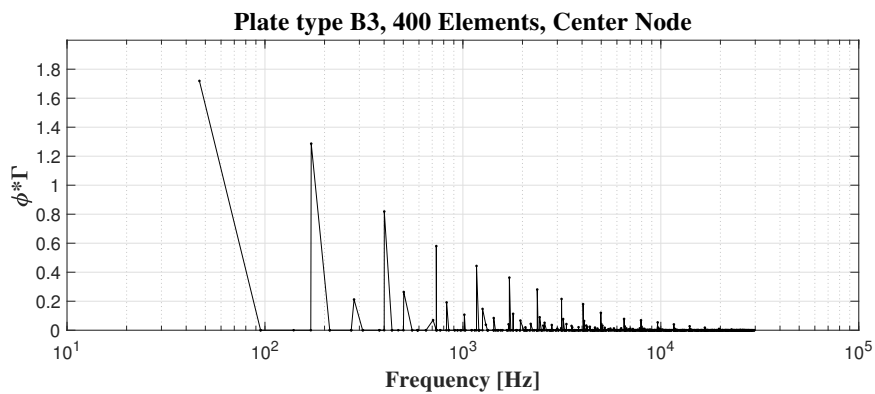


Figure A.8: Modal contribution on the vertical mid DOF of plate B3.

A. Graphs from the parameter study of modal contribution

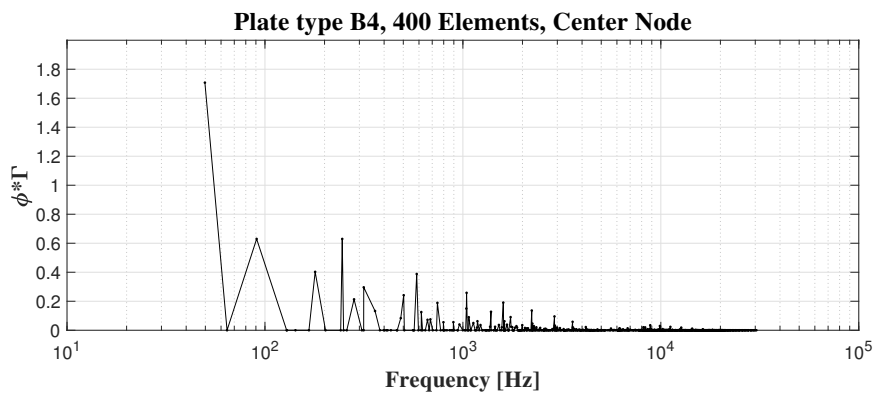


Figure A.9: Modal contribution on the vertical mid DOF of plate B4.

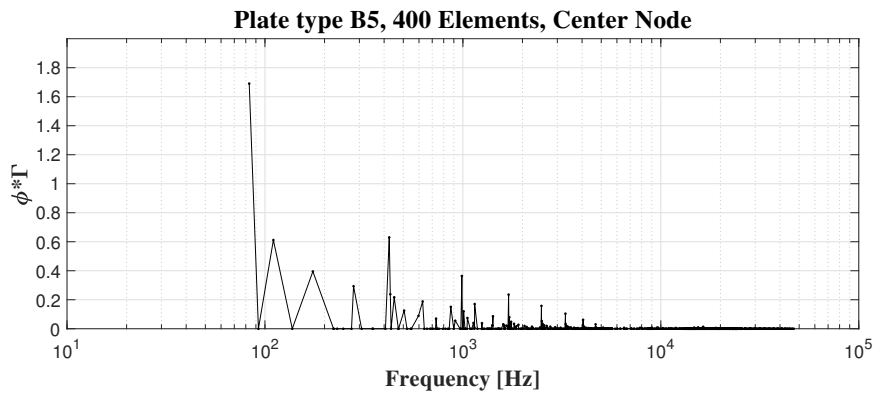


Figure A.10: Modal contribution on the vertical mid DOF of plate B5.

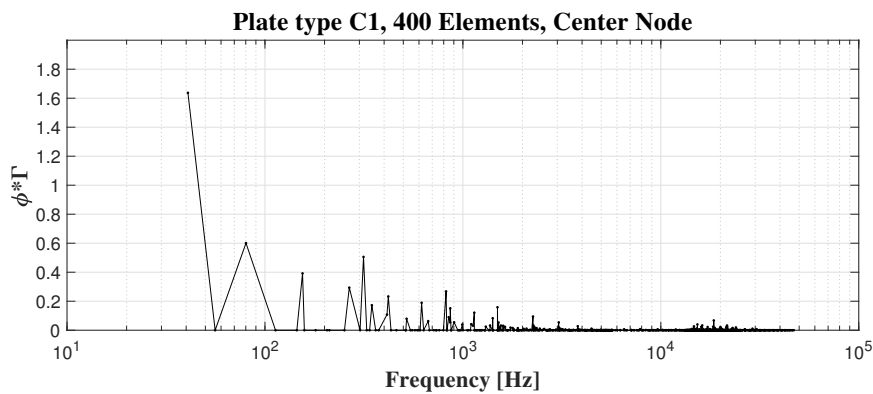


Figure A.11: Modal contribution on the vertical mid DOF of plate C1.

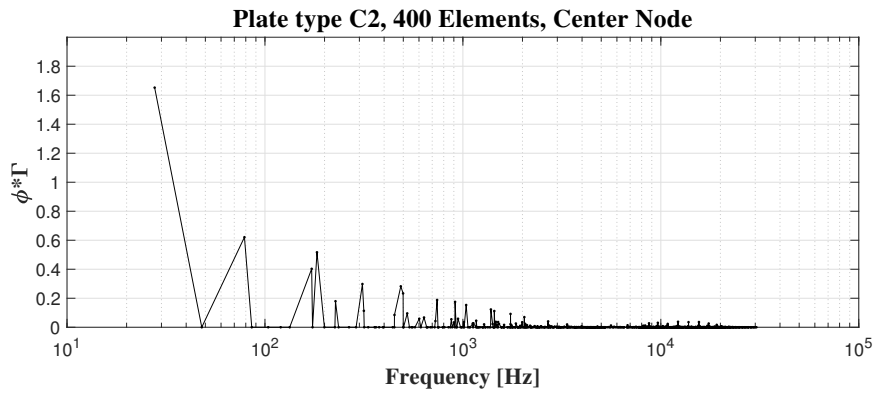


Figure A.12: Modal contribution on the vertical mid DOF of plate C2.

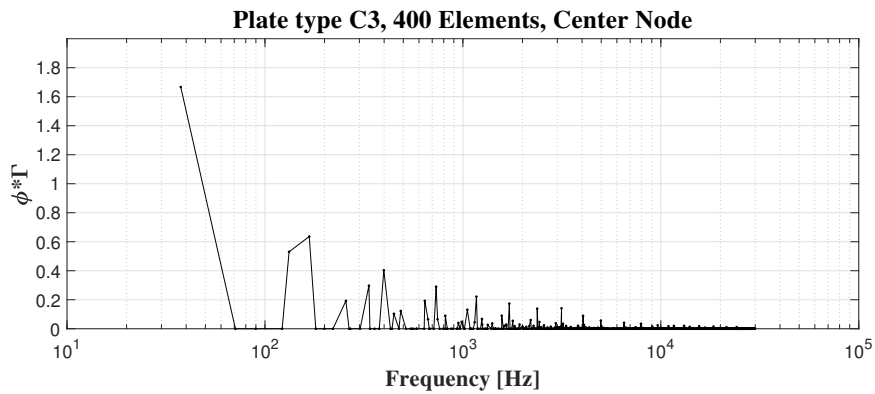


Figure A.13: Modal contribution on the vertical mid DOF of plate C3.

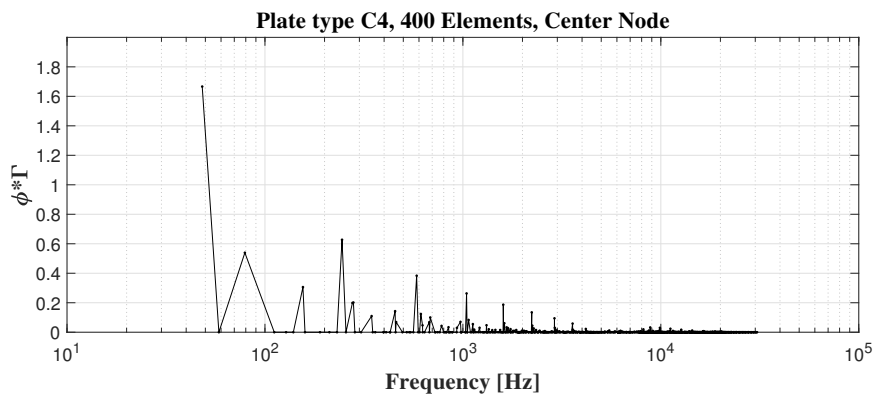


Figure A.14: Modal contribution on the vertical mid DOF of plate C4.

A. Graphs from the parameter study of modal contribution

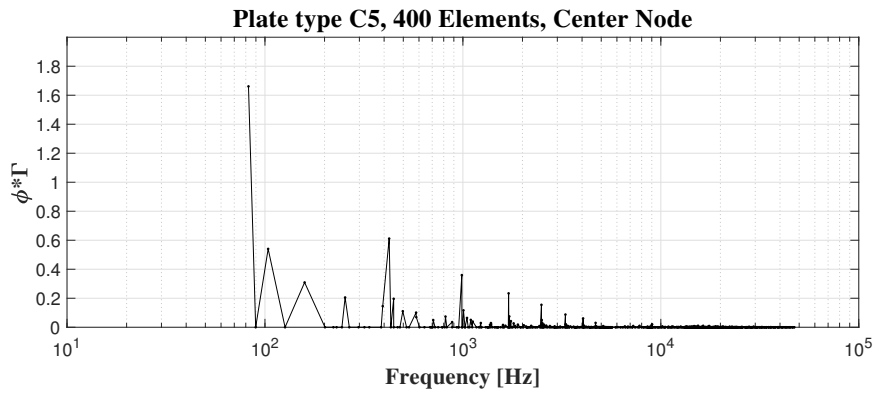


Figure A.15: Modal contribution on the vertical mid DOF of plate C5.

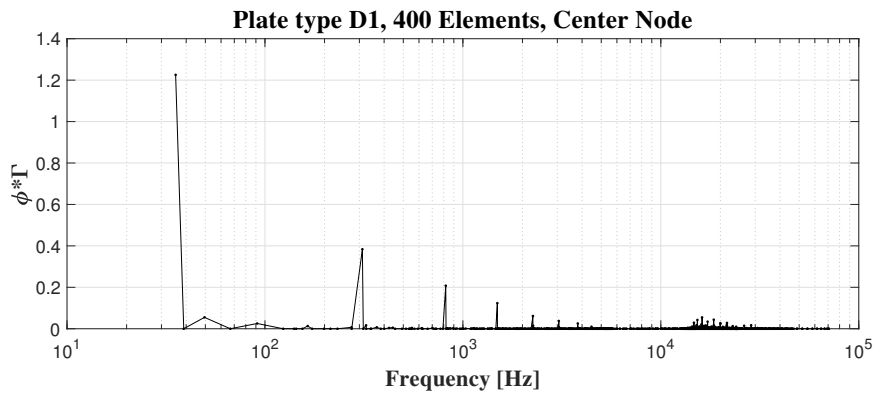


Figure A.16: Modal contribution on the vertical mid DOF of plate D1.

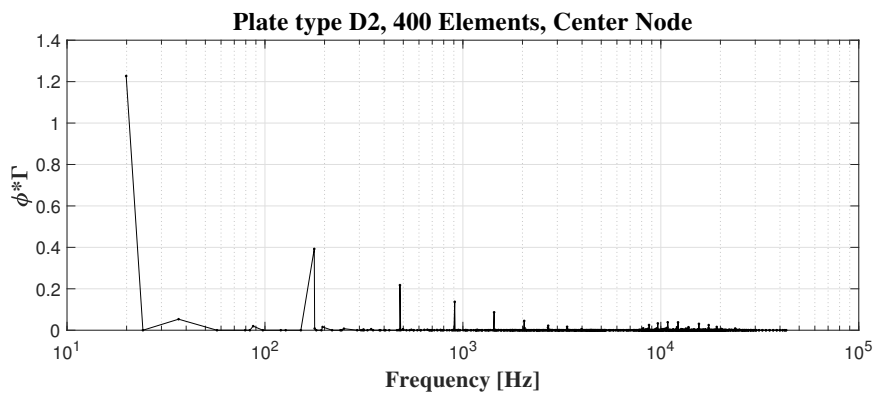


Figure A.17: Modal contribution on the vertical mid DOF of plate D2.

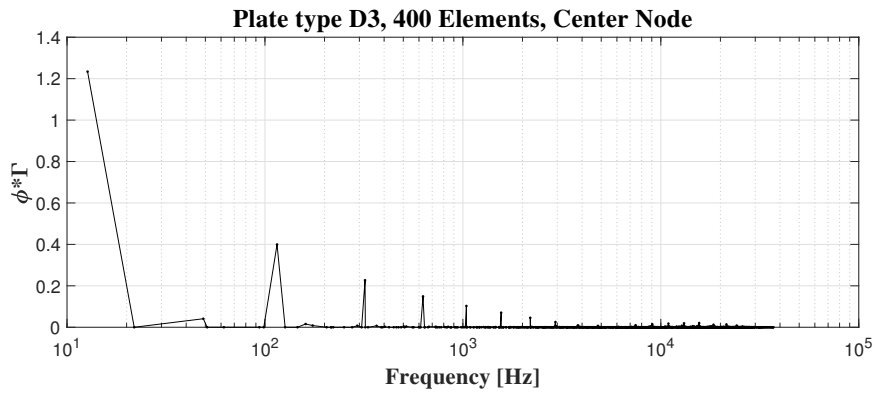


Figure A.18: Modal contribution on the vertical mid DOF of plate D3.

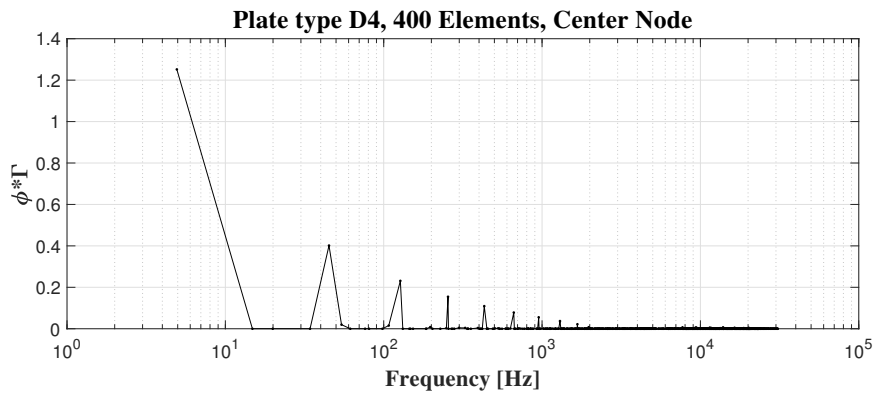


Figure A.19: Modal contribution on the vertical mid DOF of plate D4.

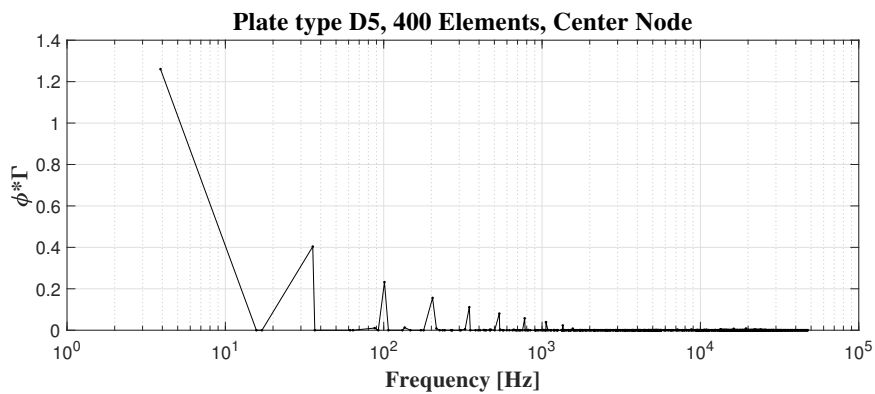


Figure A.20: Modal contribution on the vertical mid DOF of plate D5.

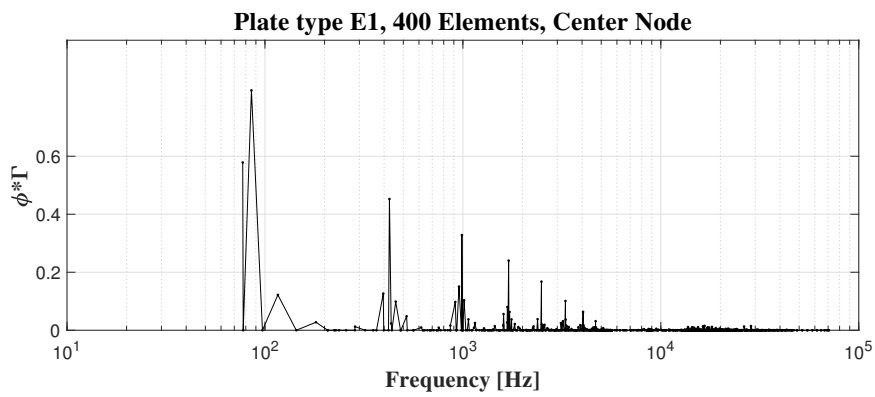


Figure A.21: Modal contribution on the vertical mid DOF of plate E1.

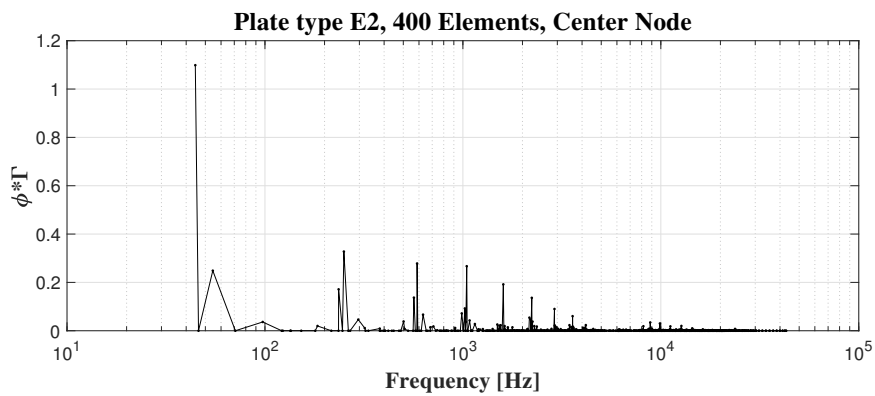


Figure A.22: Modal contribution on the vertical mid DOF of plate E2.

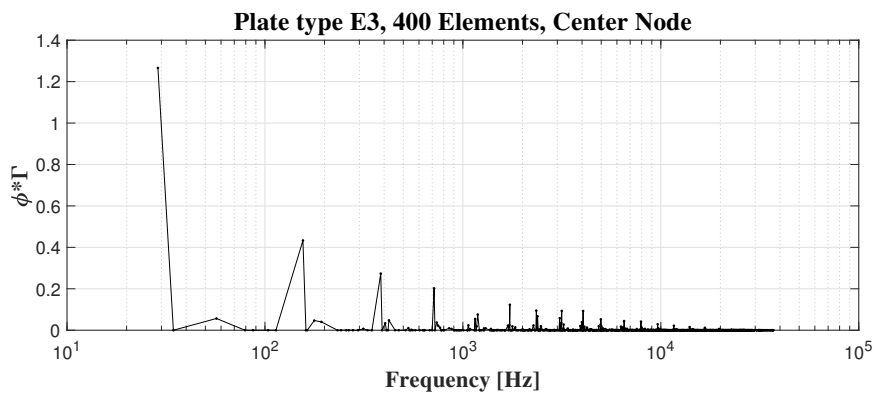


Figure A.23: Modal contribution on the vertical mid DOF of plate E3.

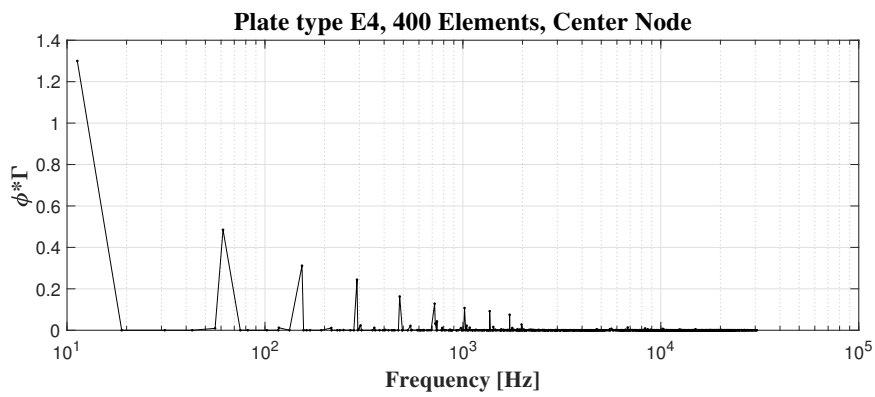


Figure A.24: Modal contribution on the vertical mid DOF of plate E4.

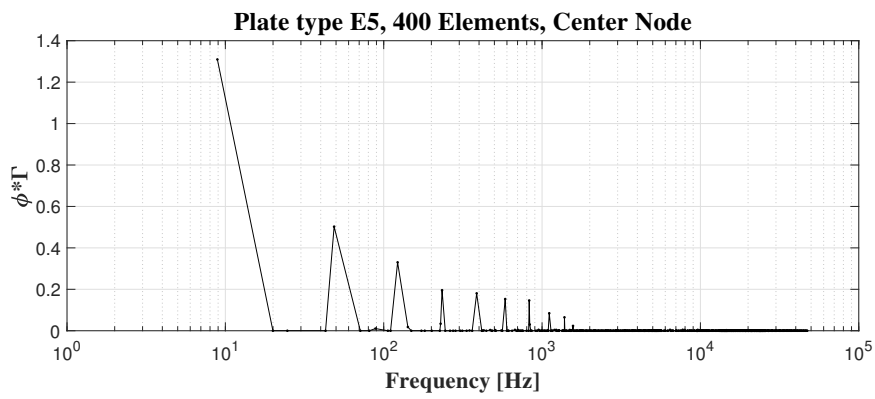


Figure A.25: Modal contribution on the vertical mid DOF of plate E5.

B

Results from the comparison of THA and RSA using a coarse mesh

Table B.1: Comparison of relative acceleration with THA and RSA using a mesh of 20×20 elements.

Plate	a_{rel} [mm/s ²]		Difference
	RSA	THA	[%]
A1/A5	1124	1345	16.46
A2/A4	992	1191	16.71
A3	922	985	6.39
B1/B5	1598	1736	7.97
B2/B4	1704	1853	8.05
B3	1702	1631	-4.35
C1	1074	1410	23.83
C2	986	984	-0.22
C3	1090	1128	3.36
C4	1816	2027	10.41
C5	1693	1681	-0.72
D1	576	594	3.09
D2	445	440	-1.18
D3	411	451	8.87
D4	476	289	-64.43
D5	431	250	-72.17
E1	858	1097	21.82
E2	780	1004	22.35
E3	580	744	21.95
E4	1145	1410	18.75
E5	675	430	-57.04

Table B.2: Comparison of relative velocity with THA and RSA using a mesh of 20×20 elements.

Plate	$v_{rel} \text{ [mm/s]} \times 10^{-1}$		Difference
	RSA	THA	[%]
A1/A5	32.64	33.46	2.44
A2/A4	25.37	31.04	18.26
A3	19.77	24.04	17.75
B1/B5	29.52	30.76	4.03
B2/B4	46.16	50.96	9.42
B3	44.92	45.56	1.41
C1	30.51	37.50	18.65
C2	27.74	34.16	18.79
C3	21.06	25.06	15.96
C4	50.24	58.70	14.41
C5	31.18	29.89	-4.34
D1	14.89	16.58	10.18
D2	11.09	11.51	3.65
D3	12.41	13.44	7.64
D4	12.37	6.64	-86.32
D5	10.48	5.53	-89.60
E1	16.98	23.14	26.64
E2	23.39	29.51	20.73
E3	16.67	19.31	13.66
E4	29.01	34.93	16.95
E5	18.42	12.43	-48.24

Table B.3: Comparison of relative displacement with THA and RSA using a mesh of 20×20 elements.

Plate	$d_{rel} [\text{mm}] \times 10^{-3}$		Difference
	RSA	THA	[%]
A1/A5	9.53	10.88	12.38
A2/A4	8.36	10.62	21.26
A3	7.80	7.66	-1.78
B1/B5	6.06	6.47	6.34
B2/B4	13.37	14.05	4.80
B3	13.72	13.47	-1.86
C1	8.71	10.86	19.73
C2	11.87	11.88	0.10
C3	6.82	7.19	5.23
C4	14.77	17.00	13.09
C5	6.48	6.30	-2.76
D1	4.93	5.07	2.78
D2	4.69	4.94	5.08
D3	4.94	5.19	4.95
D4	6.32	5.08	-24.35
D5	5.14	4.43	-16.07
E1	3.58	5.06	29.24
E2	6.73	8.32	19.16
E3	5.93	6.41	7.54
E4	8.48	10.97	22.65
E5	6.71	6.07	-10.60

C

Results from the comparison of THA and RSA using ABSSUM

Table C.1: Comparison of relative acceleration with THA and RSA using ABSSUM.

	a_{rel} [mm/s ²]		Difference
	RSA	THA	[%]
A1/A5	2212	1182	-87.12
A2/A4	2398	1291	-85.76
A3	1666	970	-71.82
B1/B5	2731	1754	-55.65
B2/B4	3135	1805	-73.67
B3	2856	1897	-50.60
C1	2163	1195	-81.06
C2	2365	1018	-132.42
C3	2182	1059	-106.02
C4	3121	2045	-52.65
C5	2527	1557	-62.22
D1	805	611	-31.74
D2	739	476	-55.23
D3	698	405	-72.26
D4	905	308	-193.67
D5	901	235	-283.40
E1	1275	1042	-22.33
E2	1229	951	-29.12
E3	1037	660	-57.11
E4	1933	1181	-63.62
E5	1216	415	-193.18

Table C.2: Comparison of relative velocity with THA and RSA using ABSSUM.

	v_{rel} [mm/s] $\times 10^{-1}$		Difference
	RSA	THA	[%]
A1/A5	48.57	35.96	-35.07
A2/A4	47.45	37.78	-25.59
A3	27.69	24.19	-14.45
B1/B5	41.07	30.85	-33.14
B2/B4	62.01	52.00	-19.26
B3	54.13	45.54	-18.87
C1	45.17	34.93	-29.31
C2	44.33	29.20	-51.80
C3	32.21	23.68	-36.01
C4	64.84	55.63	-16.56
C5	39.62	29.74	-33.22
D1	17.37	16.64	-4.38
D2	14.33	11.36	-26.12
D3	16.33	12.72	-28.41
D4	20.11	5.94	-238.57
D5	17.88	6.00	-197.86
E1	24.01	22.39	-7.26
E2	30.22	27.81	-8.69
E3	23.62	18.54	-27.36
E4	42.88	29.94	-43.24
E5	28.26	11.86	-138.33

Table C.3: Comparison of relative displacement with THA and RSA using ABSSUM.

	$d_{rel} [\text{mm}] \times 10^{-3}$		Difference
	RSA	THA	[%]
A1/A5	12.73	10.65	-19.51
A2/A4	13.22	12.37	-6.89
A3	9.00	8.08	-11.31
B1/B5	7.81	6.31	-23.75
B2/B4	15.91	14.38	-10.65
B3	13.83	13.14	-5.26
C1	11.59	10.40	-11.46
C2	14.36	13.17	-9.01
C3	8.04	6.90	-16.44
C4	17.43	16.88	-3.27
C5	7.95	6.30	-26.23
D1	5.65	5.11	-10.53
D2	5.12	4.90	-4.58
D3	5.86	5.14	-13.88
D4	8.57	5.33	-60.60
D5	7.34	4.53	-62.17
E1	5.10	4.82	-5.82
E2	8.38	7.86	-6.59
E3	7.33	6.65	-10.22
E4	12.79	9.87	-29.59
E5	9.71	6.03	-60.96

D

MATLAB code

D.1 RSA code

```
%-----%  
% RSA.m Script for calculating response spectra for  
%relative response using ground motion from excel sheet  
% By Nils Rasmak & Fredrik Hellquist (2018)  
%-----%  
clc  
clear all  
close all  
clearvars -except MPFResults  
%Checks the type of input signal chosen  
[~,storage] = xlsread("RSA_original.xlsx","Start","J2");  
choice=string(storage);  
%tot is a variable with the count of indata points  
%mass is for this script chosen as unity, while k is changed  
%based on desired frequency  
M = 1;  
%damping ratio zeta is an input that can be chosen  
zeta = xlsread("RSA_original.xlsx","Start","G3");  
%newmark coefficient alfa  
alfa = xlsread("RSA_original.xlsx","Start","G4");  
%newmark coefficient beta  
beta = xlsread("RSA_original.xlsx","Start","G5");  
%starting frequency for the response spectrum  
fstart = xlsread("RSA_original.xlsx","Start","G7");  
%ending frequency for the response spectrum  
fend=xlsread("RSA_original.xlsx","Start","G8");  
%f is used for loops  
%f = fstart;  
%number of frequency increments  
fstep = xlsread("RSA_original.xlsx","Start","G10");  
%size of frequency increment for each iteration  
df = xlsread("RSA_original.xlsx","Start","G9");
```

```

%Initial Conditions
%initial velocity
v0 = xlsread("RSA_original.xlsx", "Start", "G12"); %[m/s]
%initial displacement
d0 = xlsread("RSA_original.xlsx", "Start", "G13"); %[m]
%creates frequency vector and reads the input signal
% fVec=fCut;
% fVec=zeros(fstep,1);
% for i=1:fstep
%     fVec(i,1)=fstart*(1+df/100)^(i-1);
% end
%%

if choice == "Displacement"
Tot = xlsread("RSA_original.xlsx", "Start", "Z1");
inSignalRange=strcat('Z3:Z', num2str(Tot+2));
elseif choice == "Velocity"
Tot = xlsread("RSA_original.xlsx", "Start", "X1");
inSignalRange=strcat('X3:X', num2str(Tot+2));
elseif choice == "Acceleration"
Tot = xlsread("RSA_original.xlsx", "Start", "K3");
inSignalRange=strcat('J3:J', num2str(Tot+2));
end
timeRange=strcat('I3:I', num2str(Tot+2));
timevec=xlsread("RSA_original.xlsx", "Start", timeRange);
inSignalVec=xlsread("RSA_original.xlsx", ...
"Start", inSignalRange);
shortIndataPoints=round(Tot/3);
shortIndata=zeros(shortIndataPoints,1);
for i = 1:shortIndataPoints
shortIndata(i)=1+3*(i-1);
end

inSignalVec=inSignalVec(shortIndata');
timevec=timevec(shortIndata');

Tot=shortIndataPoints;


---


%Input signal processing
%Checks the chosen input signal format and allocates
%vector sizes based %on the number of derivatives
%needed to convert the input signal to
%acceleration
dt = timevec(2) - timevec(1);
if choice == "Displacement"

```

```

%two derivatives needed for conversion to acceleration
derivativeOrder = 2;
dgVec=zeros(Tot,1);
vgVec=zeros(Tot - 1,1);
agVec=zeros(Tot - 2,1);
for i = 1:length(dgVec)
dgVec(i) = inSignalVec(i);
end
for i = 1:length(vgVec)
vgVec(i) = (inSignalVec(i + 1) - inSignalVec(i)) / ...
(timevec(i + 1) - timevec(i));
end
for i = 1:length(agVec)
agVec(i) = (vgVec(i + 1) - vgVec(i)) / ...
(timevec(i + 1) - timevec(i));
end
elseif choice == "Velocity"
%one derivative needed for conversion to acceleration
derivativeOrder = 1;
dgVec=zeros(Tot - 1,1);
vgVec=zeros(Tot,1);
agVec=zeros(Tot - 1,1);
vtot = 0;
for i = 1:length(vgVec)
vgVec(i,1) = inSignalVec(i,1);
vtot = vtot + vgVec(i,1);
end
for i = 1:length(agVec)
agVec(i,1) = (inSignalVec(i + 1) - inSignalVec(i)) ...
/ (timevec(i + 1) - timevec(i));
end
d_past = 0;
vim = vtot / length(vgVec);
for i = 1:length(dgVec)
dgVec(i,1) = d_past + ...
(((inSignalVec(i + 1) + inSignalVec(i)) / 2) * ...
(timevec(i + 1) - timevec(i))); vim;
d_past = dgVec(i);
end
elseif choice == "Acceleration"
%no derivatives needed for conversion to acceleration
derivativeOrder = 0;
dgVec=zeros(Tot - 3,1);
vgVec=zeros(Tot - 2,1);
agVec=zeros(Tot - 1,1);
atot=0;

```

```

vtot=0;
for i = 1:length(agVec)
agVec(i) = inSignalVec(i);
atot = atot + agVec(i,1);
end
v_past = 0;
aim = atot / length(agVec);
for i = 1:length(vgVec)
vgVec(i,1) = v_past + ...
((agVec(i + 1) + agVec(i)) / 2 - aim ) * ...
(timevec(i + 1) - timevec(i));
vtot=vtot+vgVec(i,1);
v_past = vgVec(i);
end
vgVec(1,1)=0;
d_past = 0;
vim = vtot / length(vgVec);
for i = 1:length(dgVec)
dgVec(i,1) = d_past + ...
((vgVec(i + 1) + vgVec(i)) / 2 - vim ) * ...
(timevec(i + 1) - timevec(i));
d_past = dgVec(i);
end
end
maxDataPoints=min( [length(agVec); length(vgVec); ...
length(dgVec) ] );
% %


---


%% Create Response Spectrum
%Preallocate vector size based on number of time steps
%and derivative order
[~,IMPF]=size(MPFResults);
nOfPlates=IMPF/3;
% nOfPlates=length(fVec);
RSAResults={1,nOfPlates*6};
for RSALoop=1:nOfPlates
fVec=MPFResults{1,RSALoop*3-1};
fstep=length(fVec);
%when using the MPFs for frequencies%
%force
ftVec=zeros((Tot - derivativeOrder),1);
%relative acceleration
aVec=zeros((Tot - derivativeOrder),1);
%relative velocity
vVec=zeros((Tot - derivativeOrder),1);
%relative displacement
dVec=zeros((Tot - derivativeOrder),1);

```

```

%absolute acceleration
aabsVec=zeros((Tot - derivativeOrder),1);
%absolute (total) velocity
vabsVec=zeros((Tot - derivativeOrder),1);
%absolute (total) displacement
dabsVec=zeros((Tot - derivativeOrder),1);
%maximum values of absolute (total) acceleration
aabsmaxVec=zeros(fstep,1);
%maximum values of absolute (total) velocity
vabsmaxVec=zeros(fstep,1);
%maximum values of absolute (total) displacement
dabsmaxVec=zeros(fstep,1);
%maximum values of relative acceleration
arelmaxVec=zeros(fstep,1);
%maximum values of relative velocity
vrelmaxVec=zeros(fstep,1);
%maximum values of relative displacement
drelmaxVec=zeros(fstep,1);
%% Loop cycling through all the chosen frequencies
for j = 1:fstep
f = fVec(j,1);
k = 4 * pi ^ 2 * f ^ 2 * M; %[N/m] spring stiffness
W = sqrt(k / M); %[rad/s] natural frequency omega
c = 2 * zeta * W * M; %[Ns/m] damping coefficient c
%initial conditions for time loop
ag0 = agVec(1,1);
f0 = -M * ag0; %[N]
a0 = f0 / M - 2 * zeta * W * v0 - W ^ 2 * d0; %[m/s^2]
aabs0 = a0 - f0 / M; %[m/s^2]
dp = d0; %suffix p stands for previous
vp = v0;
ap = a0;
%assigns the initial conditions to the vectors
aabsVec(1,1) = aabs0;
ftVec(1,1) = f0;
aVec(1,1) = a0;
vVec(1,1) = v0;
dVec(1,1) = d0;
%[m] effective mass, used for Newmark method
meff = M + c * alfa * dt + k * beta * dt ^ 2;
%Loop cycling through the time steps starting from
%position 2
for i = 2:maxDataPoints
ag = agVec(i,1); %ground acceleration
vg = vgVec(i,1); %ground velocity
dg = dgVec(i,1); %ground velocity

```

```

ft = -M * ag;    %force
%relative acceleration
a = ( ...
-M * ag ...
- c * ((1 - alfa) * dt * ap + vp) ...
- k * ((1 / 2) * dt ^ 2 * (1 - 2 * beta) * ...
ap + dt * vp + dp)) / meff;
%relative velocity
v = ap * dt * (1 - alfa) + a * dt * alfa + vp;
%relative displacement
d = ap * (1 / 2) * dt ^ 2 * (1 - 2 * beta) ...
+ a * dt ^ 2 * beta + vp * dt + dp;
aabs = a + ag; %absolute acceleration
agVec(i,1) = ag;
ftVec(i,1) = ft;
aVec(i,1) = a;
vVec(i,1) = v;
dVec(i,1) = d;
aabsVec(i,1) = aabs;
vabs = v + vg;
vabsVec(i,1) = vabs;
dabs = d + dg;
dabsVec(i,1) = dabs;
ap = a;
vp = v;
dp = d;
end
aabsmaxVec(j,1) = max(abs(aabsVec));
vabsmaxVec(j,1) = max(abs(vabsVec));
dabsmaxVec(j,1) = max(abs(dabsVec));
arelmaxVec(j,1) = max(abs(aVec));
vrelmaxVec(j,1) = max(abs(vVec));
drelmaxVec(j,1) = max(abs(dVec));
end
RSAResults{1,RSALoop*6-5}=arelmaxVec;
RSAResults{1,RSALoop*6-4}=vrelmaxVec;
RSAResults{1,RSALoop*6-3}=drelmaxVec;
RSAResults{1,RSALoop*6-2}=aabsmaxVec;
RSAResults{1,RSALoop*6-1}=vabsmaxVec;
RSAResults{1,RSALoop*6}=dabsmaxVec;
end
%%
%clearvars -except MPFResults RSAResults
modalResponse=zeros(nOfPlates,3);
format long
for i =1:nOfPlates

```

```

Arel=RSAResults{1,i*6-5};
Vrel=RSAResults{1,i*6-4};
Drel=RSAResults{1,i*6-3};
MPF=MPFResults{1,i*3};
modalResponseA=(MPF.*Arel).^2;
modalResponseV=(MPF.*Vrel).^2;
modalResponseD=(MPF.*Drel).^2;
modalResponse(i,1)=sqrt(sum(modalResponseA));
modalResponse(i,2)=sqrt(sum(modalResponseV));
modalResponse(i,3)=sqrt(sum(modalResponseD));
end
% %%
% freqs=zeros(5,1);
% for i=1:5
% blagg=MPFResults{1,i*3-1};
% freqs(i,1)=blagg(1,1);
% end
% %% Plot Response spectrum
% axlbl=@(h)[xlabel(h,'f [Hz]'), ...
%legend('Relative','Absolute')];
%
% figure(1)
% semilogx(fVec(:,1),arelmaxVec(:,1),'k-');
% hold on
% %loglog(fVec(:,1),aabsmaxVec(:,1),'k--');
% title('Relative acceleration')
% grid on
% axlbl(gca);
% ylabel('a [mm/s^2]');
% figure(2)
% semilogx(fVec(:,1),vrelmaxVec(:,1),'k-');
% hold on
% %loglog(fVec(:,1),vabsmaxVec(:,1),'k--');
% title('Relative velocity')
% axlbl(gca);
% ylabel('v [mm/s]');
% grid on
% figure(3)
% semilogx(fVec(:,1),drelmaxVec(:,1),'k-');
% hold on
% %loglog(fVec(:,1),dabsmaxVec(:,1),'k--');
% title('Relative displacement')
% axlbl(gca);
% ylabel('d [mm]');
% grid on
% figure(4)

```

```

% semilogx(fVec(:,1), aabsmaxVec(:,1), 'k--');
% title('Absolute acceleration')
% axlbl(gca);
% ylabel('a [mm/s^2]');
% grid on
% figure(5)
% loglog(fVec(:,1), vabsmaxVec(:,1), 'k--');
% title('Absolute velocity')
% axlbl(gca);
% ylabel('v [mm/s]');
% grid on
% figure(6)
% loglog(fVec(:,1), dabsmaxVec(:,1), 'k--');
% title('Absolute displacement')
% axlbl(gca);
% ylabel('d [mm]');
% grid on
%
% axlbl = @(h) [xlabel(h, 't [s]')];
% figure(7)
% plot(timevec(1:end-1,1), agVec(:,1), 'k-');
% title('Ground acceleration')
% grid on
% axlbl(gca);
% ylabel('a [mm/s^2]');
% figure(8)
% plot(timevec(:,1), vgVec(:,1), 'k-');
% title('Ground velocity')
% axlbl(gca);
% ylabel('v [mm/s]');
% grid on
% figure(9)
% plot(timevec(1:end-1,1), dgVec(:,1), 'k-');
% title('Ground displacement')
% axlbl(gca);
% ylabel('d [mm]');
% grid on

```

D.2 MPF code

```

%-----%
% plate.m Script for calculating modal contribution for
% rectangular plates
% By Nils Rasmark & Fredrik Hellquist (2018)

```

```

%-----%
clc
clear all
close all
tic
%-----%
% This section is currently disabled due to performance
% issues, it enables reading the indata from the plate
% excel sheet
%-----%
% T = readtable('Plate.xlsx', 'Range', 'C1:C12', ...
% 'ReadVariableNames', false);
% Indata=T.Var1;
% a = str2double(Indata(1));
% b = str2double(Indata(2));
% th = str2double(Indata(3)); %Thickness of plate
% nelX = str2double(Indata(4));
% nelY = str2double(Indata(5));
% E = str2double(Indata(6)); %E-modulus
% density = str2double(Indata(7)); % density
% ny = str2double(Indata(8)); %Poissons ratio
% SideADown = string(Indata(12));
% SideATop = string(Indata(11));
% SideBLeft = string(Indata(9));
% SideBRight = string(Indata(10));
toc

% a = xlsread("Plate.xlsx", "Start", "B2");
% b = xlsread("Plate.xlsx", "Start", "B3");
% Thickness of plate
% th = xlsread("Plate.xlsx", "Start", "B4");
% nelX = xlsread("Plate.xlsx", "Start", "B5");
% nelY = xlsread("Plate.xlsx", "Start", "B6");
% E-modulus
% E = xlsread("Plate.xlsx", "Start", "B8");
% density
% density = xlsread("Plate.xlsx", "Start", "B9");
% Poissons ratio
% ny = xlsread("Plate.xlsx", "Start", "B10");
%-----%
% If the excel indata is disabled these variable settings
% needs to be enabled
SideADown = "SS"; % Fixity choices, "SS", "fixed" or "free"
SideATop = "SS";
SideBLeft = "free";
SideBRight = "free";

```

```

ifPlot="Yes";
%If "Yes", will plot nModes number of contributing modes
nModes=30; %Number of modes to plot
nelX = 20; %Number of elements X direction
nelY = 20; %Number of elements Y direction
E = 30e9; %E-modulus
density = 2500; % density
ny = 0.2; %Poissons ratio

%-----%
%Setup for FEM analysis
nel = nelX * nelY; %total number of elements
nex = nelX + 1; %number of nodes, x direction
ney = nelY + 1; %number of nodes, y direction
nNode = nex * ney; % total number of nodes
ndof = nNode * 3; %total number of Dofs
Dof = Dofs(nNode); %Creates the Dof matrix
% Creates the Edof Matrix
Edof = Edofs(nel, nelX, nelY, Dof);
%Creates the BC matrix and the number of locked Dofs
[BC,nlockedDofs] = bc(nelY, nelX, nex, ney, nNode, ...
SideADown,SideATop, SideBLeft,SideBRight);
%number of free dofs
nfreeDofs = ndof - nlockedDofs;
%These two lines creates a column vector
freeDof=linspace(1,ndof,ndof)';
freeDof(BC)=[]; %containing all free Dofs
%Vector with all free Dofs followed by all locked
%by the boundary conditions
sorted_DOOF=[freeDof;BC];
%-----%
%When studying one plate only, set a to desired size and
%plate ratio such that b gets the desired dimension
a=[3];
b=[9];
nPlate=length(a);
th = 0.2; %Thickness of plate.
%-----%
%When analysing multiple plates, set the plate ratios for
%the number of desired plates and the plate thickness in
%thVec
%plateRatio(:,1)=[1]';
%For multiple plate check
%thVec =[0.008 0.032 0.128 0.512 2.048 8.192];
%-----%
%For writing plate ratio, frequencies and PHI*MPF to an

```

```

%excel sheet this must be enabled and set to desired values.
% RatioColumn='B';
% fColumn='A';
% MPFColumn='B';


---


%When first mode frequency with corresponding MPF
%is of interest
%f_and_MPF=zeros(6,2);
%Bigloop will run one iteration per plate ratio
% specified in the plateRatio vector. If the plate ratio
%only has one value it will just run once
MPFResults={1,nPlate*3};
vertDof=zeros(nNode,1);
for i=1:nNode
vertDof(i,1)=1+(i-1)*3;
end
Maxdof=zeros(length(a),1);
for bigLoop = 1:nPlate %bigloop start
%th=thVec(bigLoop); %for analysis of several plates
%with variable %thickness, comment this and uncomment
%the single thickness parameter above
%special case analysis of multiple quadratic plates
%a=2^(bigLoop-1);
%Recalculating b dimension for each loop
%b = a/nPlate(bigLoop);
lx = a(bigLoop) / nelX; % Element width
ly = b(bigLoop) / nelY; % Element height
k=zeros(ndof, ndof); %global stiffness matrix
m=zeros(ndof, ndof); %global mass matrix
%Calculation of element stiffness and mass matrix and
%assembling into global
for i = 1:nel
[ke,me]=plateDyn(ny, E, density, lx, ly, th);
k = assem(Edof(i,:), k, ke);
m = assem(Edof(i,:), m, me);
end
%reduced global stiffness matrix w.r.t BC
k2=k(freeDof, freeDof);
%reduced global mass matrix w.r.t BC
m2=m(freeDof, freeDof);
%eigenvalues and eigenvectors
[L, eigVect]=eigen(k,m,BC(:,1));
%Norms the eigenvectors to 1
for i=1:nfreeDofs
eigVect(:,i) = eigVect(:,i)/norm(eigVect(:,i));
end

```

```

disp( 'Eigenvalue_solutions_completed' ); toc
Phi=eigVect(freeDof, :); %Extracts eigenvectors for free Dofs
f=sqrt(L)/(2*pi); %recalculates eigenvalues to Frequency [Hz]
midDof=(nex*ney/2)*3-1/2; %Identifies the middle vertical DoF
%Calculates modal participation factors
MPF=MPF_Plate(BC, ndof, k, Phi, nNode, m2, nfreeDofs);
%Midresponse is MPF*PHI
midResponse=zeros( length( eigVect ), length( MPF ) );
vertEigen=zeros( size( eigVect ) );
vertEigen( vertDof, :) = eigVect( vertDof, : );
for allMPF=1:length( MPF )
midResponse( :, allMPF ) = ( vertEigen( :, allMPF ) .* MPF( allMPF ) );
end
midResponseSquared=midResponse.^2;
allSum=sum( midResponseSquared, 2 );
allSRSS=(allSum).^0.5;
[ maxVal, Maxdof( bigLoop ) ] = max( allSRSS );
%Maxdof(:)=[316 346 631 661 946 976];
%Maxdof(:)=[661 976];
Maxdof=[midDof];
%Positions contains the mid responses that have a value
%larger than 10^-9. This is to remove MPF*PHI which
%have very low contribution
midResponseMax=(eigVect( Maxdof( bigLoop ), :))' .* MPF;
Positions=((abs(midResponseMax( :, 1 )) > 10^-100)');
%fCut and MPFCut contains the frequency and mid response
%where the contribution is larger than 10^-9;
fCut=f( Positions, 1 );
MPFCut=midResponseMax( Positions, : );
%Dimensions=[strcat( 'a=', num2str( a( bigLoop ) ) );
%strcat( 'b=', num2str( b( bigLoop ) ) )];
pos1=bigLoop*3-2;
pos2=bigLoop*3-1;
pos3=bigLoop*3;
MPFResults{1, pos1}=num2str( Maxdof( bigLoop ) );
MPFResults{1, pos2}=fCut;
MPFResults{1, pos3}=MPFCut;
%%-----%
%If the frequency and mid response is of interest, if used
%be sure to uncomment the declaration of this matrix above
% f_and_MPF( bigLoop, 1 ) = f( 1 );
% f_and_MPF( bigLoop, 2 ) = midResponse( 1 );
%%-----%
toc
disp( 'Iteration_completed' );
%run RSA.m

```

```

%%-----%
% Writes the fCut, MPFCut and ratio to excel sheet
% sizeRatio=a/b;
% sheet='Sheet3';
% nEle=length(MPFCut);
% fRange= strcat(sprintf('%c3:%c',fColumn,fColumn), ...
% num2str(nEle+2));
% MPFRange= strcat(sprintf('%c3:%c',MPFColumn, ...
% MPFColumn), num2str(nEle+2));
% RatioRange= sprintf('%c1:%c1',RatioColumn,RatioColumn);
% xlswrite('FandMPF.xlsx',fCut,sheet,fRange);
% xlswrite('FandMPF.xlsx',MPFCut,sheet,MPFRange);
% xlswrite('FandMPF.xlsx',sizeRatio,sheet,RatioRange);
% RatioColumn=RatioColumn+2;
% fColumn=fColumn+2;
% MPFColumn=MPFColumn+2;
% toc
%%-----%

end %BIGLOOP END
toc
disp('Finished!')
% clearvars -except MPFResults
% for i= 1:length(dimensions)
% %%
% set(0,'DefaultTextFontname','CMU Serif')
% nelString=num2str(nel);
% %platype=string(['316' '346' '631' '661' ...
% '946' '976']);
% for i = 1:length(a)
%figure(i)
%plotFreq=MPFResults{1,i*3-1};
%plotMPF=abs(MPFResults{1,i*3});
%semilogx(plotFreq,plotMPF,'k.-');
%hold on
%plotTitle=strcat({'Plate type'},{'D5'},{' ',''}, ...
%{nelString}, %{' '},{ 'Elements'},{ ',' , Dof '}, ...
% num2str(Maxdof(i)));
%title(plotTitle);
%xlabel('Frequency [Hz]');
%ylabel('Modal contribution');
%nTickMarks=ceil(plotMPF(1)/0.2);
%tickVecY=(linspace(0,nTickMarks*0.2,nTickMarks+1));
%yticks(tickVecY)
%grid on
%hold off

```

```

%end
%
%test=sum(midResponse ');
%
%Surface plots of all modes
% This will plot nMode number of modes, but only plot
%the modes which satisfy the condition that
%PHI*MPF> 10^-9;
% Matrix containing all the vertical Dofs,
%used for surface plot purposes
vertDofMatrix=zeros(nNode/nex , nNode/ney);
for i = 1:ney
for j= 1:nex
vertDofMatrix(i , j)=(i -1)*nex*3+j*3-2;
end
end
%-----%
intressantDof=linspace(1 , nfreeDofs , nfreeDofs)';
ModerAttKolla=intressantDof '; %intressantDof( Positions ', 1);
Zstore=zeros( nex , ney );
Z={1, nModes };
[X, Y]=meshgrid( 0: lx : a(1) , 0: ly : b(1) );
nModes=30;
%for zMatrix=1:nModes
for zMatrix=18:18
for i =1:ney
for j=1:nex
Zstore( i , j)=eigVect( vertDofMatrix( i , j) , ...
ModerAttKolla( zMatrix ) );
end
end
plotTitle=strcat( 'Mode' , { '□' } , num2str( zMatrix) , { '□' } , ...
' Natural□frequency : ' , { '□' } , num2str( fCut( zMatrix) ) );
Z{1, zMatrix}=Zstore;
hold on
figure( zMatrix)
surf(X, Y, Zstore)
daspect( [20 20 1] )
title( plotTitle)
colormap( 'gray' )
axis off
hold off
end
% %% Plot Nodegrid
% CheckDofs=[346 661 976]';
% ijIndex=zeros( length( CheckDofs) , 2);

```

```

% for i = 1:length(CheckDofs)
%     [ijIndex(i,1),ijIndex(i,2)]=find(vertDofMatrix == ...
% CheckDofs(i));
% end
% z0=zeros(21,21);
% figure(1)
% hold on
% daspect([1 1 1])
% surf(X,Y,z0)
% colormap('white')
% axis off
% NodeNum=string([106 126 211 221 231 316 336]);
% for i =1:length(CheckDofs)
%     figure(1)
%     x=X(ijIndex(i,1),ijIndex(i,2));
%     y=Y(ijIndex(i,1),ijIndex(i,2));
%     plot3(x,y,0,'ko');
% end
% hold off
% %%
% Zny=Z{1,1};
% figure(1)
% hold on
% plot3(X(20,41),Y(20,41),Zny(20,41),'o');
% %%
% Zny=-Z{1,1};
%     figure(1)
%     surf(X,Y,Zny)
%     colormap('gray')
%     axis off
%     hold off
% %%
% % Printing of all MPF*phi to excel sheet
% % All_MPF={1,length(dimensions)};
% % for i =1:length(dimensions)
% %All_MPF{1,i}=f_and_MPF(i,((abs(f_and_MPF(i,:)))>10^-9));
% % end
% % column='B';
% % sheet='testing';
% % toc
% % for i=1:length(dimensions)
% % [nEle,~]=size(All_MPF{1,i});
% % rnge= strcat(sprintf('%c2:%c',column,column), ...
% num2str(nEle+1));
% % xlswrite('Dimensions.xlsx',All_MPF{1,i},sheet,rnge);
% % column=column+1;

```

D. MATLAB code

```
% % end  
% %
```
